

POLITECNICO DI TORINO

Master's degree in Mechanical Engineering



**Politecnico
di Torino**

Master's Degree Thesis

**ECONOMIC OPTIMIZATION OF DRONE
STRUCTURE FOR INDUSTRIAL INDOOR
USE BY ADDITIVE MANUFACTURING**

Supervisor

Prof. Luca IULIANO

Company supervisors

Federico GIUFFRIDA

Orlando TOVAR

Candidate

Jorge Luis REGINO PRADO

December 2022

Acknowledgments

Al final de este trabajo y en general de esta etapa que culmino de manera satisfactoria me siento muy agradecido con todas las personas que han estado para mi y que de una u otra forma me ayudaron a realizar este sueño que inició hace más de tres años, logrando hoy el objetivo principal.

Quiero agradecer a mis padres y a mi hermana que siempre me han acompañado en cada tramo con su apoyo incondicional y que han depositado en mi la confianza y el amor necesario para lograr cada cosa que quiero en la vida. Este logro es de todos nosotros, sin ustedes no habría llegado a este punto.

Agradezco a mis amigos que me brindaron su apoyo muchas veces cuando los necesité y que me ayudaron a que el camino fuera más ameno. Amigos con los que siempre conté como Mena, Alfredo y Over. A la manada, que son como mi familia foránea y que desde el inicio me acogieron y me brindaron su amistad. En especial también a mis amigos de Colombia y a todas las personas que esta experiencia me dio la oportunidad de conocer durante el camino.

Voglio anche ringraziare ai ragazzi dal CIM4.0, dove ho svolto la mia tesi. A Federico, che è stato mio relatore durante il progetto, per il suo supporto e anche a tutti i ragazzi dell'ufficio con cui ho condiviso e da cui ho imparato cose nuove.

Abstract

The forthcoming industrial environments will require a high level of automation to be flexible. In this sense, Industry 4.0 encourages the integration of new autonomous systems digitally interconnected that can interact with humans. This thesis is developed at CIM 4.0 in the frame of the FIXIT project aiming to produce an autonomous system integrated by a UAV and a UGV. As a result, a combined system that complies with the Industry 4.0 requirements is created and mainly serves an operator by performing inspection tasks.

This work is focused on redesigning the UAV airframe. Normally these structures are manufactured with some conventional techniques like molding which limits building complex structures and presents high costs in most cases. In this sense, the scope is to create a personalized structure at a lower price than the standard airframes by implementing one of the industry 4.0 pillars: additive manufacturing. The topology optimization method is integrated into the design process to create a mass-customized structure with optimum structural properties. The role of Additive manufacturing in this work is crucial to obtain an innovative, customized system with an optimum cost considering the prices on the market.

The thesis is performed in different phases, starting from the definition of the UAV configuration and the propulsion system. Then a multi-material comparison and the analysis of different airframe designs are performed considering the cost and structural performance. Following this is the detailed design, in which other necessary features like the landing system, devices' supports, and protection structures are designed. Finally, is performed the manufacturing phase in which a functional prototype is printed through FDM technology.

The result is a lightweight customized airframe with good mechanical properties and optimum cost that is well integrated with the electronic components and landing system, enabling its autonomous performance characterized by repeatability and effectiveness.

CONTENTS

- Introduction 10
 - Brief about Unmanned vehicles..... 10
 - The role of additive manufacturing 13
 - The thesis purposes 15
- 1. Preliminary design: UAV configuration 16
 - 1.1. Airframe..... 16
 - 1.1.1. Selection of the UAV configuration..... 17
 - 1.2. Electronic components 19
 - 1.2.1. Propulsion unit 19
 - 1.2.2. Controlling components and sensors 25
 - 1.3. System configuration summary and connection scheme 28
- 2. Additive manufacturing..... 30
 - 2.1. AM for polymers..... 32
 - 2.1.1. Fused deposition modelling (FDM) 33
 - 2.1.2. Selective laser sintering (SLS) and Multi Jet Fusion (MJF) 35
 - 2.2. Additive manufacturing over conventional technologies 36
 - 2.3. Limitations of AM in UAVs..... 39
 - 2.4. Parameters influencing the cost 41
- 3. Structure optimization techniques 42
 - 3.1. Topology optimization technique 42
 - 3.2. Finite elements method 46
- 4. Airframe design and optimization 51
 - 4.1. Multi-material Material Comparison and selection 52
 - 4.2. Loading conditions..... 54
 - 4.2.1. Nominal condition 56
 - 4.2.2. Impact conditions 56
 - 4.2.3. Dynamic model 57
 - 4.3. Design constraints..... 66
 - 4.3.1. Structural components 66
 - 4.3.2. Electronic components 68
 - 4.4. Topology optimization 69
 - 4.4.1. Material configuration..... 69
 - 4.4.2. Design and non-design space 70

4.4.3.	Fasteners and contacts between bodies	72
4.4.4.	Load cases definition	74
4.4.5.	Shape controls	76
4.4.6.	Optimization settings	77
4.5.	Results	78
4.5.1.	Quad X	78
4.5.2.	Quad X with cylindric section	79
4.5.3.	Quad H and Quad I.....	80
5.	Optimum final design and printing	81
5.1.	Final design and other considerations	83
5.2.	Supports for electronic components	85
5.3.	Propellers protection for indoor flights.....	87
5.4.	Landing structure.....	87
5.5.	Final analysis.....	92
5.6.	Printing process and assembly	93
6.	Conclusions.....	98
	References	100

List of tables

Table 1 : UAV components specifications 28

Table 2 : Multi-material comparison53

Table 3 : FDM Material properties53

Table 4 : Test report by the motor supplier [26]55

Table 5 : Loading conditions of different manoeuvres 66

Table 6 : Critical load cases75

Table 7 : FEM analysis results 81

Table 8 : Mass and cost of the system with each material95

List of Figures

Fig 1 :	Forecast of the Drone market in North America [9]	11
Fig 2 :	Timeline of the development of additive manufacturing technologies and their applications in UAV [16].....	13
Fig 3 :	AM opportunity in the drone market	14
Fig 4 :	Requirements for the selection of UAV application [4].....	17
Fig 5 :	Octo-quad configurations [24]	18
Fig 6 :	Motor AT2312 specifications [26].	20
Fig 7 :	AT2312 motor with accessories [26]	21
Fig 8 :	Graph of propeller 6040 - diameter and pitch [27].....	21
Fig 9 :	Selected Propeller Multistar 9050 [28].....	22
Fig 10 :	Selected Lipo 3S 8000mAh Battery [29].....	23
Fig 11 :	Selected Electronic Speed Controller (ESC) 40A, 2-4S [30]	24
Fig 12 :	Pixhawk 2.4.8 [32]	25
Fig 13 :	Kit Nvidia Jetson Nano [33]	26
Fig 14 :	UWB pozyx module [34]	27
Fig 15 :	Initial UAV ZD550 Airframe [35].	29
Fig 16 :	Connection diagram of the main electronic components	29
Fig 17 :	Additive manufacturing process chain [36].	31
Fig 18 :	Development of AM over time [36].	31
Fig 19 :	AM technologies for polymers [36].	33
Fig 20 :	FDM process description [36]	34
Fig 21 :	Ultimaker S5 [38].....	34
Fig 22 :	Process description of a) SLS and b) MJF [39]	35
Fig 23 :	Comparison in the design process between AM and conventional methods [16] ..	37
Fig 24 :	Relation between cost and complexity in AM [36].	38
Fig 25 :	Topology Optimized component example [36].....	38
Fig 26 :	Topology optimization Steps [51]	46
Fig 27 :	Airframe Design path	51
Fig 28 :	Series 1585 Test Stand [27].....	54
Fig 29 :	Relation between thrust-rpm and torque-rpm	55
Fig 30 :	Rotating direction and motor enumeration of the system [24].....	57
Fig 31 :	Drone manoeuvres. a) roll motion b) vertical motion c) pitch motion d) yaw motion	58

Fig 32 :	Reference frames of the system	59
Fig 33 :	Description of Motors moments and thrust.....	63
Fig 34 :	Airframe measures in mm from the model in Solidworks.....	63
Fig 35 :	The initial main body of the airframe.....	67
Fig 36 :	The relative position of the motor supports	68
Fig 37 :	Settings of material properties.....	70
Fig 38 :	Non-design space	71
Fig 39 :	Design spaces: a) Quad X b) Quad H c) Quad I d) Quad X with cylindric section	71
Fig 40 :	Implementation of fasteners in Inspire.....	72
Fig 41 :	Location of the joints in the different bodies	73
Fig 42 :	Contacts between bodies in Inspire.....	73
Fig 43 :	Loadings over the motor support during flight.....	74
Fig 44 :	Impact conditions over the motor support	75
Fig 45 :	Constraint and concentrated mass in the main body	76
Fig 46 :	Symmetric shape control	76
Fig 47 :	Quad-X resulting structure	78
Fig 48 :	Quad-X cylindric resulting structure.....	80
Fig 49 :	Quad-H resulting structure.....	81
Fig 50 :	Results of FEM simulation: Quad-X, Quad-X cylindric, Quad H – Divergent Scale	82
Fig 51 :	Top and bottom plates' final design.....	84
Fig 52 :	Structure assembly – integrated with arms, main body, and motor supports	84
Fig 53 :	Structural analysis of the optimized structure	85
Fig 54 :	Support structures for electronic components: Battery, UWB, GPS, and depth camera	86
Fig 55 :	Propeller guard integrated with the motor support.....	87
Fig 56 :	Assembly of the structure with the arms.....	89
Fig 57 :	Landing structure before optimization with load cases: case a)Top case b)Bottom	90
Fig 58 :	Optimized landing structure	90
Fig 59 :	Description of the landing system with the constraints	91
Fig 60 :	Finite element analysis of the complete structure	92
Fig 61 :	The final model of the complete system	93
Fig 62 :	Preview of the printing process: left: XT-CF20, right: PA6CF	95
Fig 63 :	Printing preview of the support structures for electronic components	96

Introduction

In the ongoing fourth industrial revolution, industry 4.0, the main goal is to move into automation and integration of cyber-physical systems [1]. These systems are digitally connected and can interact with each other and with operators by exchanging information and performing multiple tasks. Industry 4.0 combines automated systems, cloud computing, the internet of things, and advanced manufacturing technologies to create an intelligent manufacturing system and operate more efficiently [2]. This fourth revolution has begun recently and is growing fast, focused on providing customization, enhancing flexibility and productivity by digitalizing the processes in the industry, being more practical and less wasteful.

The forthcoming industrial environments will require a high level of automation to be flexible and adaptive enough to comply with the increasingly faster and low-cost market demands. In this sense, autonomous vehicles and collaborative robots have an ever-greater role in the industry 4.0 implementation. In this context, the FIXIT project was born at the Competence Center CIM 4.0 to develop a product that complies with the industry 4.0 requirements, from automated vehicles to additive manufacturing and augmented reality to the internet of things.

FIXIT project consists of an autonomous driving system integrated by an Unmanned Aerial Vehicle (UAV) and an Autonomous Mobile Robot (AMR). This system intends to carry out inspection activities in indoor and outdoor industrial or logistic environments, providing interactive support and assistance for the human operator. Therefore, the system collects information in the field, which is processed to identify anomalies in industrial procedures. Finally, an operator who benefits from the assistance provided by augmented reality corrects these anomalies.

Brief about Unmanned vehicles

The automation robots that have emerged with industry 4.0 include unmanned vehicles, which are driven without the driver being on board the vehicle. Unmanned vehicles consist of the following [3]: Unmanned Ground Vehicles (UGVs), which are part of mobile robots (AMR); Unmanned Aerial Vehicles (UAVs), which are unpiloted aircraft, commercially called “drones” and Unmanned Marine Vehicles (UMV). UGVs operate on the ground performing manufacturing activities like part-feeding and material handling [4, 5, 6]. Instead, UAVs work in the air and have been used widely, from military operations to package delivery, one of the most exploited applications.

UAVs or drones appeared in the 20th century for military applications due to the need to perform dangerous activities for humans. Thanks to technological advances and consequently costs decreasing, now they are used in multiple non-military applications, like product delivery, aerial photography, infrastructure inspection, policing and surveillance, science, racing, and others [7, 8]. Currently, many types of drones exist, varying widely from the size of a butterfly to the size of a plane, and are classified principally based on the airframe or structure configuration and can be subclassified according to the application or the number of rotors.

Drones are considered the next breakthrough in industry 4.0 [1]. Therefore, they are increasingly used in different applications in the industry; consequently, the drone market is growing faster and faster. The most extensive use is expected in inspection and maintenance applications where the operation is risky and ineffective because the operator can not access the zone, e.g., environments like refineries, pipelines, mines, and others [1]. North America is an example of this evolution, where the forecast is an expansion of the commercial drone market from 2021 to 2028 at a compound annual growth rate (CAGR) of 55.2%, as shown in figure 1 [9].

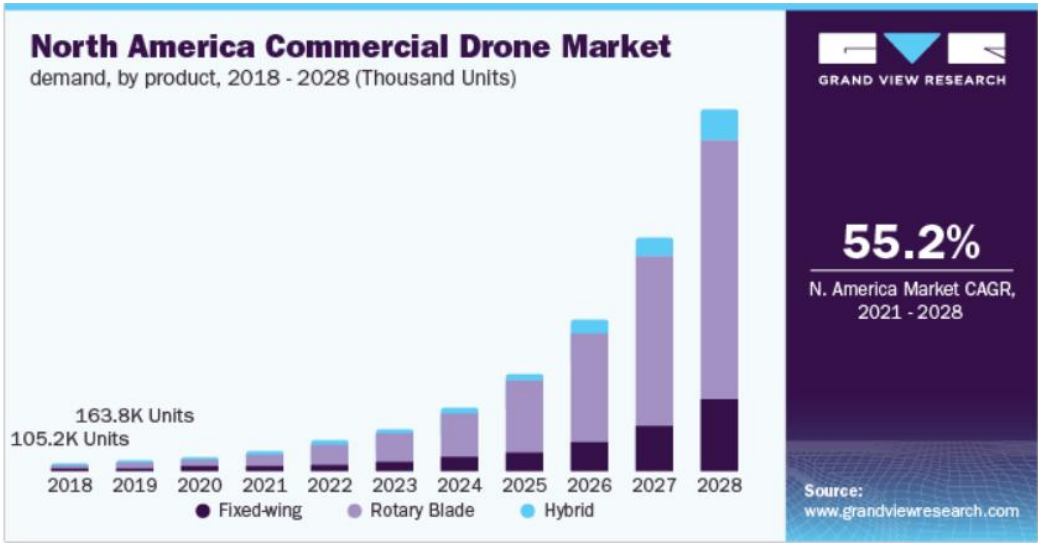


Fig 1 : Forecast of the Drone market in North America [9]

Integrating advanced technologies such as Artificial Intelligence (AI) and Machine Learning (ML) in drones offers significant growth enabling the expansion of the applications. Drones, combined with AI technology, can better understand their surroundings, map areas accurately, track and monitor the movement of specific objects, and offer precise analytical feedback [9]. Today UVs can be integrated with different technological components such as cameras, laser range finders, motion capture systems, and wireless communication technologies, which

enable the implementation of UAVs for indoor operations [4, 10, 11, 12]. For instance, equipped with an imaging device and sensor, a UAV can perform inspection tasks in a harsh environment, both visual and sensory inspection [4].

As mentioned before, the FIXIT project is focused on developing a multi-nodal vehicle that commutes the capacity of an autonomous mobile robot with the capabilities of an intelligent flying vehicle. From the point of view of the operation, the missions of a UAV are characterized by high movement speeds, high agility that allows for reaching hard-to-reach spaces, low load capacity, and short duration. On the contrary, the missions of an AMR are characterized by the low speed of movement but with a load capacity even higher than its weight. The interest in integrating a combined UAV-UGV system is due to the possibility of complementing and taking advantage of the different features of each one.

The integration of combined UAV-UGV systems starts with developing combined path-planning algorithms between the two systems. These algorithms guarantee the maximization of efficiency in path generation, which translates into less energy expenditure for the same operations. Both elements can assume primary or support roles depending on the application. In general, the combined systems ensure the maximization of the covered area, compared to the separate use of each one individually [13].

The applications of these systems are multiple and include the delivery of goods to private users, providing relief in emergencies, distributing seeds and pesticides in agriculture, and carrying out inspections in the civil and industrial fields [13]. In inspection applications, these systems appear to be valid substitutes for stationary sensors for monitoring, as they guarantee more flexibility without the limitations of fixed sensors in the inspection activities. It is necessary only to equip the UAV or UGV with the proper sensor when its use is required.

The FIXIT project paid particular attention to the inspection applications, which operate in places or regions, both indoor and outdoor, where human operation is complex, risky, and consequently expensive. Then a system equipped with various sensors, e.g., ultrasonic, laser, Lidar distance sensors and stability, and orientation sensors or stereoscopic cameras can discover anomalies or problems in industrial equipment and, in this way, avoid time-consuming, dangerous, and costly human inspections [1] [14] [15].

The role of additive manufacturing

Industry 4.0 is looking to increase flexibility in manufacturing and be more friendly to the environment improving quality and productivity along with mass customization by innovating design and manufacturing processes. It introduces new products with customized features at optimal cost and the possibility of collecting and analyzing data to identify whether the product is suitable for the customer. Additive manufacturing (AM) fulfills these and other upcoming requirements. For this reason, it is one of the pillars and plays a vital role in Industry 4.0, where digital manufacturing and customization are essential.

AM offers multiple possibilities and solutions to industry 4.0. For instance, the application of this technology in the aerospace sector and autonomous systems like UAVs is constantly increasing. Particularly AM is changing the way drones are made by creating innovative and complex structures, both for the frame and other functional parts and accessories, decreasing the costs without taking care of the constraints present with the traditional methods. UAVs match perfectly with additive manufacturing since getting a high-quality customized drone with the exact features for a specific purpose is possible.

The relationship between drones and additive manufacturing is recent. The first fully printed drone was produced in 2011, as shown in figure 2. From there, this relationship does not stop growing and is enhancing more and more because these advanced technologies can address most of the challenges and solutions for drone building. Today is easier to produce a lightweight and resistant drone through AM, where the short lead times allow to make as many iterations as are necessary and save time in the development process.

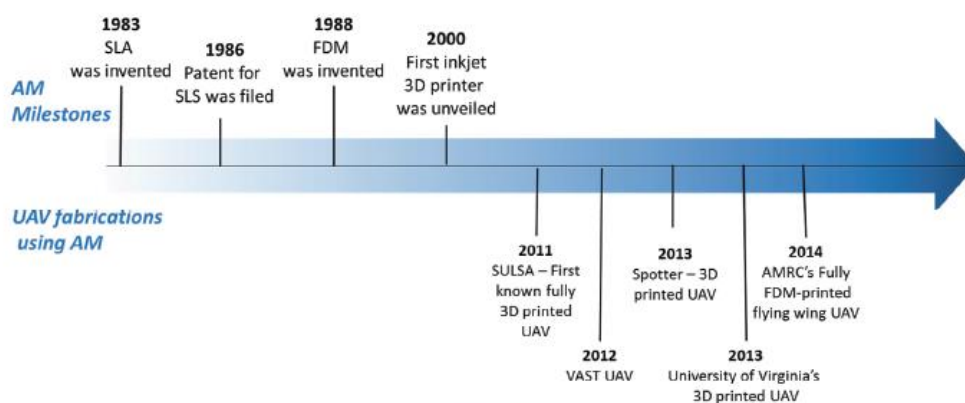


Figure 2

Fig 2 : Timeline of the development of additive manufacturing technologies and their applications in UAV [16].

FDM, SLA, polyjet, and SLS have been used to either fully print the UAV structures or fabricate certain parts of UAV structures [16]. The Marine Corp [17, 18] found a solution to replace a costly Raven drone with a 3D print drone to get real-time images of dangerous areas. The total system applying AM only costs \$615 while the Raven drone costs \$30000, and with the printed drone was easier to assemble and replace broken parts. Due to the disaster that occurred in the past, In Japan, a customized 3D printed drone with an extended flight time and a reinforced frame was designed by Yuki Ogasawara and Ryo Kumeda to work in emergencies like an earthquake, locating people needing help [19]. In delivery applications, the demand is increasing, so a research group from KU Leuven [20] developed a 3D-printed drone that can transport a charge of 5 kg and reach a speed of 150 km/h. CargoCopter, as it is called, combines the benefits of fixed-wing drones with those of multi-rotor drones resulting in a hybrid solution that performs a transition from hover flight into an efficient cruise flight.

Additive manufacturing is aiming to dominate the growing drone market. Recent surveys have suggested that the fabrication of small-volume manufacturing UAVs will increase tremendously by 2025, focused principally on Materials, Design, structure, and printer Technology [16, 21]. AM has ample opportunity in this area, and the use of its technologies will increase more and more to produce drone components now and in the future.



Fig 3 : AM opportunity in the drone market

The thesis purposes

This thesis is done in the frame of the FIXIT project. It aims to redesign and optimize the structure of a UAV that will be part of a combined autonomous system consisting of a UAV and an AMR, used as support for an operator in industrial inspection and maintenance. This work is developed in the following phases:

- ✓ Preliminary design
- ✓ Airframe design and optimization
- ✓ Detailed design and final considerations
- ✓ Printing process

The preliminary design consists of selecting the airframe configuration as the definition of the propulsion unit and the controlling components necessary to power the system, control the drone's movements, and enable the performance of the desired tasks, respectively.

The phase of design and optimization is the most important. This phase begins with a multi-material analysis of different AM technologies. Then the volumetric and assembly constraints for the design of the structure and the static and dynamic loads to which it will be subjected are evaluated. Finally, the topology optimization of the structure is performed based on the definition of different design spaces, from which various design hypotheses were obtained through the use of Inspire 2021 and SolidWorks 2020 software. These structures were then compared from a mechanical and functional point of view: the best result was subjected to detailed modifications aimed at reducing the mass and redesigning the stress concentration zones.

The phase of final considerations consists of the design of the other components like support structures for electronic devices, protections for indoor flight, and the landing system, which is necessary to provide the autonomous landing of the UAV on the AMR structure.

Finally, the last phase is the printing process, where a functional prototype is produced to validate the structure's final design and fix eventual issues, mainly from the point of view of the assembly. This process is performed in the printer Ultimaker S5 provided by the competence centre in which is developed the project, CIM 4.0.

1. Preliminary design: UAV configuration

Any UAV configuration has two main elements: the airframe and the electronic components. For an optimum UAV design, those elements need to be well integrated and complemented because the selection of the mounted electronic components depends on the shape and type of frame and vice-versa. As the current work is focused on optimizing the UAV airframe, it is essential to guarantee the drone's structural integrity and optimum flight using an efficient propulsion unit, a proper controlling system, and sensors to ensure autonomous flight.

1.1. Airframe

The airframe is the drone structure that houses the propulsion unit, which includes the motors, propellers, battery, controlling components, and relevant sensors. The airframe design is one of the essential steps since, in UAVs, the space is restricted and should be such that all the required sensors and payloads can be mounted on it without compromising the flight performance [22].

Different types of airframes are used according to the need or application. These can be divided principally into three types:

- **Multicopter:** These drones are composed, in general, of multiple motors that power propellers to generate vertical thrust with excellent control over the position. In general, they are cheap and suitable also for indoor applications. The structure consists principally of the following:

The main body is the central structure of the frame, where the arms, the electronic components for control and power, the carcass, and the landing structure are fixed.

The arms are the elements that are joined to the main body and support the motors.

The landing structure ensures the drone's stable and optimal landing and enables the battery to recharge when the drone is on the recharge platform.

The multi-rotors are named according to the number of arms/rotors. In the market, they typically have three arms (tricopter), four arms (quadcopter), six arms(hexacopter), or eight arms (octocopter). Quadcopters are the most common due to their better stability capacity than tricopters and lower complexity and cost than hexacopters and octocopters.

To ensure the dynamic stability of flight, the multirotor must have a symmetric structure with counter-rotating propellers to cancel out the overall angular momentum that the motors generate on the structure.

- **Fixed wing:** In this type of airframe, horizontal axis propellers are used to generate thrust in the direction of flight, and fixed-wing geometry generates vertical thrust. They are suitable for large, open worksites. They are speedy and efficient, with longer flight times.
- **VTOL (vertical take-off and landing):** This airframe generates vertical thrust by a system of vertical axis propellers. They take off and land vertically as a quadcopter but act like fixed-wing drones in flight. They combine elements from both quadcopter and fixed-wing designs. They are high-efficiency systems suitable for large scale, but the cost is also high.

1.1.1. Selection of the UAV configuration

For the selection of the UAV configuration, the type of application must be well analyzed, considering the following elements [4]: the task that is the activity the drone will perform like inspection; the environment that consists of the surroundings and spaces in which the drone will operate and the UAV operation features which refers to the devices that support the UAV operation, e.g., UAVs equipped with grippers, imaging device or sensor. Therefore, it is possible to define a cycle to define a proper system configuration, as shown in figure 4.

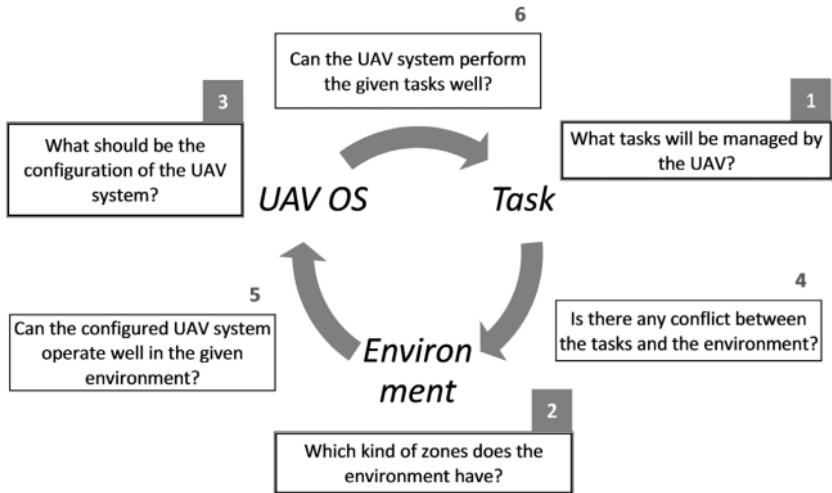


Fig 4 : Requirements for the selection of UAV application [4].

In this case, as mentioned before, this application is for indoor and outdoor flights. It aims at providing interactive support for the human operator in inspection activities within an industrial or logistic environment. Another critical parameter to take into account is the cost. According to the project's requirements, the best option is an octa-quad frame, a quad-type multirotor frame with eight motors/propellers: two motors in each arm (one facing up and the other facing down). This type of frame offers the possibility to have sufficient thrust and more strength in a compact and lighter design than the octocopter configuration. This configuration ensures the parallel engine in case of failure and takes advantage of the high stability and low cost. In this configuration, the double propellers rotate in opposite directions, balancing one other with the inertia force [23].

The quad-type airframes can be divided according to the relation of the propeller system with the flight direction as follows [23]:

Quad X: This is the most common configuration, in which two propellers lead (with an even number of propellers). In general, the most suitable for positioning electronic components and sensors.

Quad H: This is a not typical configuration, where the construction is based on the H-shaped with two propellers leading.

Quad +: In this configuration, one propeller is leading (at least four propellers).

Quad V: This is a rare configuration where two propellers lead onto outstretched arms.

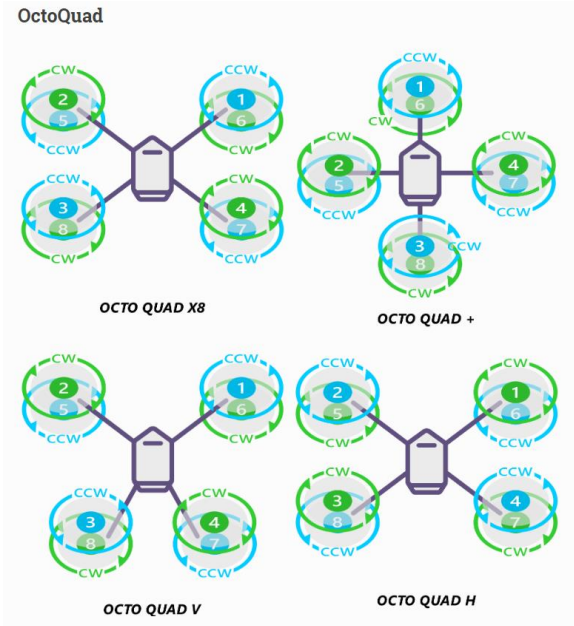


Fig 5 : Octo-quad configurations [24]

For this case, the configuration is selected after evaluating principally the mechanical properties of each one and the dimensional constraints of the electronic components that will be discussed forward.

1.2. Electronic components

The electronic components are the second part of the UAV system. Its function is to power and controls the complete system. To select these components, parameters like the drone's total weight, the airframe's volume, the system's complexity, and the level of autonomy in choosing the sensors are necessary. The electronic components can be divided into two categories according to the function they perform: the propulsion unit, composed of the components that power the system, and the controlling components and sensors, whose role is to control the movements of the drone and enable the performance of the desired tasks.

1.2.1. Propulsion unit

The propulsion unit is the first step in selecting the electronic components and is composed of the motors, the propellers, the battery, and the Electronic speed controllers (ESC). To define the propulsion unit is necessary to make some assumptions considering the application to determine the required quantity of thrust, which is the force perpendicular to the propellers required to provide motion to the drone [25]. In the drone field, the thrust can be measured in grams or Newtons (1N = 100gf).

In this case, the quadcopter is for inspection flights and support for the operator, so the drone does not need to reach high speeds or carry an extra payload. In this sense, the initial total mass of the drone, including the whole system (structure and electronic components), is about 2,8 kg. Then the required thrust to keep the drone at hover is equal to the system's weight and is calculated by the equation (1).

$$T_{Hover} = M_{drone} * 9.8 \frac{m}{s^2} = 27,5 N \quad (1)$$

As the drone needs to perform different operations, not only hover, the drone must guarantee a higher thrust than hover, for example, at the take-off where it is necessary also to overcome the inertia and the drag. Therefore the Thrust-to-weight ratio (TWR) is the relation between the maximum thrust that can be reached and the weight of the system. TWR is one of the most critical parameters in drone building. The TWR is different drone by drone, depending on the application. In this case, a minimum TWR of 2,5 suits this drone's requirements. Then the total thrust can be calculated by equation (2)

The terminology of the motors is explained as follows: the first numbers refer to the dimensions of the stator; for example, for the selected motor, the diameter of the stator is 23mm, and its height is 12mm. The number of Kv refers to the motor speed in RPM when applying one volt, so in this case, the motor spins at 1150 RPM when 1 volt is applied, but the mean is more complex because Kv also relates to the torque generated by the motor. The more Kv, the less efficient the motor gets since it requires more current to deliver the same torque. Therefore, a higher Kv motor does not mean that the propeller will spin faster because sufficient torque is also needed to accelerate and rotate the propeller faster. More Kv means, in general, less torque.



Fig 7 : AT2312 motor with accessories [26]

Propeller

The propellers generate the thrust through the rotational movement transmitted by the motors. The principal parameters of the propellers are the diameter, pitch, weight, number of blades, and material. Commonly propellers are defined by their size in a four-digit number in terms of their diameter and pitch. The diameter indicates the diameter, in inches, of the circle that the propeller generates during rotation, while the pitch refers to the amount of travel in one spin. For example, a propeller 6040 has a 6.0” diameter and a pitch of 4.0”, as shown in figure 8.

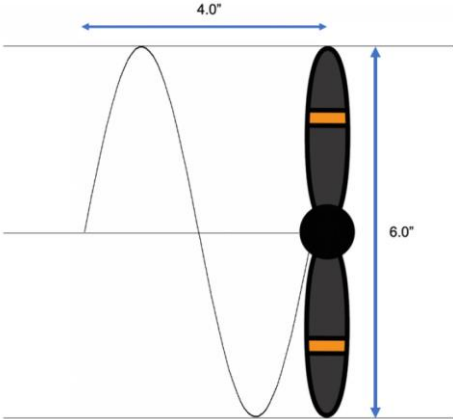


Fig 8 : Graph of propeller 6040 - diameter and pitch [27]

Another critical parameter is the material because it is related to the weight of the propeller. The most common propeller materials have a good balance of strength and weight, such as nylon, carbon fiber, fiberglass, or stainless titanium [27].

The propeller selection is crucial since thrust depends exclusively on the geometry and velocity of the propeller and the air velocity. Longer propellers can generate higher thrust at a certain speed, but more power from the motor is necessary to get them spinning. Also, something similar happens with the number of blades, more propeller blades produce more thrust, but they also have higher heat loss and lower efficiency [27].

All the propellers mounted in the drone must have the same diameter and pitch. Generally, in the motor specifications is possible to find some recommendations about the optimum propellers to have an efficient system. In this case, a propeller 9050 (diameter 9" and pitch 5") is selected because the motor supplier recommended it for the AT2312 to get the required thrust and optimal performance. In cases where there are no specifications about the propellers, it is necessary to compare different propellers by testing and then select the most efficient. The propeller efficiency is obtained as the ratio between the thrust and the mechanical power.



Fig 9 : Selected Propeller Multistar 9050 [28].

Battery

Usually, the batteries used in UAVs are rechargeable LiPo (Lithium-Polymer) batteries due to the high energy density by weight compared with other batteries like nickel batteries. LiPo batteries are different from traditional Li-Ion batteries because the first ones use a porous gel-like compound instead of a liquid. They are also trendy because they are less likely to leak or combust [27]. This type of battery comes with some specifications that are important to the battery selection and drone building:

Battery capacity: is the most critical parameter, commonly given in mAh or Ah, and is defined as the amount of current that can provide the battery in one hour.

Voltage: this is the working rating voltage of the battery and is helpful to know the theoretical motor speed using the motor Kv (RPM/Volt).

Cell configuration refers to the number of cells and the battery layout. The voltage provided by the battery is distributed among the cells. For example, a 3S LiPo battery has three cells in series (S) with a nominal voltage of 3.7V, so $3 * 3.7 = 11.1V$ is the voltage rating of this battery.

Discharge rate (C rating): This parameter refers to the capacity of the battery to discharge quickly and helps calculate the maximum current provided by the battery. For instance, with a battery whose capacity is 8000mAh and discharge rate of 30C is possible to discharge it at 30 times the capacity of the battery ($8Ah * 30 = 240Ah$) and would be discharged working in this condition in two minutes ($(8Ah / 240Ah) * 60 = 2$ minutes).

According to the motor/propeller set, there are some battery recommendations. The volume energy density is essential as it defines the size for the proper battery fit on the drone. Still, more important is the energy density from the point of view of performance and also the cost because a higher energy density means a more expensive battery.

For this system, at 100% throttle, the motors draw a maximum current of 18A each, so the eight motors require 144A of current. Also, the consumed energy by the other electronic components and the required flight duration need to be considered in the battery selection. The motor manufacturer recommends 2-4 S batteries. In this sense, the selected battery is a LiPo Gens ace 4S 5000mAh 50C, with three series cells working at 3,7V. The maximum amount of current that can provide by this battery is 250A which is sufficient to supply the maximum current required by the motors and the other electronic components. The maximum current is calculated by equation (4).

$$I_{max} = Capacity * C_{rating} = 5Ah * 50 = 240A \quad (4)$$



Fig 10 : Selected Lipo 3S 8000mAh Battery [29]

Electronic speed controller

The electronic speed controllers (ESC) control the power provided to the motors from the battery. For instance, if the throttle on the controller is 50%, the ESC delivers 50% of the regime. Each motor is connected to its own ESC. The connections of the ESC are configured as follows: on one side, the ESC has three connectors to connect to the coils of the brushless motor. On the other side, has two wires, one red (positive) and one black (negative), to connect to the battery through a power distribution board. It also has a connection to the flight controller, which controls each motor's throttle according to the signal read by the receiver.



Fig 11 : Selected Electronic Speed Controller (ESC) 40A, 2-4S [30]

In this case, the communication between the flight controller and the ESC to convey throttle information is done by the protocol PWM (pulse width modulation), so the output of the ESC is a PWM signal. This type of signal has a constant amplitude but a variable pulse duration or duty cycle (DC). The objective of this protocol is to generate an analogue signal from a digital one. The ESCs must be independent for each motor as motors generally have different rotational speeds, which is essential for the dynamics of the flight, in particular for stability and movement.

For the selection of the ESC, the most important is that the current rating must be higher than the current required by the motors, in this case, higher than 18A, to prevent overheating and to guarantee a safe range when the working condition is at maximum throttle. Then an ESC with a maximum current of 40A recommended for 2-4S batteries is selected, which meets the requirement of the motor.

1.2.2. Controlling components and sensors

These components are necessary for autonomous flight, allow the proper performance and ensure the correct functioning of the propulsion system and motion of the drone. This group of components is like the brain of our complete system. The main components in this group are the following:

Flight controller

The FC (flight controller) is the most critical component in this group. The FC monitors and controls all drone operations and can vary in complexity. Although the operator can control the motion on the ground by radio control, the drone must have an automatic control system that allows it to be stable and perform operations without human intervention. These operations should be guaranteed when the flight controller is selected [31]:

- Gyroscopic stabilization: it is the automatic stabilization capacity of the drone.
- Self-leveling is the ability to maintain a specific orientation during movement.
- Altitude Holding: The drone can maintain a fixed altitude without the pilot having to adjust the throttle manually.

This drone uses the FC PixHawk 2.4.8 to control the system, one of the most implemented flight controllers in drone applications. It has an internal programmable memory, sensors such as accelerometers, an internal barometer, and GPS. This FC accepts input connections from an external GPS and radio receiver to receive a radio signal from a device such as a radio control to manual driving by an operator from the ground. Finally, it can be connected to a microcomputer to be controlled autonomously without the need to receive orders from the ground [31].



Fig 12 : Pixhawk 2.4.8 [32]

The essential element of the FC is the internal measurement unit (IMU) which contains the sensors with which the drone can recognize its orientation in space. The IMU includes three gyroscopes and three accelerometers of class Micro Electro Mechanical Systems (MEMS) for the control in XY Z axes. The gyroscopes allow measuring the rotation of the FC on each axis, while the accelerometers allow measuring acceleration on each axis. This measured data is processed according to a Proportional Integrative Derivative (PID) algorithm, which gives as output the rotation speed of the motors [31].

Nvidia Jetson Nano

In this case, using an Nvidia Jetson Nano was considered after some simulations in a virtual environment. The jetson nano is a kit that helps perform multiple tasks like object detection and image classification. This component is also known for its good computational power and performance at a low cost.



Fig 13 :Kit Nvidia Jetson Nano [33]

UWB pozix

This component provides information about positioning and motion, and it is very accurate. Its principal element is an ultra-wideband (UWB) transceiver which uses a radiofrequency transmission technique for indoor positioning systems. This system consists of fixed anchors positioned at known points in an indoor environment and an antenna placed on the object to be tracked. It also has a set of sensors (accelerometer, gyroscope, compass pressure sensor). This component is required to implement an autonomous system inside the drone. It can process logical information, such as the route to follow and the obstacles present, and physical measurements, such as acceleration and atmospheric pressure.



Fig 14 : UWB pozyx module [34]

Depth camera D435i

An intel RealSense depth camera is mounted. This camera is designed for fast-moving applications like the UAV system and offers a wide field of view with a global shutter on the depth sensor. In this application, the camera helps to perform the landing operation by detecting a marker in the ground and guiding the drone's precise landing.

RTK GPS

The GPS mounted in the drone uses RTK technology (Real Time Kinematic), a technique that offers satellite positioning producing accurate results to the centimeter. This technology measures satellite data against a ground station to obtain precise information in real-time.

Transmitter (Tx) and receiver (Rx): These two components allow the drone's control remotely from the ground using a wireless signal. These components perform control of all the operations of the drone, like throttle, pitch, roll, or yaw. This system uses a 2.4GHz frequency for communication, which serves better than other radio frequency controllers since it does not present signal conflicts.

Telemetry module

This device controls the drone using ground station software (on a PC or tablet). The kit has two modules, one ground module to connect to the PC and the air module mounted on the drone. The telemetry module used has a transmission band of 433 MHz.

Magnetometer

This component is a geomagnetic sensor that permits accurate heading and orientation calculations by eliminating the noise in the magnetic field measurements. It Provides a heading reference for the drone to navigate through waypoints and eliminates magnetic disturbances due to motor coils and metal parts.

Lidar

This component is a sensor typically used in autonomous vehicles to have a 3D view of the surroundings for safe operation. In this case, it measures the drone's height relative to the ground. Its maximum operating range is 12m, sufficient for indoor applications.

1.3. System configuration summary and connection scheme

All the components described above are the necessary selected components for building the initial UAV system. The specifications of these components are given in table 1. This table shows two main parameters: the price and the weight of the complete system, which are some of the main parameters to optimize. This initial configuration was proper to program the system and test the drone's flight operations. These testing operations were done by some colleagues working on the autonomous flight and the landing system of the drone. Once this is done, the idea is to optimize the initial UAV airframe, shown in figure 15, through additive manufacturing and topology optimization, maintaining the selected electronic components necessary for the drone's functioning. The physical connection scheme of the main features of the UAV system is shown in figure 16.

Quantity	Component	Dimension (mm)	Weight (g)	Price (€)
1	Quadcopter frame ZD550	550x395	675	193,66
8	2312 1150KV Brushless Motor	23x12	480	280
8	Propeller 9050	229	56	47
1	LiPo Battery	1637x43x34	436	65
8	ESC	68x24	132	84
1	Flight controller	82x47x16	41	146
-	Other electronic components	-	980	2184
Total			2800	3000

Table 1 : UAV components specifications



Fig 15 :Initial UAV ZD550 Airframe [35].

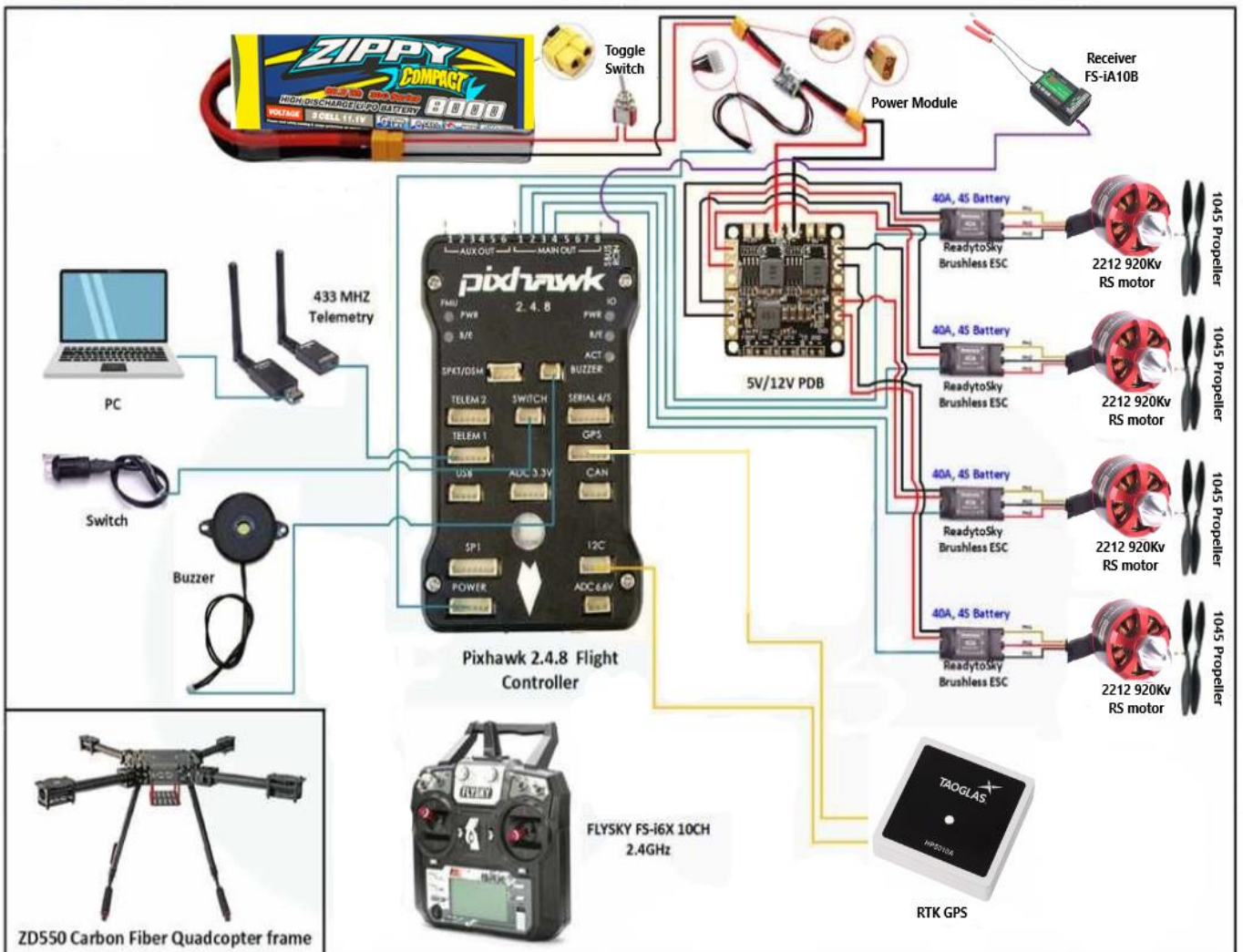


Fig 16 : Connection diagram of the main electronic components

2. Additive manufacturing

Additive Manufacturing (AM) is a new technology compared with conventional manufacturing methods and still has significant potential. Unlike traditional techniques that use material removals, such as milling, machining, carving, shaping, or other means, AM techniques are based on the deposition or treatment of the raw material, layer upon layer, in precise geometric shapes, producing minimal material waste. AM offers the possibility of creating parts with complex geometry using data from computer-aided design (CAD) software or 3D object scanners.

The manufacturing process starts with the design of the component by computer-aided design (CAD) software that is used to create .stl (standard triangulation language) files that essentially "slice" the object into ultra-thin layers. This process triangulates the external surface of the piece starting from the CAD file, approximating it to triangles with variable shapes and sizes according to the piece's surface and the calculation parameters. The shape and position of the individual triangles are calculated according to some parameters that identify the precision with which the approximation is carried out. The main parameters are:

- Chordal error: represents the maximum allowable distance between the mathematical surface of the model and the triangle used to approximate it.
- Normal deviation: represents the maximum angle between the normal to the triangle used for the approximation and the normal to the original surface at the same point.

After that, the model is oriented correctly, such as the z-axis being the building direction, and the STL model is sliced by a sequence of parallel slicing planes based on a layer thickness entered by the user. For that, stair stepping is a characteristic of additive manufactured parts. The result of this slicing process is a parameterization of the individual sections of the piece. Then each two-dimensional section is processed by the software to generate a list of instructions. Subsequently, This information guides the path of a nozzle or print head as it precisely deposits material upon the preceding layer or, depending on the technology, guides a laser or electron beam that selectively melts in a bed of powdered material. As the material cools or cures, it fuses to form a three-dimensional object.

Finally, the last step is post-processing, where parts receive finishing touches such as smoothing and painting but differ depending on the technology used. Sometimes the finishing process can enhance a part's surface characteristics, geometric accuracy, aesthetics, and

mechanical properties, so it is an essential step in the manufacturing process. Some tasks are removing supports, draining and rinsing, surface finishing, post-curing, or heat-treating.

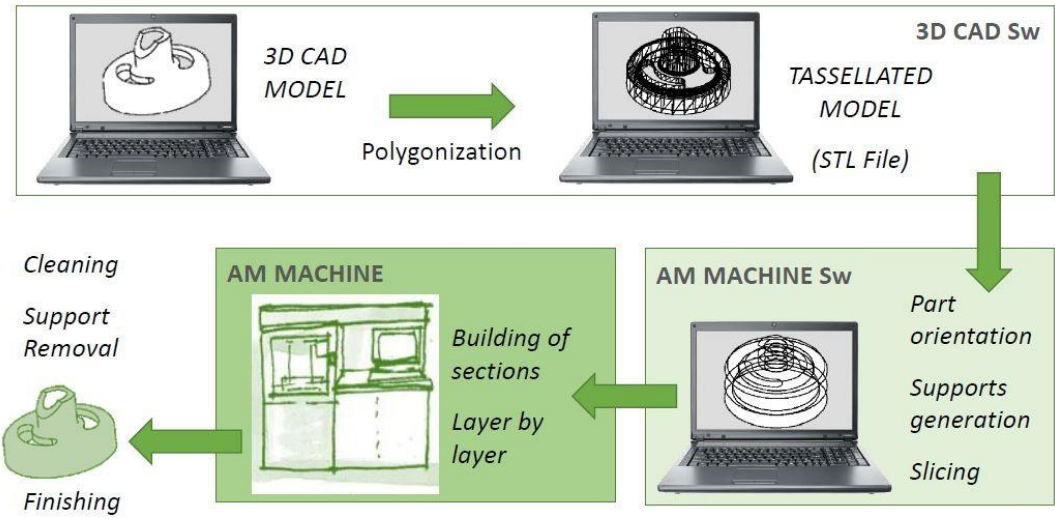


Fig 17 : Additive manufacturing process chain [36].

Over time the growth of the AM has been fast and has evolved from using the technology only for prototyping conceptual designs to today, where high-performance and end-use components can be made, as is shown in figure 18. Also, the range of materials with which it is possible to work in AM has increased in the last years, and it is one of the topics that are most researched nowadays in this technology. There is a wide variety for multiple applications, like components with high-impact strength or high-temperature use, to mention a few. Today is possible to print high-perform composite materials with excellent mechanical properties.

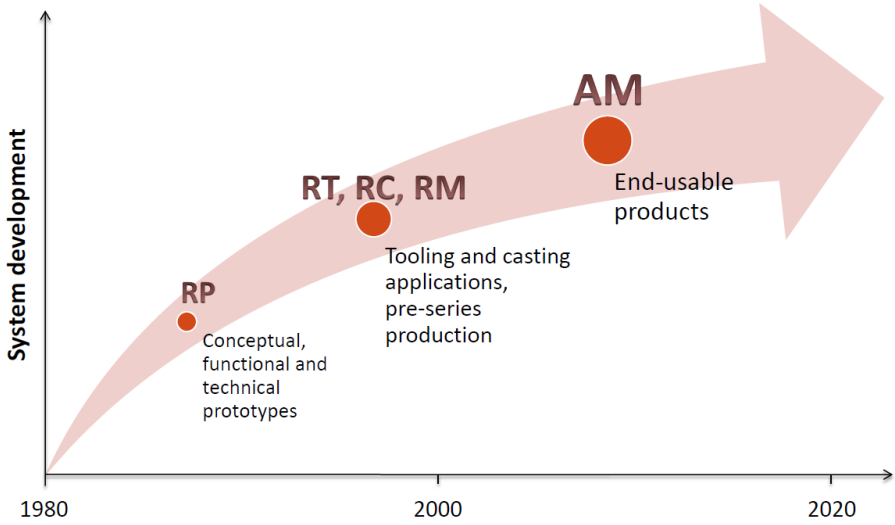


Fig 18 : Development of AM over time [36].

Topology optimization will be discussed further since it is one of the main topics applied in this work. Today there is also the possibility of concurrent application of topology optimization (and generative design) and additive manufacturing where the principal purpose is basically “put material only where it is needed.” Topology optimization consists of optimising the material distribution in the piece to be designed. Thanks to this technique, producing complex shape geometries is no longer a problem.

Generative design is more of a design exploration process in which parameters and goals are set, such as performance, spatial requirements, materials, and costs. The software will create high-performing design options based on those constraints. The generative design software resolves conflicting design constraints, so it can focus only on innovating.

The primary design rules for AM could be summarized as [36]:

- ✓ Do not consider conventional design principles
- ✓ Capitalize on the capabilities of AM technologies
- ✓ Rethink the whole assembly towards integrated freeform design; reduce the parts count by intelligent integration of functions
- ✓ Use as little raw material as possible (therefore as little energy as possible) to optimize the design towards the highest strength and lowest weight
- ✓ Feel free to use freeform designs; use undercuts and hollow structures if they are useful
- ✓ Design the optimal shape of the part according to functionality

2.1. AM for polymers

In this project, the drone airframe is made through the polymeric AM, the technology commonly used for this type of application since it is the most suitable to have lightweight parts with high mechanical properties, which is a critical requirement in the drone’s building. Polymeric AM techniques are also the most used thanks to their low cost and greater ease of use than metallic ones. They offer the possibility of creating parts in a wide range, from prototyping to producing finished components in small series. The different processes in AM for polymers can be classified according to the type of raw material: powder, liquid or solid, as shown in figure 19.

AM for Polymers

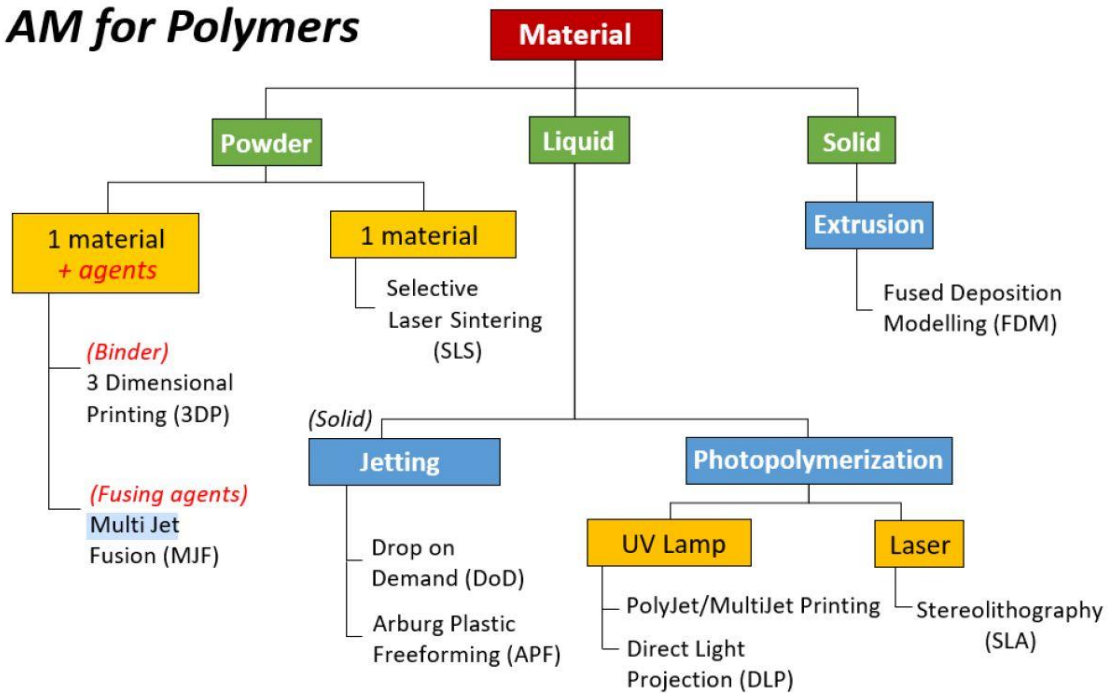


Fig 19 : AM technologies for polymers [36].

Concerning the purpose of this thesis, the AM polymeric technologies considered are the following: fused deposition modelling (FDM), selective laser sintering (SLS), and multijet fusion (MJF). FDM is the principal technique to take into account since it is most suited in the UAV field thanks to its flexibility and lower cost without requiring extensive infrastructure, which is able at CIM 4.0, where the project is done. Printing with materials reinforced with fibers is possible, which helps obtain the final drone version. The other processes to consider are selective laser sintering (SLS) and multijet fusion (MJF), which are powder bed fusion technologies used to manufacture resistant and lightweight drone parts in the industry [37].

2.1.1. Fused deposition modelling (FDM)

The FDM is an extrusion process where the materials are selectively distributed through a nozzle or orifice. It uses a heating chamber to liquefy polymer fed into the system as a filament. A tractor wheel arrangement pushes the filament into the chamber, which generates the extrusion pressure. The materials used in this technology are thermoplastics like ABS, PLA, PC, ASA, PA, PEEK, and others. Since this technology is a direct deposition, it also allows the simultaneous use of different materials so that it is possible to generate the supports in another thermoplastic material that can be soluble, in water, for example.

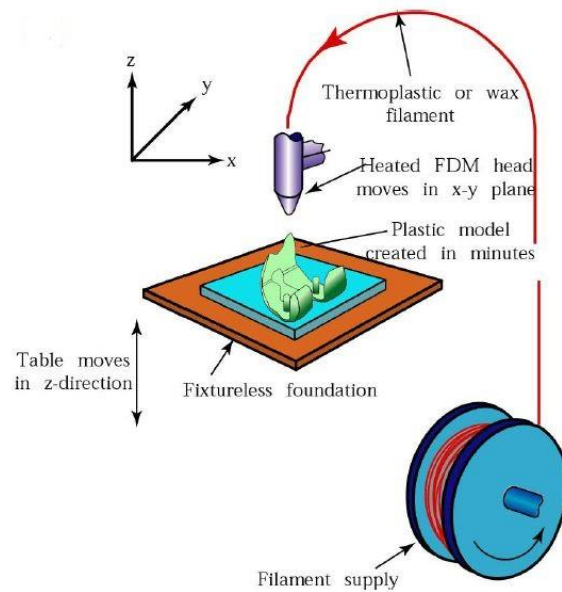


Fig 20 : FDM process description [36]

FDM is widely used to print critical structures of UAVs due to its ability to print high-strength materials. However, due to the small build volume of the standard machines, the designs are mostly printed in modular parts and later connected using carbon rods to improve the stiffness [16]. As mentioned before, at CIM 4.0 company is possible to work with the FDM process. There is an Ultimaker s5 printer, a last-generation machine with great features, such as a dual extrusion system that enables the printing of composites. The build volume is 330x240x300 mm and is compatible with over 200 materials, so in this sense, the prototype and even the final parts of the drone could be made with this printer, and the process is detailed forward.



Fig 21 : Ultimaker S5 [38].

2.1.2. Selective laser sintering (SLS) and Multi Jet Fusion (MJF)

SLS and MJF are processes based on powder bed fusion, which is used thermal energy to fuse regions of a powder bed selectively. These two technologies are similar and share the following features: thermal sources to induce the fusion, methods to control powder fusion to a certain region of each layer, and methods to add smooth powder layers. Additionally, they do not require support structures. In particular, the SLS technology uses a low-power laser beam as a primary heat source that provides enough energy to exceed the polymer's melting temperature and an infrared lamp as a secondary source that enables the uniform heating of the newly deposited layer of powder.

The MJF is a more recent technology developed by HP that, instead of using point laser radiation to sinter the part, uses an infrared lamp that provides radiation to the entire area to be solidified simultaneously. This technology also utilises an inkjet head to deposit two agents: a fusing agent impregnated to the particles to facilitate the absorption of radiation and, therefore, the particle's fusion, and a detailing agent to inhibit the heat transfer toward the surrounding. The result of this is a process ten times shorter than SLS.

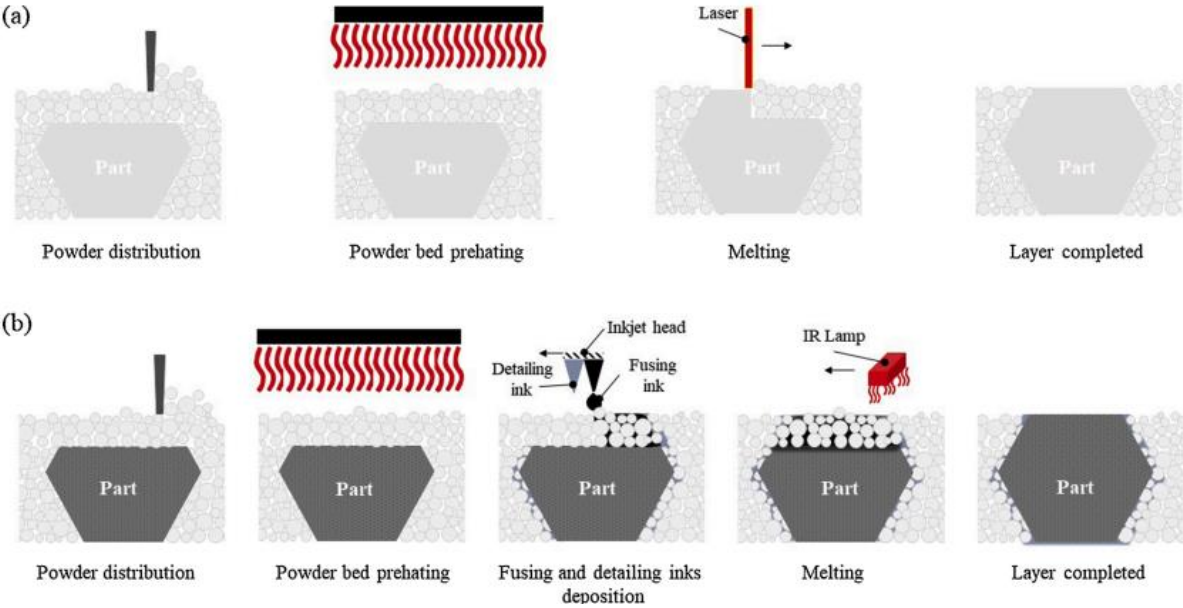


Fig 22 : Process description of a) SLS and b) MJF [39]

These technologies can produce the final parts for drone applications due to the high mechanical properties and performance of the components obtained. Some materials used are Nylon PA 12, which offers good resistance and waterproofness, and new high-performance materials like PA11 CF, carbon-fibre-reinforced material with advanced mechanical properties

characterized by an excellent strength-to-weight ratio, ideal for manufacturing both resistant and lightweight drones parts [37]. However, these technologies are limited in this case by the higher cost and printing requirements, so the use of FDM for drone building with composite materials is preferred in the first instance.

2.2. Additive manufacturing over conventional technologies

An important fact to discuss in this work is the reason why fabricating the UAV with AM technology. Usually, the conventional technologies used to produce the drone structure include CNC hot-wire and injection moulding. Still, they are process dependent, which limits building complex lightweight structures and presents disadvantages like a high cost for moulds, multi-step, labour-intensive processes, and long processing times [16]. AM offers the possibility of fixing those drawbacks being a design-oriented technology, so in this sense, AM can exploit mainly the following features:

- Creating lightweight parts meets an essential requirement for a flying device. So is possible to design a drone structure thinking about weight reduction without taking care of the complexity, and as a result, a light and robust drone is obtained.
- Flexibility and design-driven characteristics allow focus on innovation and adaptation since it is possible to create highly complex parts customized to supply a specific need and provide value-added to the pieces. Therefore the drone airframe can be personalized to fit the functional features and the exact components required for the particular application.

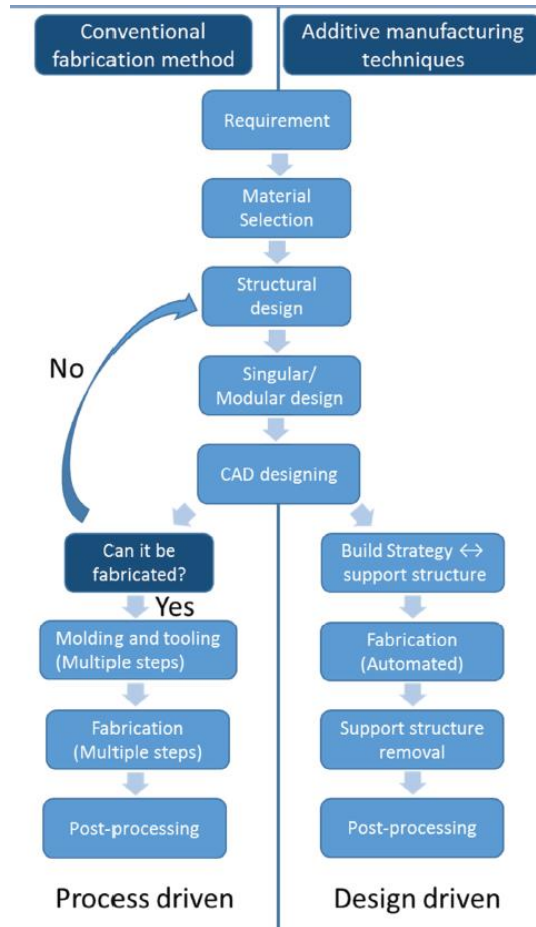


Fig 23 : Comparison in the design process between AM and conventional methods [16]

- It prints modular designs to have a convenient and easy assembly, reducing the assembly time and possibly repairing the UAV parts with a quick part swap. Therefore, it is possible to reduce the number of parts of the UAV by optimizing them with more elaborate shapes than moulded parts, which leads to optimising the total mass of the drone.
- AM enables to customize the structure according to the wanted budget. From the point of view of the cost, the economic benefit is presented in the low quantity production, so in this case, which is necessary to produce one unit is an advantage. Also is possible to relate the cost with the complexity of the parts. Using conventional technologies exists a limit of complexity in which the maximum cost is reached. Instead, using AM can get more complex components at a low cost, so there is a range of complexity for “free,” as shown in figure 24.

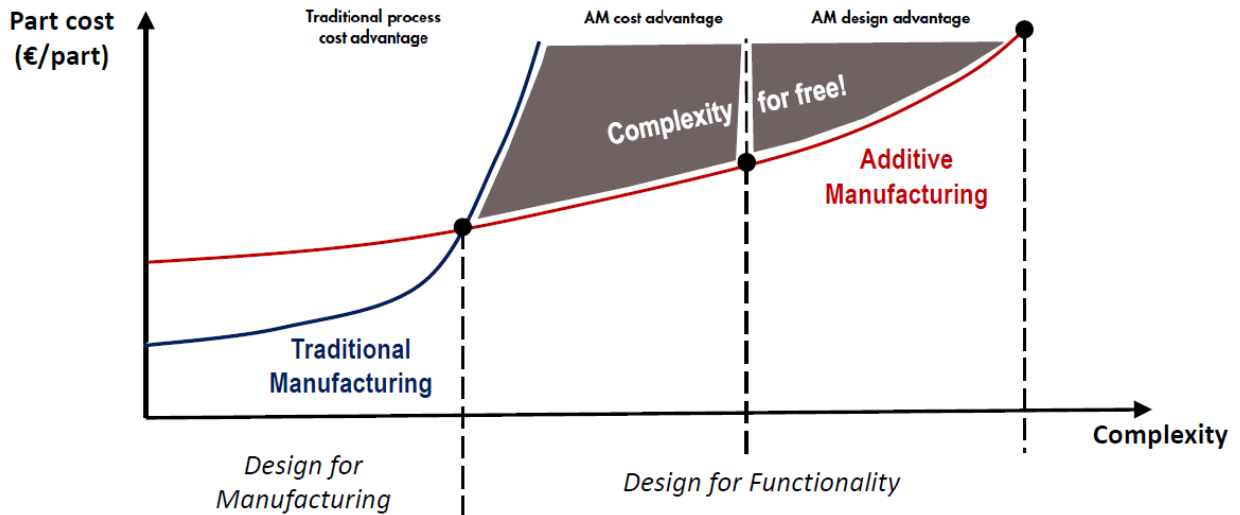


Fig 24 : Relation between cost and complexity in AM [36].

- The use of AM combined with Generative and topology optimization techniques offers the possibility to improve the weight and strength of the components through mass customization and will be discussed deeper.

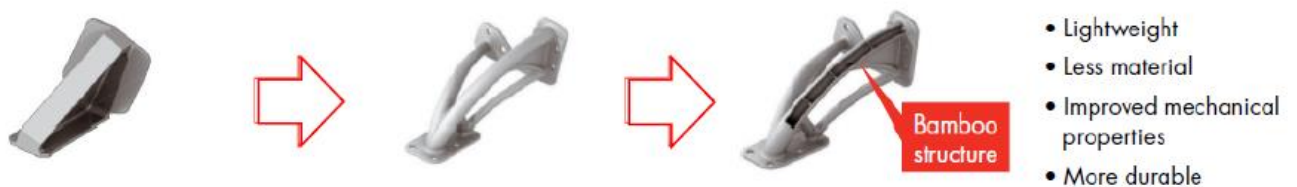


Fig 25 : Topology Optimized component example [36].

- Fast production since there are no necessary significant changes in the manufacturing setup, enabling virtual inventories of personalizable UAV parts that can be printed at any time instead of large inventories of stock parts.
- From the point of view of sustainability, the AM produces less waste material, and there is the opportunity of melting old or broken parts to print new ones [40].

Finally is important to mention the active market interest in AM technology which will allow this technology to develop more and more, improving some limitations that will be discussed forward.

In the specific case of this work, as mentioned before, it aims to optimize the UAV airframe through AM, taking into account the supports for electronic components, the landing structure, the case for protection, and accessories. This is done considering the following parameters:

- Strength and impact resistance
- Weight
- Price
- Ease of assembly
- Aesthetic

From the point of view of the structure, the UAV can be improved in two ways [16]:

- AM can obtain topology-optimized structures creating shapes varying the size and type of cellular structure in different parts, providing more flexibility in the design and assembly. Also, the performance of a structure with a conformal truss with variable strut sizes and orientation is superior to a uniform truss [16, 41, 42], so it is possible to have a complex structure of arm for the drone with variable thickness depending on the critical points in which are applied the loads.
- Using composite materials in the UAV industry is always more common since they offer high strength, low weight, high corrosion, fatigue resistance, and easy processing. For instance, carbon-fibre-reinforced plastics (CFRP) stand out for the niche application of UAVs [16]. The CFRP material consists of a load-bearing fibre and a load-transmitting resin material. It is known for its high specific strength-to-weight ratio, but with conventional technologies is complex to work and requires a mould. Using AM instead can be manufactured easier, and the most common technology is FDM since it is only necessary to have the proper nozzle to print with fibres like the Ultimaker S5 printer.

2.3. Limitations of AM in UAVs

The relationship between UAVs and additive manufacturing is in constant growth and development, as the motivation to use AM is to satisfy the user requirements that are constantly growing. However, some limitations are still being improved [16]:

- High-performance materials like CFRP are limited to printing only in straight and horizontal directions. Having a free orientation of the fibre is difficult, so it is very complex to have curved structures.
- Anisotropic behaviour is present in some processes like FDM, which induces a thermal gradient due to the quick cooling of extruded material from melting to printer chamber temperature, resulting in the creation of inner stresses responsible for the weak bond between two deposition lines. As a result of this thermal gradient, the material grows in a specific direction inducing different mechanical properties for each X, Y, and Z direction [43, 44].

A detailed characterization of the material is necessary to know the mechanical properties of the component in all directions. In this case, carbon fibres can be introduced in the z-direction to enhance mechanical strength. It is possible to compensate for this limitation by modifying some printing parameters like the build orientation, the raster angle, the layer thickness, and the feed rate or doing some post-processing heat treatment to increase the mechanical properties in all directions.

- Porosity is induced due to incomplete densification in the layer-by-layer process. Porosity is undesirable as the strength of the printed part will be less than the predicted strength of the material. Improvement in densification is required to reach the desired mechanical parameters of design.
- Platform size can be a limitation if the UAV is very large. In this case, it is not a problem since it is possible to exploit the modularity capacity of AM to optimize the structure.
- In current FDM technology, layer resolution and tolerances limit UAV design capability. Lower resolutions result in improved part quality and finish, but they also increase printing time [45].

Even with current limitations, it will take only a few technological improvements to transform this technology into a manufacturer of on-demand drones. Manufacturing an inexpensive UAV can be reduced to a one-person job [45], and the flexibility of this process makes 3D printing now and in the future an optimum solution for UAV testing operations and producing final drone versions.

2.4. Parameters influencing the cost

The economic factor is essential in the realization of this work, so the parameters that affect the cost from the point of view of the additive manufacturing process are analyzed to know the contribution to the total cost of the UAV and try to reduce it.

- Material quantity (piece and supports): The idea is to select a composite material for the structure at a low cost with high mechanical properties to reduce material consumption. The selection of material is detailed forward in the design process. In the printing supports, is used a thermoplastic material soluble in water.
- Printing time to produce a sample: Depend on the technology, the material, and the part orientation
- Machine: The machine selected in the first instance is the Ultimaker S5, which is available at CIM 4.0.
- Other operation costs (preliminary and post-processing activities)
- Labor

The most critical parameters to analyze are the part building's printing time and material consumption. It has been shown that the material consumption and the printing time are closely and significantly influenced by input parameters, especially the sample orientation on the printing bed [41]. Therefore, the manufacturing time and the material quantity can vary starting from the input parameters: part orientation, layer thickness, and deposition speed. With the software that sets the printing parameters (Ultimaker Cura), it is possible to predict the time and material consumption and obtain the price of the printed part. Then from the point of view of economics, the following considerations are taken into account:

- The manufacturing time is the most important indicator to consider to print simple parts where the geometry is not complex, like the support structures for electronic components mounted on the drone or some pieces for protection.
- To print complex parts, instead, like the arms of the drone, which have unique shapes and different thicknesses along the structure as a result of the topology optimization, it is better to consider the quantity of material as the most important economic indicator due to the additional need to build and support the model [46].

3. Structure optimization techniques

Optimizing the structure is an iterative process and is the essential activity of this work. The primary purpose of the optimization process is to get optimal design solutions by implementing accurate and fast design analysis techniques. In this sense, this process includes some steps that are performed to obtain a robust and lightweight airframe to improve the system's efficiency by increasing the flight time and reducing the cost of the drone. This iterative process consists mainly of the following points: a multi-material comparison and selection, the geometry obtention through topology optimization, and the finite element analysis to validate the results [47, 48].

The topology optimization (TO) [49] is the core of this step. It is defined as a mathematical procedure in which the distribution of the material in a specified domain is optimized by complying with given constraints and minimizing one or more designated functions. The TO is part of the material distribution method [50], which aims to find the optimum layout of a linear elastic structure. This method also addresses other features of the structural design problem by sizing and shape optimization. In a sizing problem, the parameters to optimize are the structure's thickness, area, or inertia. In a shape problem, the objective is to get the optimal shape of the domain defined as the design variable.

3.1. Topology optimization technique

The topology optimization process maximizes the structure's performance by fulfilling parameters such as load conditions, boundary conditions, constraints, and material properties. In particular, the TO works in two ways: to maximise the stiffness or minimise the mass, obtaining a connected and continuous structure. The optimization process is usually described as a system of differential equations that are transformed into a system of algebraic equations thanks to the finite element method.

Mathematically the problem is defined as follows [50]: supposing a body in a domain Ω^{mat} and this domain is part of a more extensive reference domain Ω in \mathbb{R}^2 or \mathbb{R}^3 and it is less than or equal at a minimum volume V . Then is possible to define the optimal design by referring to the reference domain, as the problem of finding the optimal stiffness $E_{ijkl}(x)$ which is a variable over the domain. As the goal is to maximize stiffness or reduce the deflection of the structure stressed by a load, this effect is equivalent to the maximum reduction of the work done by external forces. So it is possible to write the objective function with the principle of

virtual work of an elastic body at the equilibrium u and for an arbitrary virtual displacement v :

$$a(u, v) = \int_{\Omega} E_{ijkl}(x) \varepsilon_{ij}(u) \varepsilon_{kl}(v) d\Omega, \quad (5)$$

Where $\varepsilon_{ij}(u) = \frac{1}{2} \left(\frac{\partial u_i}{\partial x_j} + \frac{\partial u_j}{\partial x_i} \right)$: linearized strains

And $l(u) = \int_{\Omega} f u d\Omega + \int_{\Gamma_T} t u ds$: the load in linear form.

Therefore, the maximum stiffness (minimum compliance) problem takes the form:

$$\begin{aligned} & \min_{u \in U, E} l(u) \\ & \text{such that: } a_E(u, v) = l(v), \quad \forall v \in U \\ & E \leq E_{adm} \\ & \int_{\Omega^{mat}} 1 d\Omega \leq V \end{aligned} \quad (6)$$

Young's modulus of material E must be less than or equal to an admissible value E_{adm} , where $E_{adm} = 0$ represents the absence of material.

To solve the problem of equation (6) by computational tools, the typical solution is to discretize the problem by the finite element method (FEM). In this case, there are two fields involved, the stiffness E and the displacement u . Assuming the same finite element mesh for both fields and discretising E as constant in each element, it is possible to write the discrete form of equation (6) as follows:

$$\begin{aligned} & \min_{u, E_e} f^T u \\ & \text{such that: } K(E_e) u = f, \\ & E_e \in E_{adm} \end{aligned} \quad (7)$$

Where u is the displacement vector and f is the load vector. Also, the stiffness matrix K depends on the stiffness E_e in element e , enumerated as $e = 1, \dots, N$, and K can be written in the form:

$$K = \sum_{e=1}^N K_e(E_e),$$

Where K_e : it is the global element stiffness matrix.

To validate Hooke's law [31], the elastic deformation energy U takes a quadratic form in the deformations:

$$U = \frac{1}{2} \int_{\Omega} E_{ijkl}(x) \varepsilon_{kl}(u) \varepsilon_{kl}(v) d\Omega \quad (8)$$

Furthermore, the elastic potential energy W linked to the action of external forces is equivalent to the opposite of the work performed by the forces mentioned before and can be expressed as:

$$W = - \int_{\Omega} f^T u d\Omega \quad (9)$$

Therefore is possible to calculate the variation of the elastic energy U :

$$\begin{aligned} \delta U &= U(\varepsilon + \delta\varepsilon) - U(\varepsilon) = \\ &= \frac{1}{2} \int_{\Omega} (\varepsilon_{kl}(u) + \delta\varepsilon_{kl}(u))^T E_{ijkl}(x) \varepsilon_{kl}(v) d\Omega - \frac{1}{2} \int_{\Omega} \varepsilon_{kl}(u) E_{ijkl}(x) \varepsilon_{kl}(v) d\Omega \end{aligned} \quad (10)$$

And also the variation of the potential energy W :

$$\delta W = W(u + \delta u) - W(u) = - \int_{\Omega} f^T (u + \delta u) d\Omega + \int_{\Omega} f^T u d\Omega \quad (11)$$

In the case in which the internal stresses and deformations are not independent of each other and are linearly elastic dependent, the principle of virtual works can be written as:

$$\int_{\Omega} \varepsilon_{kl}(u) E_{ijkl}(x) \delta\varepsilon_{kl}(v) d\Omega - \int_{\Omega} f^T \delta u d\Omega = 0 \quad (12)$$

Moreover, replacing the energy variations previously calculated in equation (13) is obtained:

$$\delta(U + W) = 0 \quad (13)$$

Where $\Pi = U + W$ represents the internal elastic energy stored by the body. The expression, therefore, corresponds to the principle according to which, in stationary conditions, the elastic energy of a body does not vary, which can be expressed with the equation (14)

$$\frac{\delta\Pi}{\delta u} = 0 \quad (14)$$

The topology optimization in drones and aerospace applications fits naturally since one of the targets in these applications is weight reduction. The process starts with the initial design model in which the constraints, external forces, and material properties are put, and then the software, using the finite element method, analyzes the structure and removes redundant material to produce an optimized design. From the point of view of the manufacturing process, topology optimization creates free-form designs that are difficult to make using traditional manufacturing methods. This point is where additive manufacturing takes on greater importance because the design output by topology optimization can be manufactured directly by a 3D printer.

In this case, the software used for topology optimization is Altair Inspire. The process, in general, can be described thoroughly step by step as follows:

- ✓ **Design of the initial geometry** in which is created the initial frame or space to be optimized
- ✓ **Define the non-design space** that includes the keep-out geometrical volumes or fixed locations like the support parts for the drone's motors.
- ✓ **Define the loading conditions, constraints, and material properties** applied to the structure.
- ✓ **Generate the mesh** through the finite element method: It considers the minimum geometric design envelope and breaks down the design space into smaller areas such as applied load points, mounting locations, and constrained areas. Then it creates a mesh that can be refined to get a better result. Finite element analysis then evaluates the mesh's stress distribution and strain energy to find the optimum load or stress that each element can handle.
- ✓ **Choose the optimization objective** that can be to maximize the stiffness or minimize the mass of the structure.
- ✓ **Run the topology optimization:** The process that is performed by the software
- ✓ **Evaluation and analysis of the results:** The software offers different options to analyze the results and identify the critical areas by evaluating the deformation, von misses stress or safety factor.
- ✓ Finally, the structure can be **exported**, and the optimized model can be modified, for example, to obtain a proper assembly or to suit manufacturing.

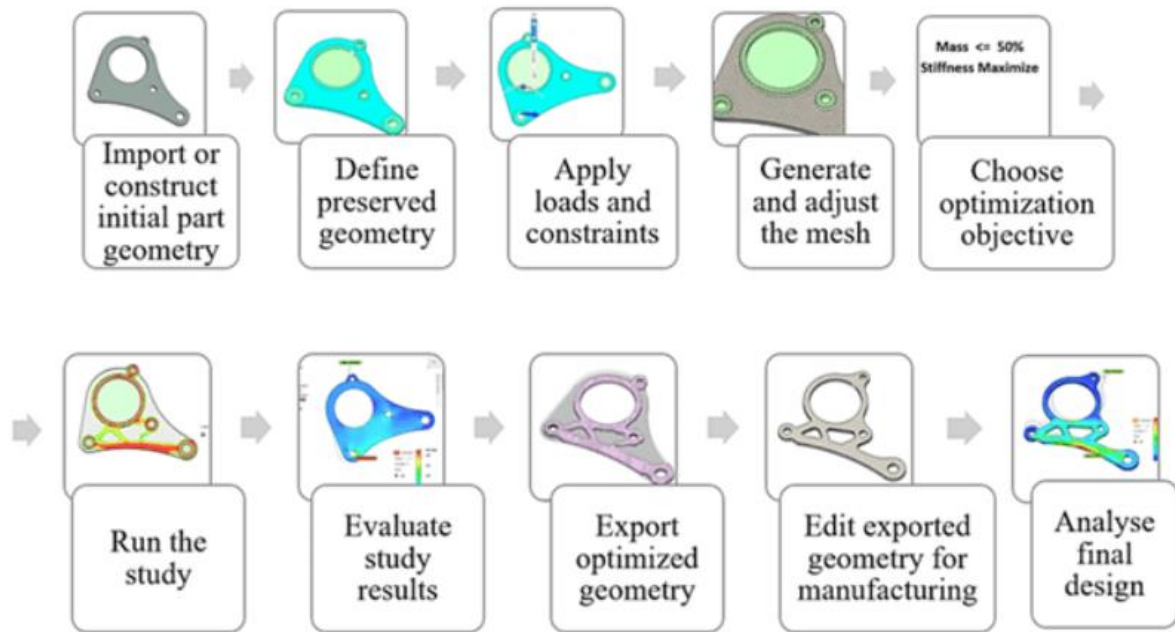


Fig 26 : Topology optimization Steps [51]

3.2. Finite elements method

The described optimization problem is numerically solved through the finite element method, a well-known helpful method to solve differential equations and perform engineering analysis in several fields like structural, fluids, and electromagnetic. As this is a space-dependent problem, it can be expressed by partial differential equations (PDEs), which are complex to solve analytically. Therefore, these PDEs are usually approximated with numerical model equations by discretizing and solving them through the finite element method.

FEM transforms the space domain into the union of many subdomains of elementary shapes, such as triangles and rectangles or tetrahedra and prisms, leaving the equations unchanged. The approximating functions of the solution are identified through the values that the dependent variable assumes in the domain's nodes (element vertices). The problem assumes a finite number of unknowns. The approximating functions, or functions of form, are chosen among those particular functions with a known trend, usually polynomial but also trigonometric.

The FEM method [31, 52] aims to write the stiffness relationship of an element, allowing the expression of the field of displacements, deformations, and stresses inside the element. The procedure is described as follows:

- The first phase includes describing the element, numbering the nodes, and identifying the displacement field. For each point on the element, the extent of its displacements $\{\delta\}$ is described. For each node, it will be possible to write its displacement vector $\{f_i\}$ and a vector of the applied forces $\{F_i\}$. These last, combined sequentially, will form the vector of the nodal displacements and the nodal forces relating to the element as follows:

$$\{f\} = \{\{f_1\}, \{f_2\}, \{f_3\}, \dots, \{f_n\}\}^T$$

$$\{F\} = \{\{F_1\}, \{F_2\}, \{F_3\}, \dots, \{F_n\}\}^T$$

- It is now necessary to choose a function that approximates the field of displacements, which must respect two requirements of completeness and two of compatibility so that a monotonous convergence of the result is ensured:
 1. The function chosen must ensure the ability to describe all the rigid motions of the element without the onset of a residual tension state
 2. The function must ensure the possibility of expressing at least all the states of constant deformation on the whole element. However, the continuity of the deformation field is not required
 3. The function must guarantee the continuity of the displacement range on the structure; that is, no tears or overlaps are allowed
 4. The function must be free of singular points in its domain, so it must ensure the continuity of the displacement field within the element, Indicating with $\{\delta_i\}$ the i -th displacement. For each point of the element, we can write:

$$\delta_1(x_k) = \alpha_1\phi_{11}(x_k) + \alpha_2\phi_{12}(x_k) + \alpha_n\phi_{1n}(x_k)$$

$$\delta_2(x_k) = \alpha_1\phi_{21}(x_k) + \alpha_2\phi_{22}(x_k) + \alpha_n\phi_{2n}(x_k)$$

⋮

$$\delta_i(x_k) = \alpha_1\phi_{i1}(x_k) + \alpha_2\phi_{i2}(x_k) + \alpha_n\phi_{in}(x_k)$$

Where x_k are the coordinates of the point considered in the local reference system, ϕ_{ij} are the chosen functions, and α_j are the coefficients. The coefficients α_j should be at least equal to the number of degrees of freedom. In compact form, it can be written as:

$$\{\delta(x_k)\} = \begin{Bmatrix} \delta_1(x_k) \\ \delta_2(x_k) \\ \dots \end{Bmatrix} = \begin{bmatrix} \phi_{11} & \phi_{12} & \dots \\ \phi_{21} & \phi_{22} & \dots \\ \dots & \dots & \dots \end{bmatrix} \begin{Bmatrix} \alpha_1 \\ \alpha_2 \\ \dots \end{Bmatrix} \Rightarrow \{\delta(x_k)\} = [\delta(x_k)]\{\alpha\}$$

- Then, it is necessary to Join the displacement range of the element to the nodal displacements. The chosen function for the displacement range must be such as to assume the values of the nodal displacements:

$$\{f\} = \begin{bmatrix} \delta(x_k)^1 \\ \delta(x_k)^2 \\ \dots \end{bmatrix} = \begin{bmatrix} [\phi(x_k)]_1 \\ [\phi(x_k)]_2 \\ \dots \end{bmatrix} \begin{bmatrix} \alpha_1 \\ \alpha_2 \\ \dots \end{bmatrix} = [A]\{\alpha\} = \{f\}$$

The matrix A collects the values of the functions ϕ_{ij} calculated in the nodes. It is square and invertible. Therefore the coefficients α_j can be obtained:

$$\{\alpha\} = [A]^{-1}\{f\}$$

Then, we can write the displacement field as a function of the nodal displacements:

$$\{\delta(x_k)\} = [\phi(x_k)][A]^{-1}\{f\} = [M(x_k)]\{f\}$$

Where M_{xk} is the shape functions matrix.

In this case, the functions are of the Lagrangian type because a value is imposed at specific points: the nodes. If the value of the derivatives is also imposed, then the functions are said to be Hermitian.

- The deformation field of the element and the displacement field are joined. The field of deformations $\{\epsilon(x_k)\}$ is studied. Two different behaviors can be observed:

The element deforms inside the plane: $\{\epsilon(x_k)\} \leftrightarrow \frac{d\{\delta(x_k)\}}{d(x_k)}$

The element deforms outside the plane: $\{\epsilon(x_k)\} \leftrightarrow \frac{d^2\{\delta(x_k)\}}{d(x_k)^2}$

Moreover, in general, it is possible to write:

$$\begin{aligned} \{\epsilon(x_k)\} &= \text{diff}\{\delta(x_k)\} = \text{diff}\{[M(x_k)]\{f\}\} = \text{diff}\{[\phi(x_k)][A]^{-1}\{f\}\} = [C][A]^{-1}\{f\} \\ &= [B]\{f\} \end{aligned}$$

- The next step is to join the element's nodal loads and nodal displacements. The field of stresses $\{\sigma(x_k)\}$ is linked to the field of deformations through the elastic characteristics of the material contained in the matrix $[D]$ as follows:

$$\{\sigma(x_k)\} = [D]\{\epsilon(x_k)\}$$

Where $[D]$ is called the constitutive matrix of the material, and it turns out to be square.

If there are residual deformations $\{\epsilon_0\}$ and residual stresses σ_0 , it becomes:

$$\{\sigma(x_k)\} = [D]\{\{\epsilon(x_k)\} - \{\epsilon_0\}\} + \{\sigma_0\}$$

- The next step is to join the stress field and the field of nodal displacements of the element. As the hypotheses of the finite element method are defined, the single elements exchange forces only through the common nodes. For the assumptions made, a single movement must be associated with a node. For the continuity assumptions, moreover, the force exchanged by two elements in a node must be equal and opposite. For these reasons, it is easy to calculate the value of the forces exchanged through the principle of virtual works.

Indicating the vector of the virtual nodal displacements $\{f^*\}$ and the field of equivalent virtual deformations $\{\epsilon\}$, the works of the internal and external forces can be calculated as follows:

$$L_{est} = \{f^*\}^T \{F\}$$

$$dL_{int} = \{\epsilon^*\}^T \{\sigma\} dV$$

Considering this: $\{\sigma\} = [D][B]\{f\}$

It is possible to express the following integral:

$$L_{int} = \int_V \{\epsilon^*\}^T \{\sigma\} dV = \int_V \{f^*\}^T [B][D][B]\{f\} dV = \{f^*\}^T \int_V [B][D][B] dV \{f\}$$

And by equality, the works:

$$L_{est} = L_{int} \Rightarrow \{f^*\}^T \{f\} = \{f^*\}^T \int_V [B][D][B] dV \{f\}$$

Considering the stiffness relation $F=K f$ and simplifying the vectors of the nodal displacements, the following relation is obtained:

$$[K] = \int_V [B][D][B] dV$$

This approximation is better when the choice of functions is accurate. In case there are external surfaces forces $\{p\}$ or external volume forces $\{v\}$:

$$\begin{aligned} L_{est} &= \{f^*\}^T \{F\} + \int_{\Omega} \{f^*\}^T [N]^T \{p\} dS + \int_V \{f^*\}^T [N]^T \{v\} dV \\ &= \{f^*\}^T \{F\} + \int_{\Omega} \{\delta^*\} \{p\} dS + \int_V \{\delta^*\} \{v\} dV \\ &= \{f^*\}^T (\{F\} + \{F_p\} + \{F_v\}) \end{aligned}$$

Where F_p and F_v are the vectors of the equivalent nodal loads relative to the surface and volume forces, which can be calculated as:

$$\begin{aligned}\{F_p\} &= \int_{\Omega} [N]^T \{p\} dS \\ \{F_v\} &= \int_V [N]^T \{v\} dV\end{aligned}$$

If there is a residual stress field $\{\sigma_0\}$ or an independent deformation field $\{\epsilon_0\}$:

$$\{\sigma\} = \{\sigma_0\} + [D](\{\epsilon\} - \{\epsilon_0\})$$

Then, it is possible to recalculate the work of the internal forces as follows:

$$L_{int} = \int_V \{\epsilon^*\}^T \{\sigma\} dV = \int_V \{\epsilon^*\}^T \{\sigma_0\} dV + \int_V \{\epsilon^*\}^T [D] \{\epsilon\} dV - \int_V \{\epsilon^*\}^T [D] \{\epsilon_0\} dV$$

Moreover, substituting the following relation: $\{\epsilon(x_k)\} = [B(x_k)]\{f^*\}$

It is possible to write the work as follows:

$$L_{int} = \{f^*\}^T \int_V [B]^T \{\sigma_0\} dV + \{f^*\}^T \int_V [B]^T [D] [B] dV \{f\} - \{f^*\}^T \int_V [B]^T [D] \{\epsilon_0\} dV$$

In compact form, it will be:

$$L_{int} = \{f^*\}^T \{[K]\{f\} - \{F_\epsilon\} - \{F_\sigma\}\}$$

Where $\{F_\epsilon\}$ is the vector of nodal loads equivalent to the strain field $\{\epsilon_0\}$:

$$\{F_\epsilon\} = \int_V [B]^T [D] \{\epsilon_0\} dV$$

Moreover, $\{F_\sigma\}$ is the vector of nodal loads equivalent to the stress field $\{\epsilon_0\}$:

$$\{F_\sigma\} = - \int_V [B]^T \{\sigma_0\} dV$$

Finally, the stiffness in the general case can be expressed as:

$$\{\{F\} + \{F_p\} + \{F_v\} + \{F_\epsilon\} + \{F_\sigma\}\} = [K]\{f\}$$

- The last step defines the relationship between the nodal stress vector $\{\sigma\}$ with the nodal displacement vector $\{f\}$ as follows:

$$\{\sigma(x_k)\} = [D][B]\{f\}$$

This relation can be expressed in a compact form:

$$\{\sigma(x_k)\} = [H]\{f\}$$

4. Airframe design and optimization

This phase is the most critical phase of the project. The design and optimization of the airframe are performed in several stages, as shown in figure 27. First, a multi-material comparison is made based on different parameters to obtain the most suitable solution for the material airframe. Then the design process follows with evaluating the dimensional and assembly constraints, the service conditions, impact, and dynamic analyses where the different flight manoeuvres and the different loading conditions acting on the drone airframe are evaluated. Finally, is performed the topology optimization and finite element analysis which is the iterative process performed through Altair inspire to get the optimal structure.

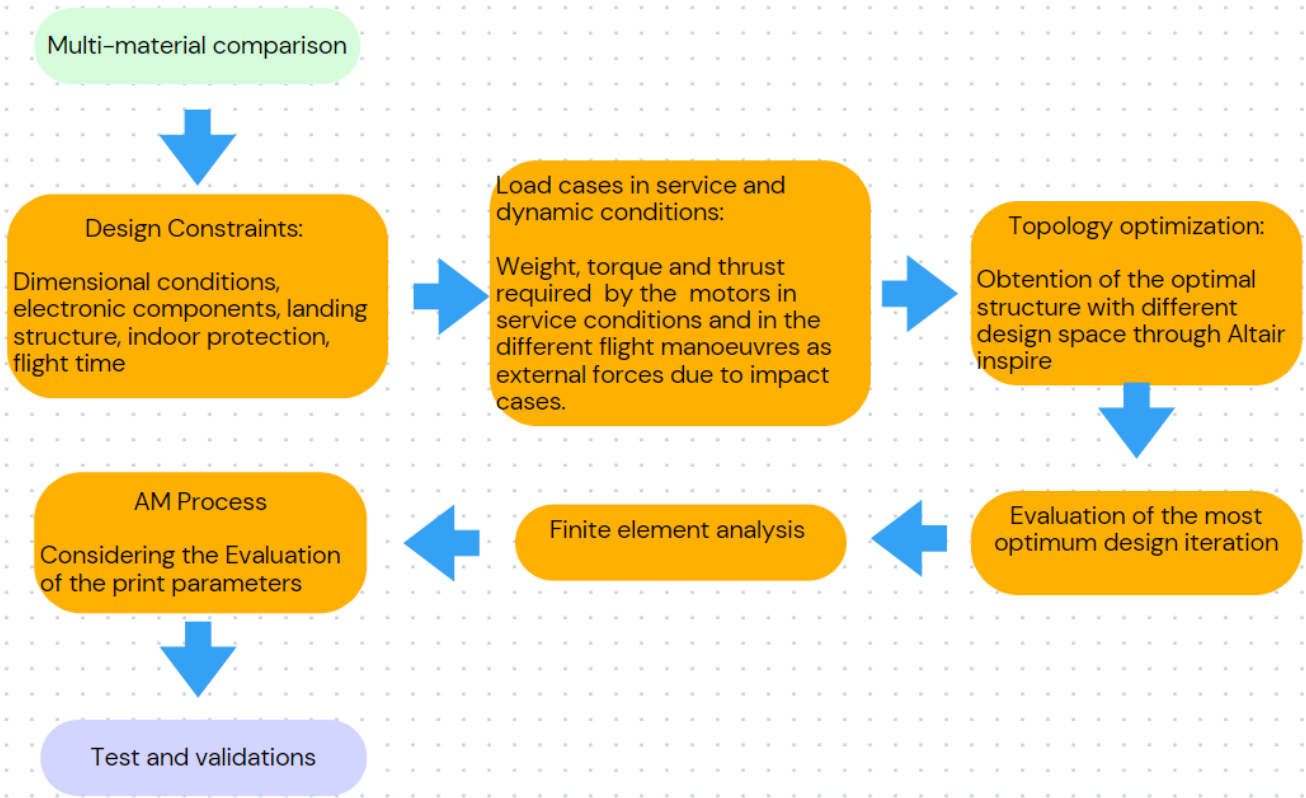


Fig 27 : Airframe Design path

4.1. Multi-material Material Comparison and selection

The multi-material analysis focuses only on the AM for polymers due to the ability to produce high-strength and lighter-weight structures than AM for metals. It is performed considering the drone airframe's final high quality and cost. Initially, the scope is to find a material processed by FDM, which is cheapest and easiest to work, with properties similar to the high-performance material commonly used for aerospace applications, particularly for drone building, such as PA11 CF processed with SLS or PA12 processed with multijet fusion.

In this sense, the analysis was performed considering the following parameters, which have different weights or importance in the selection:

Cost is one of the most important in this case since it is one of the parameters to optimize and plays a role in the decision-making process. The material cost is crucial as obtaining a printed drone is cheaper than a commercial one produced with traditional methods.

Mechanical strength measured in MPa is the principal mechanical property to know the material's resistance and to have a first safety factor according to the maximum loads applied over the structure. In this case, it is essential to have high strength as the system is subjected to dynamic behaviour.

Strength-to-weight ratio is a parameter that relates the strength of the material to its density. This parameter is measured in $\frac{MPa}{g/cm^3}$. A high strength-to-weight ratio represents a lightweight material with high mechanical properties, one of the most critical requirements.

Impact resistance is another important parameter as the drone is exposed to falls and impacts due to failures in flight, so a structure with good stiffness is required to prevent parts from breaking. This parameter is measured in $\frac{kJ}{m^2}$, and is obtained by impact tests like the Charpy test.

The temperature of the application can be defined by the HDT or Heat Deflection Temperature, which indicates the temperature at which a specimen is subjected to bending loads and deforms in a plastic way. This parameter is not crucial since the UAV is not a high-temperature application. However, the correct performance of the material at 60 degrees is verified with the material supplier, which is approximately the maximum temperature reached by the electronic components.

Different materials, considering their availability on the market, are compared and listed in table 2. The comparison focuses mainly on the polymers' FDM and powder bed fusion

technologies. The analysis is performed by searching the optimal mechanical properties-price relationship.

FDM						
Material	Tensile Strength MPa	Density g/cm ³	Impact strength Charpy (un) kJ/m ²	Strength-to-weight	Price Euro/kg	Supplier
PLA BASF [53]	34,7	1,24	13,2	27,98387097	28,00 €	BASF
PLA pro [53]	48	1,25	20,4	38,4	33,00 €	BASF
Ultrafuse ABS [53]	36,3	1,04	36,4	34,90384615	28,00 €	BASF
Ultrafuse PA (Nylon) [53]	61,4	1,11	23	55,31531532	55,00 €	BASF
PA12 [54]	41,1	1,03	27,4	39,90291262	80,00 €	fabbrix
Nylon carbon [54]	66,3	1	41,1	66,3	90,00 €	fabbrix
PET CF 15 [53]	63,2	1,36	27,8	46,47058824	73,00 €	BASF
BASF Ultrafuse PAHT CF15 [53]	103,2	1,23	20,6	83,90243902	87,00 €	BASF
PLA/PHA [55]	61,5	1,24	30,8	49,59677419	40,00 €	Colorfabb
XT-CF20 [55]	76	1,35	60	56,2962963	55,00 €	Colorfabb
PA6-CF (20%) [56]	105	1,2	13,3 (ISO 179 Notched)	87,5	78,50 €	Polymaker
SLS						
PA11 CF SLS [57]	81	1	113,65	81	150,00 €	Sinterit
PA11 CF SLS [53]	71	1,07	63	66,35514019	130,00 €	BASF

Table 2 : Multi-material comparison

From the point of view of performance and mechanical properties, the powder Nylon PA11 reinforced with carbon manufactured with SLS technology is the best option. However, the cost of this technology and the material, one of the most critical parameters, is very high compared with FDM. In addition, at the company, there is an Ultimaker S5 to take advantage of the FDM process principally. Therefore to have a lower cost and high-quality drone, another analysis is performed filtering by the high-performance FDM materials, and those listed in table 3 are obtained.

FDM						
Material	Tensile Strength MPa	Density g/cm ³	Impact strength kJ/m ²	Strength-to-weight	Price Euro/kg (without taxes)	Supplier
XT-CF20 [55]	76	1,35	60 (ISO 180 Unnotched)	56,2962963	55,00 €	ColorFabb
PA6-CF (20%) [56]	105	1,2	13,3 (ISO 179 Notched)	87,5	78,50 €	Polymaker
Ultrafuse TPU 64D [53]	32	1,15	115 (ISO 179 Notched)	27,82608696	46,60 €	BASF

Table 3 : FDM Material properties

The optimum selected materials under the parameters mentioned are the XT-CF20, a high-quality Amphora copolyester-based filament loaded with 20% carbon fibres, supplied by ColorFabb, and the PA6-CF, a Nylon 6 reinforced with 20% of carbon fibres, provided by Polymaker. These materials are perfect low-cost options for parts needing high strength and stiffness with a lightweight. Another good point is that those are available in the Ultimaker marketplace, so the settings to do the printing process are performed easily in the “Cura” software since the materials are in its library.

4.2. Loading conditions

As described in section 2, the selected propulsion unit mainly comprises the AT2312 motor and the propeller 9050. To perform the analysis of the loading conditions is necessary to test and characterize the motor/propeller set. Usually, this process is done using a test stand in which the motor and propeller are mounted, and the data is read while the electronic speed controller throttles the power at different points. This type of test stand, shown in figure 28, is commonly used to get information about thrust, torque, voltage, current, power, and efficiency to optimize the propulsion system and, therefore, the UAV's performance. In this case, the motor supplier gives the test report where it is possible to get the thrust and torque motor at different speeds that will be useful to determine the loads over the structure. The recollected data of the motor/propeller configuration is shown in Table 4.

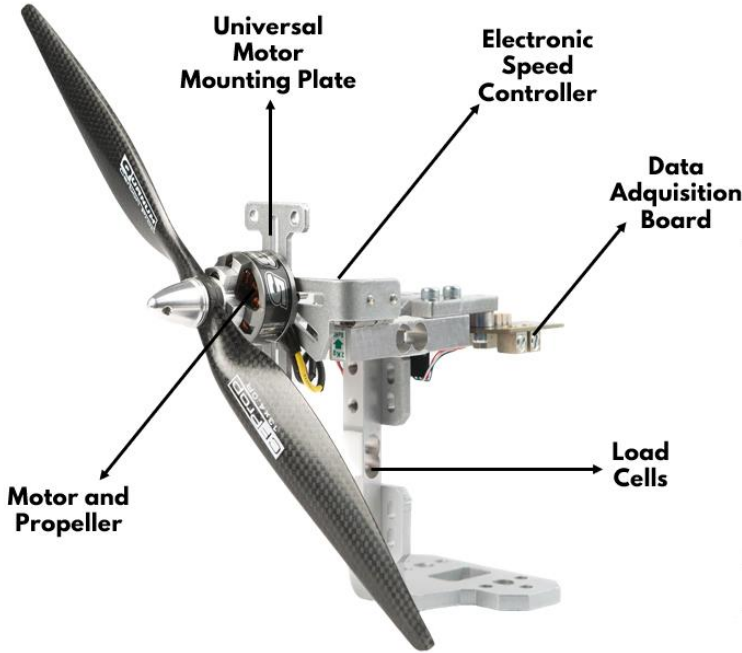


Fig 28 : Series 1585 Test Stand [27]

Throttle (%)	Current (A)	RPM	Torque (N.m)	Thrust (N)
40	3,9	5239	0,053	3,29
45	4,58	5554	0,061	3,71
50	5,32	5867	0,068	4,18
55	6,11	6211	0,075	4,74
60	6,92	6508	0,082	5,29
65	8,11	6885	0,092	5,98
70	9,55	7258	0,103	6,77
75	10,88	7595	0,113	7,42
80	12,58	7987	0,126	8,17
90	16,45	8665	0,151	9,76
100	18,03	8960	0,16	10,29

Table 4 : Test report by the motor supplier [26]

According to the data in table 4, it is possible to relate the thrust and the torque of the motor/propeller configuration with the motor speed (RPM). The relations can be approximated with a polynomial function, as shown in figure 29.

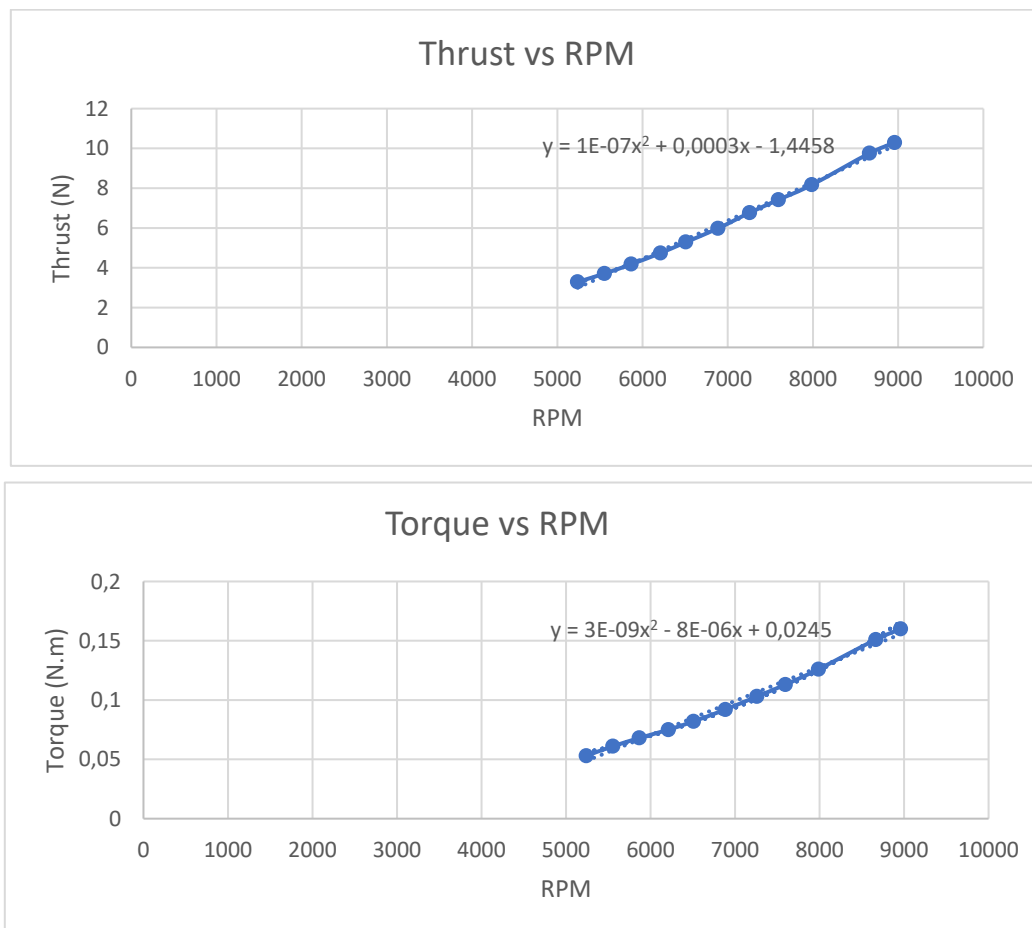


Fig 29 : Relation between thrust-rpm and torque-rpm

4.2.1. Nominal condition

The nominal condition of service is analyzed mainly based on the weight of the complete system, which is initially 2,8kg. As was performed above in the propulsion unit section 2.2.1, assuming a thrust-to-weight ratio TWR of 2,5, the thrust required by each motor is 8,6N. The thrust is also helpful to find the speed in rpm at this point. Then is possible to calculate the torque by the polynomial function that relates RPM with the torque described before.

$$M(T = 8,6N) = 0,133 \text{ N.m}$$

The maximum theoretical torque generated by this motor is also obtained, assuming an instant in which the ESC supplies the total current of 40A. Calculating this point is considered the torque constant, defined as the inverse of the speed constant. The speed constant is 1150kv for the selected motor, so the torque constant is expressed as follows:

$$K_t = \frac{1}{K_v} \frac{60}{2\pi} = 0,0083 \frac{Nm}{A}$$

Moreover, the maximum torque is obtained:

$$M_{max} = K_T i_{max} = 0,332 Nm$$

4.2.2. Impact conditions

The drone structure must also be designed to withstand other external loads, such as those represented by fall down during flight, which can occur accidentally in the event of a broken part or collisions with objects that could affect the drone's stability. In this sense, it is considered the worst case in which the system falls from a height of 20m which is the typical maximum height for this drone in indoor applications. For this purpose is used the impulse-momentum theorem which relates the impulse with the change in the momentum.

$$I = Ft = mv \tag{15}$$

Where : $I = \text{impulse}; F = \text{impact force}; t = \text{impact time duration};$

$m = \text{mass of the system}; v = \text{velocity at the instant of impact}$

To calculate the velocity at the instant of impact is possible to relate the potential with the kinetic energy as follows:

$$E = mgh = \frac{1}{2}mv^2 \tag{16}$$

$$v = \sqrt{2gh} = 19,8 \frac{m}{s}$$

Therefore, knowing the mass of the system, which is equal to 2,8kg and considering an impact time duration of 0,25 s, it is possible to calculate the impact force by the equation (15)

$$F = \frac{mv}{t} = 220N$$

This obtained force is considered to be applied in multiple impact cases in different positions and different directions.

4.2.3. Dynamic model

To perform a complete proper topology optimization to obtain an optimal design is necessary to analyze the dynamics and the different drone manoeuvres and evaluate the most critical loading conditions over the structure due to those operations. First, it is necessary to define the systems and some assumptions. In this case, the drone is an octa-quad type in which each pair of motors in each arm rotate in opposite directions and are enumerated, as shown in figure 30. Motors 1, 3, 5, and 7, represented in blue, rotate in the counter-clockwise direction, and motors 2, 4, 6, and 8, represented in green, turn in the clockwise direction.

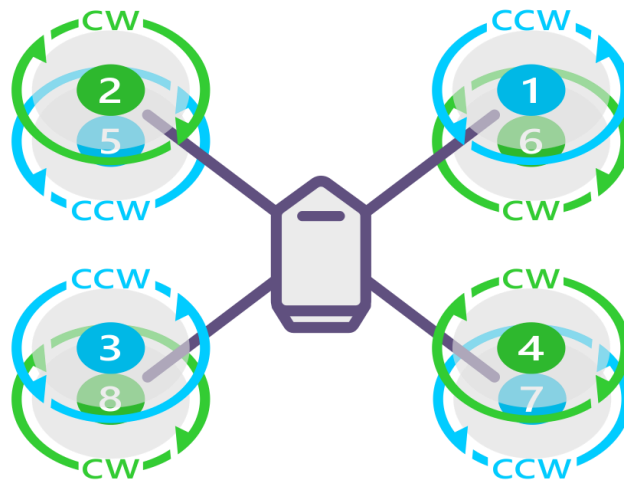


Fig 30 : Rotating direction and motor enumeration of the system [24]

The loading analysis is done based on the specifications of the initial structure to optimize, which is the ZD550 airframe. The different manoeuvres performed by the drone are roll, pitch, yaw, and vertical movement, as shown in figure 31. These different movements are achieved by varying the speed of specific motors on the quadcopter.

- Roll: Change the relative speed of the right and left rotors
- Pitch: Change the relative speed of the front and back rotors
- Yaw: Change the speed of the clockwise rotating pair and counterclockwise rotating pair
- Vertical motion: Increase the speed of all motors to go up or decrease the speed of all motors to go down.

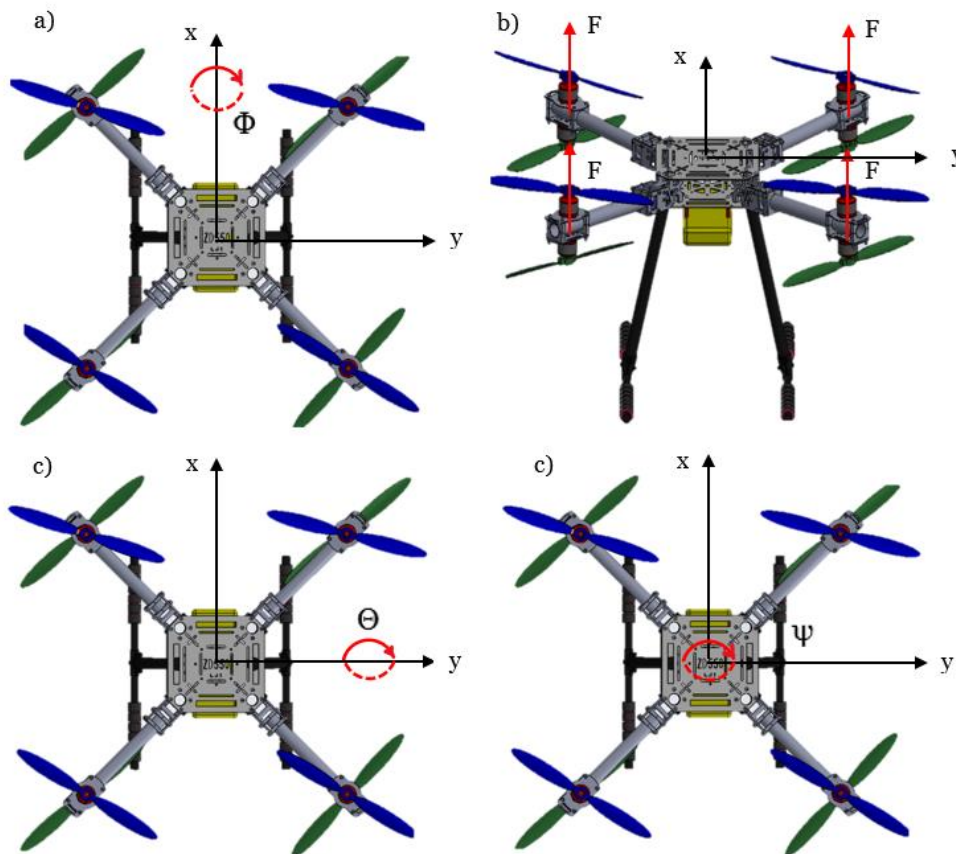


Fig 31 : Drone manoeuvres. a) roll motion b) vertical motion c) pitch motion d) yaw motion

Two coordinate frames are usually considered to study the drone dynamics and describe the different motions. A body-fixed frame and an inertial frame, as shown in figure 32. The body frame has the origin at the centre of mass of the drone and is the most crucial reference frame since the movements of the UAV are expressed on it. These two reference frames are related, so the parameters measured in the inertial frame can be transformed in the body frame and vice-versa.

In order to perform the dynamic analysis, the system is treated as a quadcopter for simplicity and considering that the motors facing down are symmetric concerning the motors facing up rotating at the same speed and opposite direction to cancel out the overall angular momentum on the structure. Also, the following assumptions are taken into consideration [58]:

- ✓ The structure of the quadcopter is rigid and symmetrical, with the four arms coinciding with the body's x- and y-axes.
- ✓ The propellers are rigid.
- ✓ The rotational motion of the quadcopter is independent of its translational motion.
- ✓ Drag and thrust forces are proportional to the square of the propeller's speed.

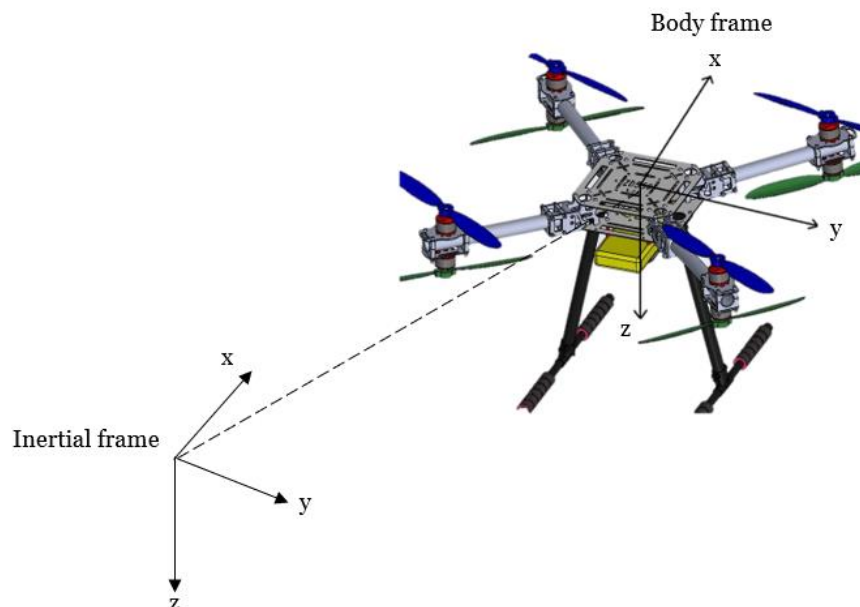


Fig 32 : Reference frames of the system

- **Vertical motion Dynamics**

This section analyzes the translational motion of the drone. The drone moves vertically due to the thrust generated by the motors. The total thrust is the sum of thrust generated by all the motors:

$$T_{total} = T_1 + T_2 + T_3 + T_4 + T_5 + T_6 + T_7 + T_8$$

- ✓ Hover: The necessary thrust to hover is equal to the weight of the drone

$$m_{drone}a = \sum F \quad \text{At hover } a_z = a_y = a_x = 0$$

So the sum of forces in z vertical direction is: $T_{hover} = m_{drone}g$

$$T_{hover} = 27,5N \quad \text{and the thrust of each motor: } T_{motor} = \frac{T_{hover}}{8} = 3,44N$$

- ✓ Vertical to take-off: To calculate the thrust to make the motion from stationary to climb is necessary to consider the drag force, which is the opposing force to the motion of the drone produced by the viscosity of air. This drag force is overcome by the thrust force produced by the propeller and is defined as follows:

$$Drag = D = 0,5\rho v^2 C_d A$$

Where,

D: drag force

ρ : air density at sea level = $1,225 \text{ kg/m}^3$

v : speed of climb to take-off

C_d : drag coefficient of the body

A: total surface area

In this case, the desired speed of climb is $2 \frac{m}{s}$ and the drag coefficient is equal to 2 based on the test results of a flat plate [59].

As the climb is vertical, only there is acceleration in the z-direction, so: $a_z > 0$; $a_x = a_y = 0$

Then:

$$m_{drone}a_z = T_{takeoff} - m_{drone}g - D$$

If we supposed the takeoff at constant speed: $a_z = 0$, and then the thrust required to takeoff is the sum of the weight and the drag as follows:

$$T_{takeoff} = m_{drone}g + D = T_1 + T_2 + \dots + T_8; \text{ where } T_1 = T_2, \dots, T_8$$

- **Rotational dynamics**

In order to perform the analysis of the rotational dynamics is considered the classical dynamics of a quadcopter under the considerations mentioned initially where the two motors on the same arm generate equal thrust in each condition.

The rotational motion of the drone is obtained through Euler's equation presented in the equation

$$I\alpha + v \times Iv = M$$

where,

I - inertia matrix

α – angular acceleration in body frame

v - angular velocity vector in body frame

M - torque/moment vector acting on the quadcopter in the body frame

The angular velocity vector is defined as:

$$v = [\dot{\phi} \quad \dot{\theta} \quad \dot{\psi}]$$

Where ϕ, θ, ψ represent the rotation about the x,y, and z-axis, respectively. The angular acceleration can be defined as \dot{v} .

The inertia matrix is defined as a diagonal matrix due to the symmetry of the drone structure as follows:

$$I = \begin{bmatrix} I_{xx} & 0 & 0 \\ 0 & I_{yy} & 0 \\ 0 & 0 & I_{zz} \end{bmatrix}$$

The moment vector M represents the moments about the respective axis and describes the different rotational manoeuvres of the drone as follows [60]:

$$M = \begin{bmatrix} db(\omega_4^2 - \omega_2^2) \\ db(\omega_1^2 - \omega_3^2) \\ k(\omega_1^2 + \omega_3^2 - \omega_2^2 - \omega_4^2) \end{bmatrix} = \begin{bmatrix} M_x \\ M_y \\ M_z \end{bmatrix}$$

where,

b - thrust coefficient

k - aero drag coefficient

d - moment arm

ω_n – speed of motor n

As mentioned before, the different manoeuvres of the drone are achieved by changing the velocity of specific motors according to the desired maneuver. The facing-up motors in image 33 rotate at the same speed as each facing-down.

Roll: to generate a rolling moment about the x-axis, it is necessary to vary only the velocity of the fourth and the second motor by the same squared amount dw . Expressed in the moment vector M:

$$\begin{bmatrix} M_x \\ M_y \\ M_z \end{bmatrix} = \begin{bmatrix} db(\omega_4^2 + dw - (\omega_2^2 - dw)) \\ 0 \\ 0 \end{bmatrix} = \begin{bmatrix} db(2dw) \\ 0 \\ 0 \end{bmatrix}$$

Pitch: similarly, a pitch moment which is a moment about the y-axis, is achieved by varying the velocities of the first and third motors by the same squared amount dw . Expressed in the moment vector M:

$$\begin{bmatrix} M_x \\ M_y \\ M_z \end{bmatrix} = \begin{bmatrix} 0 \\ db(\omega_1^2 + dw - (\omega_3^2 - dw)) \\ 0 \end{bmatrix} = \begin{bmatrix} 0 \\ db(2dw) \\ 0 \end{bmatrix}$$

Yaw: for achieving a yaw moment about the z-axis, it is necessary to speed up the first and third motor and slow down the second and fourth by the same amount dw . Expressed in the moment vector M:

$$\begin{bmatrix} M_x \\ M_y \\ M_z \end{bmatrix} = \begin{bmatrix} 0 \\ 0 \\ k(\omega_1^2 + dw + \omega_3^2 + dw - (\omega_2^2 - dw) - (\omega_4^2 - dw)) \end{bmatrix} = \begin{bmatrix} 0 \\ 0 \\ db(4dw) \end{bmatrix}$$

In all the described cases (roll, pitch, and yaw), the vertical thrust remains constant, and the drone should not change the altitude in the z-direction since the increase in thrust due to the motors speeding up is compensated by the motors slowing down.

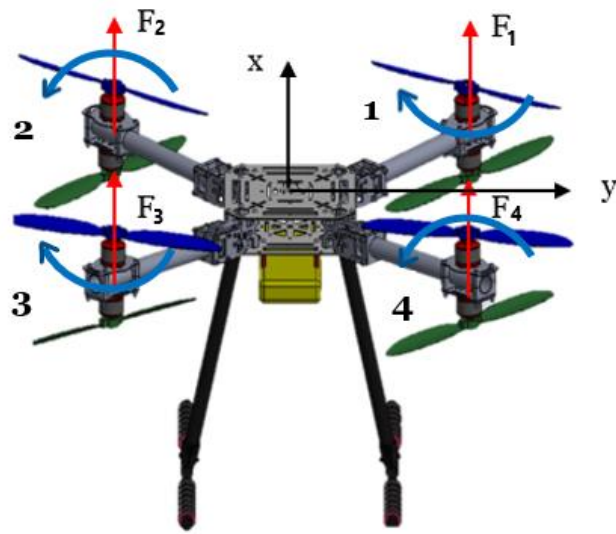


Fig 33 : Description of Motors moments and thrust

- **Definition of parameters**

As mentioned before, the analysis of loading conditions is done based on the parameters of the initial airframe ZD550, which is the structure to optimize. The structure's mass with the electronic components mounted is approximately 2.8kg.

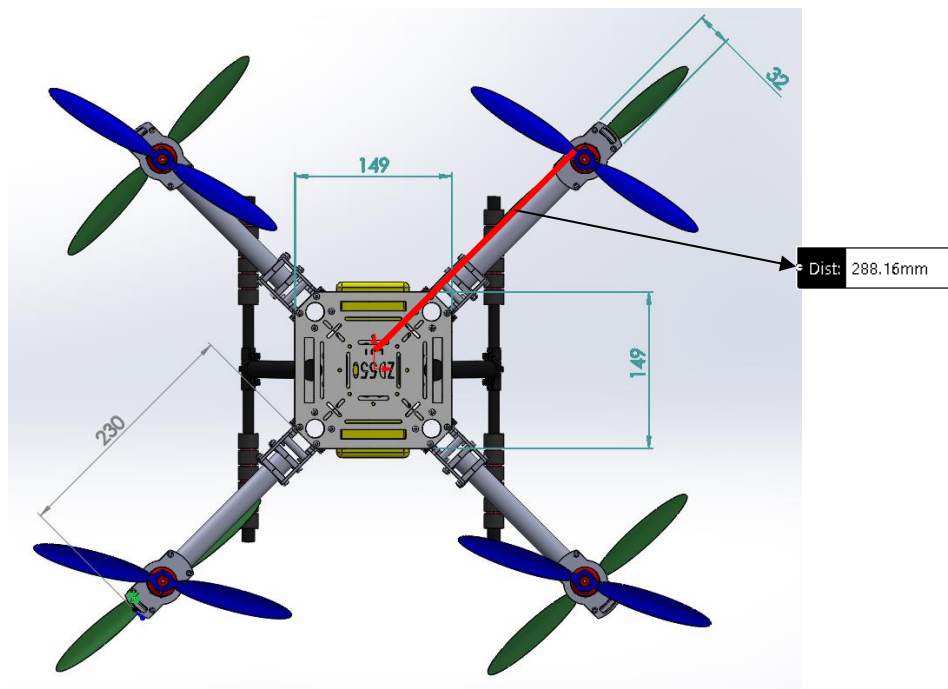


Fig 34 : Airframe measures in mm from the model in Solidworks

Area to drag force calculation

The total area for drag is calculated as the sum of the superficial area of each arm plus the area of the central plate of the main body. The measures of the structure for this calculation are shown in figure 34.

$$A = 0,0516m$$

Moments of inertia: The inertia values in each axis are taken from the calculation performed automatically by Solidworks on the initial drone model.

$$I_{xx} = 0,05565 \text{ kgm}^2$$

$$I_{yy} = 0,05580 \text{ kgm}^2$$

$$I_{zz} = 0,06382 \text{ kgm}^2$$

Moment arm: the arm d to calculate the moments is the distance from the centre of a motor to the centre of the airframe. This measure is shown in figure 34, taken from the CAD model.

$$d = 0,288m$$

Torque and thrust coefficients: The equations to obtain the torque and thrust coefficients are taken from a similar dynamic model [61, 62].

The theoretical torque generated by a propeller is calculated as follows:

$$Q = C_Q \rho n^2 D^5 \quad (17)$$

where,

C_Q - non-dimensional torque coefficient

n - propeller speed, [rps]

D - propeller diameter, [m]

ρ - air density, $\frac{kg}{m^3}$

The torque coefficient k , is presented in equation (18):

$$k = \frac{C_Q \rho D^5}{3600} \quad (18)$$

The non-dimensional torque coefficient of the 9050 propellers is taken from the APC Propeller Performance Database [63] $C_Q = 0,044$. The propeller diameter is 0,2286m, and the air density is taken at sea level, $1,225 \frac{kg}{m^3}$. Then:

$$k = 9,35 \times 10^{-9} \frac{Nm}{rpm^2}$$

On the other hand, the theoretical thrust generated by a propeller is calculated as follows:

$$T = C_t \rho n^2 D^4$$

where,

C_t - non-dimensional thrust coefficient

n - propeller speed, [rps]

D - propeller diameter, [m]

ρ - air density, $\frac{kg}{m^3}$

The thrust coefficient b , is calculated by equation (19)

$$b = \frac{C_t \rho D^4}{3600} \quad (19)$$

The non-dimensional thrust coefficient is taken from the APC Propeller Performance Database [63] $C_t = 0,110$. And taking the diameter and density defined before, then:

$$b = 1,022 \times 10^{-7} \frac{N}{rpm^2}$$

Finally, the motor's calculation of thrust and torque for each movement is performed by varying the speed of the motors according to the desired maneuver considering the points near of maximum throttle (between 90-100%). The thrust and torque are obtained from the test report given by the motor supplier, which relates the thrust and torque with the motor's RPM. Then these values are compared with the values obtained with the theoretical model described before. As a result, the test presents thrust and torque values that are slightly bigger than the theoretical model. Therefore the analysis considers mainly the test report, and the resulting loading cases are summarized in table 5, where T represents the thrust o each motor and Q is the torque.

Loading conditions								
Maneuver	T1,T6 [N]	T2,T5 [N]	T3,T8 [N]	T4,T7 [N]	Q1,Q6 [Nm]	Q2,Q5 [Nm]	Q3,Q8 [Nm]	Q4,Q7 [Nm]
Takeoff	3,46	3,46	3,46	3,46	0,053	0,053	0,053	0,053
Hover	3,43	3,43	3,43	3,43	0,053	0,053	0,053	0,053
Lift	8,58	8,58	8,58	8,58	0,133	0,133	0,133	0,133
Roll (to the right)	9,82	10,28	10,28	9,82	0,153	0,160	0,160	0,153
Roll (to the left)	10,28	9,82	9,82	10,28	0,160	0,153	0,153	0,160
Pitch (forward)	10,28	10,28	9,82	9,82	0,160	0,160	0,153	0,153
Pitch (backward)	9,82	9,82	10,28	10,28	0,153	0,153	0,160	0,160
Yaw (clockwise)	10,28	9,82	10,28	9,82	0,160	0,153	0,160	0,153
Yaw (counterclockwise)	9,82	10,28	9,82	10,28	0,153	0,160	0,153	0,160

Table 5 : Loading conditions of different manoeuvres

4.3. Design constraints

The constraints to design the new optimized structure are given mainly by the initial system composed of the airframe ZD550 and all the previous electronic components. A compact, lightweight design is sought, avoiding, as had been done initially, adding additional plates to the central body to support the electronic components. Additionally, it is necessary to consider the constraints due to the landing structure and the protection parts for indoor flight. It is also considered a modular design in which the frame can be easily assembled and integrated with new features and possible quick part swaps of eventually broken parts. The detailed constraints are described as follows:

4.3.1. Structural components

The first step is to define the drone's main body considering the total volume of the electronic components put inside this space, such as the PCB, the Nvidia Jetson Nano, and the receiver. The main body has to consider the ease of assembling these components and the possibility of changing their location inside the main body. The result is an initial central body composed of two plates of dimension 279x179x3 mm with some extruded cuts and separated each from the other by 37 mm, as shown in figure 35, ensuring enough space to contain the electronic components and the connection between them. This initial central body will be designed in detail later, creating holes and geometries to fix the electronic components and enable an easy connection between them.

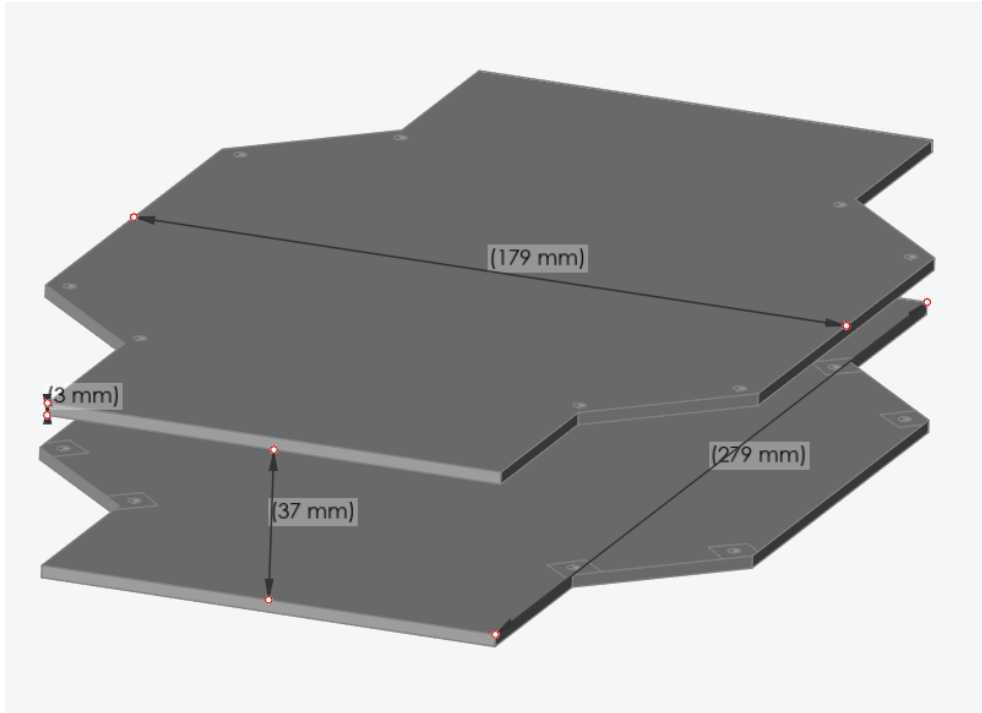


Fig 35 : The initial main body of the airframe

The flight controller defines the position of the supports where the motors are mounted since it performs the flight control starting from some variables, such as the position of the motors about the FC origin and the system mass centre, located on the vertical axis of the FC. This condition means that it is necessary to maintain the relative position of the motors of the initial system. Therefore the motor supports are located on the corners of a square with a diagonal of 550mm, separated by 37mm like the initial airframe, as shown in figure 36. Increasing the vertical distance between the plane, on which the motors are mounted, and the UAV's centre of mass improves the stability during flight; however, as this distance increases, the moments of inertia related to the rolling and pitching movements also increase. A compromise between these two effects defines this distance. The direction of the rotation of the motors also coincides with the original arrangement.

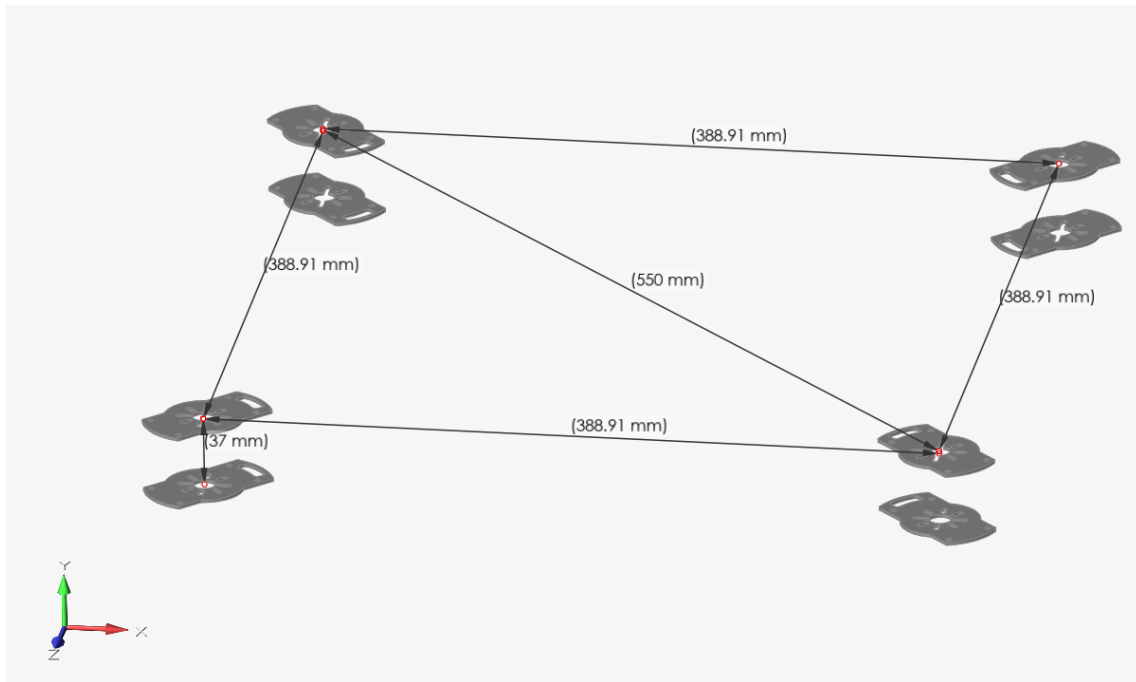


Fig 36 : The relative position of the motor supports

Additionally, the design must ensure that the propellers can rotate without interference with the landing structure or another part of the structure. The landing structure is located in the lower part of the UAV, so this zone must be as accessible as possible. Therefore, it is necessary to put as many electronic components as possible around the drone's centre to ensure stability. A good design involves positioning the battery at the bottom of the low plate, as it has a simple geometric shape and a very high mass density. Another point is that the landing structure can not interfere with the propellers facing down. Hence, a conical landing structure connected to the arms is suitable for achieving a precise landing, maintaining stability, and meeting this requirement.

4.3.2. Electronic components

The electronic components' constraints involve all the requirements for the optimum flight. Some features are positioned according to their functioning, while others are set to avoid interference with the structure. In this sense, it is necessary to make sure that:

- The electronic speed controllers, which have a rectangular geometry, should be positioned on a planar surface inside the arm if possible.
- The Pixhawk autopilot is positioned in the centre (with the arrow pointing forward) at the top of the frame.

- The GPS is positioned above the Pixhawk and with the same orientation, in the highest position away from interference.
- The depth camera is positioned below the main body in the lowest position with the lens oriented to the bottom to have a wide vision without obstruction to capture the marker in the landing base where the drone lands with precision.
- The lidar is positioned so that it points downward and unobstructed towards the floor to have a correct height measurement of the drone concerning the ground.
- The radio telemetry antenna must protrude from the main body of the structure.
- The components located at the top, such as the GPS, the telemetry, and the magnetometer, should not be covered by carbon fibre structures to avoid signal interference.

4.4. Topology optimization

The topology optimization performs an iterative process to obtain an optimum structure that leads to the final design. In this case, this process evaluates different structure configurations as geometries. Mainly four models were considered based on the defined main body: quad X, quad H, quad I, and quad X with a cylindric shape. The software to make the topology optimization is Altair inspire. This process starts with an initial target model to optimize, designed in Solidworks, and finishes with the optimized structure that can be modified with the “Polynurbs” tool. The main phases of performing this optimization process are described as follows:

4.4.1. Material configuration

After importing the geometry inside the environment of “Inspire,” the first step is to define the material and assign the selected material to each part of the model. As described before, the material selection results were on two plastic materials reinforced with carbon fibres: the PA6CF and the XT-CF20, whose properties are introduced in the software, as shown in figure 37. After, a first structural analysis is performed to know the initial safety factor of the structure and be sure that it is possible to optimize and remove material. In this case, the analysis is performed with the XT-CF20, which has less strength assuring the proper structural performance of both materials.

Material	E	Nu	Density	Yield Stress	α	λ
PA6CF	7.453E+3 MPa	0.430	1.200E-6 kg/mm ³	105.000E+00 MPa	17.300E-06 /K	16.200E-03 W/(mm ² K)
XT-CF20	6.200E+3 MPa	0.400	1.350E-6 kg/mm ³	76.000E+00 MPa	17.300E-06 /K	16.200E-03 W/(mm ² K)

Fig 37 : Settings of material properties

4.4.2. Design and non-design space

The definition of these spaces is one of the most critical phases of the entire topological optimization process. The design and non-design space describe specific structure volumes, leading to the final result of the optimization. The non-design space is the volume that remains without changing the material distribution. In this space, the loading conditions to which the structure is subjected and the system's constraints are applied. The software interprets the volume used for optimization as an essential constraint, and its shape and extension significantly vary both the result obtained and the time taken to achieve it.

The non-design space is composed of the following:

- The main body described before, where the electronic components are mounted
- The cylindric partitions that separate the two plates of the main body where the fasteners that join the arms with the plates are inserted
- The supports, where the motors are fixed with screws

This space is the same for all the airframe configurations compared and is obtained after defining the structure's assembly and integrating the system's electronic components into Solidworks's CAD software. These components are designed in such a way as to have minimum weight with sufficient resistance to withstand the forces that occur in the different load cases. The result is shown in figure 38.

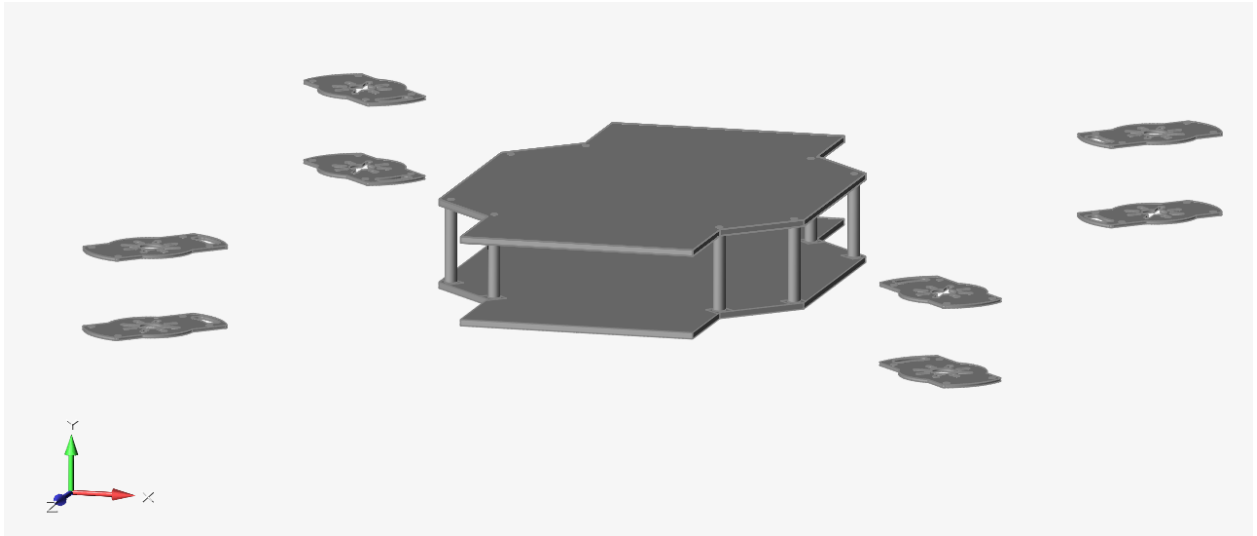


Fig 38 : Non-design space

On the other side, the design space is the volume of work composed of the parts or zones where the material distribution is optimized. As this volume is modified during the topology optimization is crucial that there are no loading conditions applied over this space. The design space comprises the arms of the drone. Different spaces were designed according to the typical drone configurations and structure geometries to compare their results and select the most optimum design. Four models are optimized: quad X, quad H, quad I, and quad X with a cylindrical section. These different design spaces are shown in figure 39.

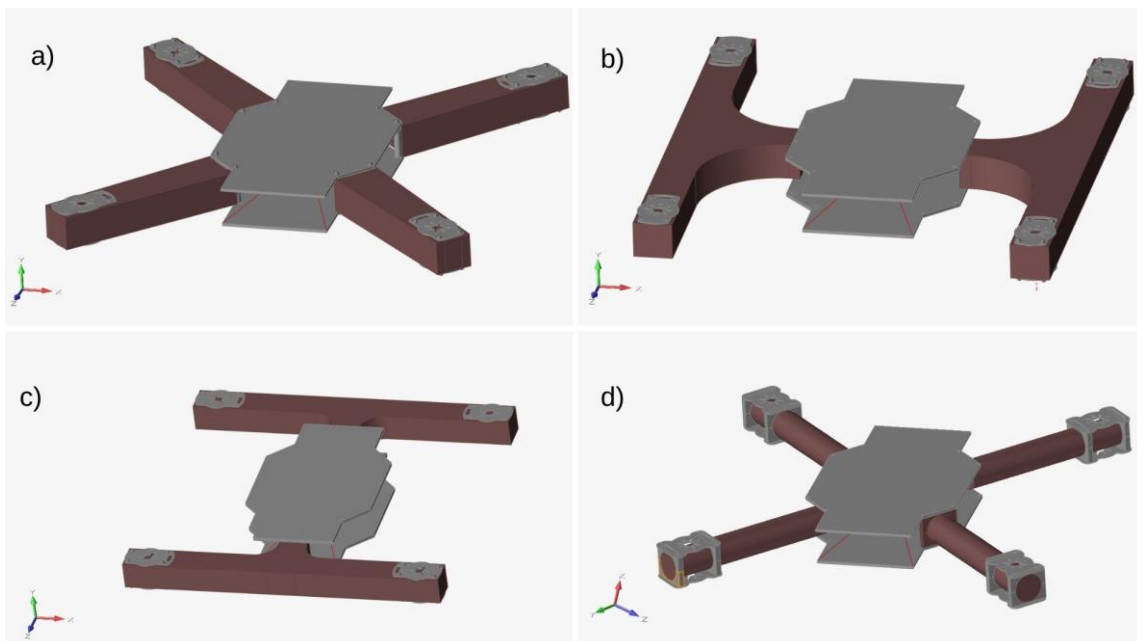


Fig 39 : Design spaces: a) Quad X b) Quad H c) Quad I d) Quad X with cylindric section

4.4.3. Fasteners and contacts between bodies

Another feature to set in the preparation of the model is the fasteners, which the software can insert automatically. Inspire can recognize the type of fastener necessary according to the holes and the geometry of the structures to join. However, it also can be modified manually and selected among bolts, screws, grounded bolts, or grounded screws. The addition of the fasteners is helpful to have a better realistic approach to the structure assembly to get better results in the optimization process performed by the software. In this case, the nuts and bolts are applied to join the arms with the main body and motor supports, as shown in figure 40.

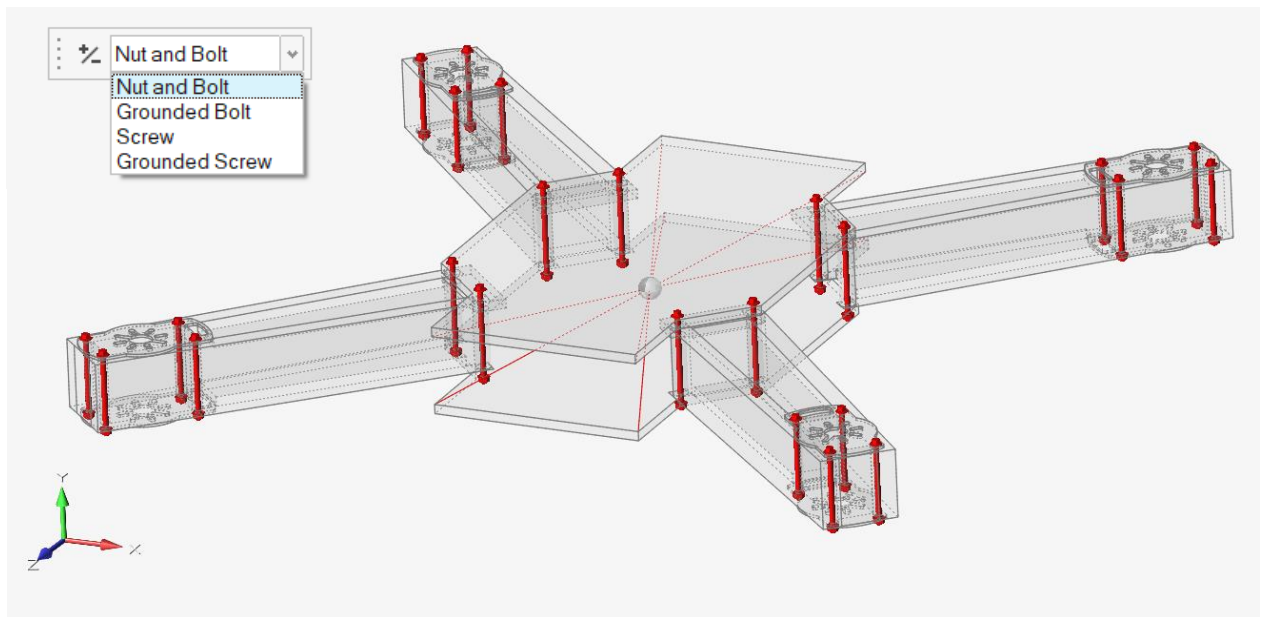


Fig 40 : Implementation of fasteners in Inspire

The joint between the main body and each arm is created by generating two cylindric partitions inside the arms structure with a 6mm diameter, as shown in figure 41. These two cylinders are created around the hole located at the joint with the main body and are defined as non-design space not to change their shape and have excellent structural strength. The joint between the arm and the motor supports automatically detects the holes through the parts and generates the bolts.

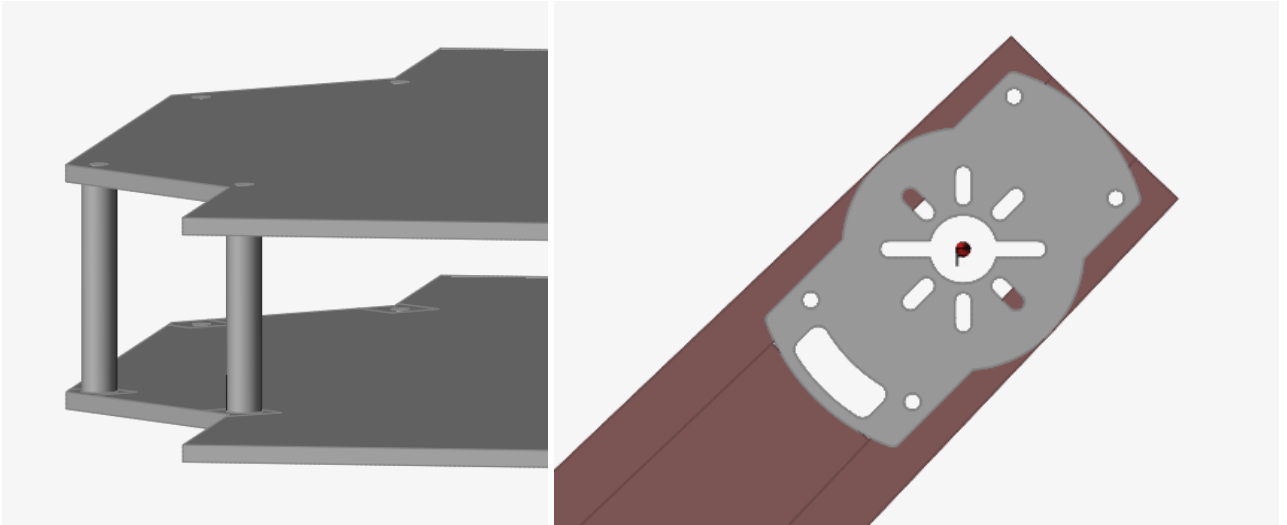


Fig 41 : Location of the joints in the different bodies

Once the fasteners are defined over the structure, verifying and modifying the type of contact between bodies is the next step. Inspire defines three types of contact conditions: bonded, which means the two bodies in contact are fused like in a unique part; contacting, which means that the two bodies are in contact and joined, like in this case by fasteners; and no contact which means that one body does not touch the other. It is essential to set these contacts properly to perform an optimum simulation and get more realistic results. In this case, the contacts where fasteners join the parts are set contacting (green). The cylindric partitions belong to the arm, so the type of contact between them is bonded (blue), as shown in figure 42.

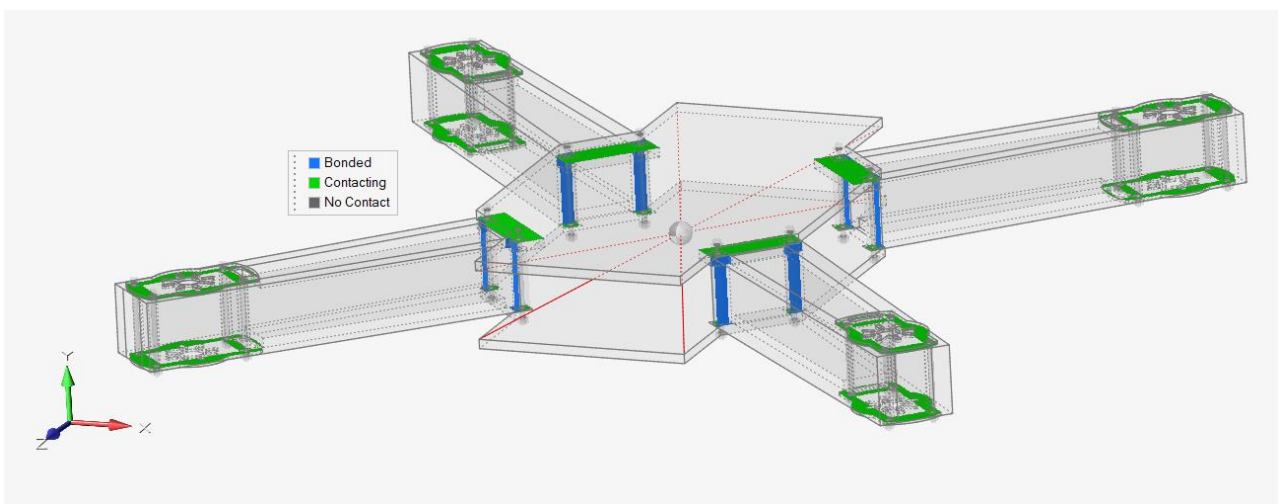


Fig 42 : Contacts between bodies in Inspire

4.4.4. Load cases definition

The next phase sets the loading conditions to which the structure will be subjected. As described before, the system is analyzed in nominal, dynamic, and impact conditions. A good practice for performing the topology optimization process is to apply the loads only over the non-design space, so in this case, the loads and constraints are applied to the motor supports and the main body.

✓ **Motor supports**

The thrust, the reaction to the motor torque, and different impact loads are applied to the motor support. Different thrust and torque values are set in different load cases according to the maneuver like take-off, yaw, roll or pitch, considering the most critical, according to the results obtained in the previous loading conditions analysis. These load cases are summarized in table 6. The direction and the location of the loads do not change, and they are described as follows:

- **Thrust:** This force is generated by the motor vertically up. It is applied over the support surface at the center of the circumference that coincides with the motor shaft.
- **Torque:** This torque is the reaction generated to counter the torque of the motor, so the value is the same as the motor torque in each load case. It is considered at the center of the motor support, like the thrust.

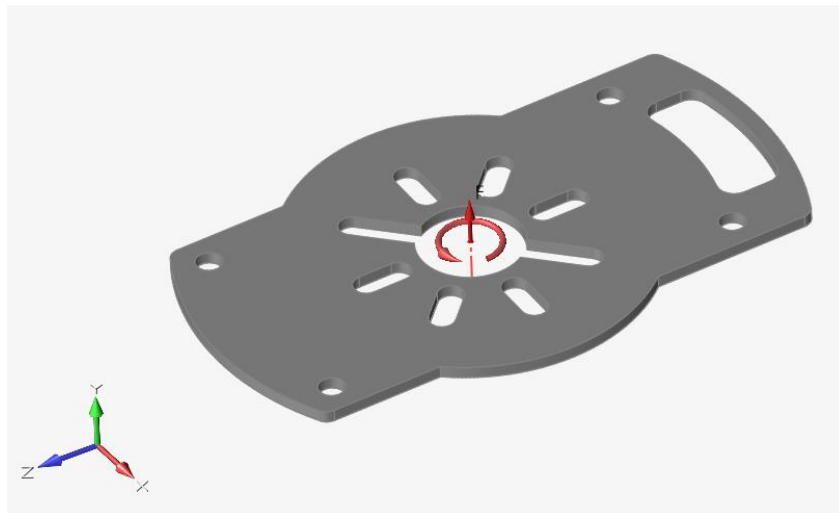


Fig 43 : Loadings over the motor support during flight

Loading conditions								
Load case	T1,T6 [N]	T2,T5 [N]	T3,T8 [N]	T4,T7 [N]	Q1,Q6 [Nm]	Q2,Q5 [Nm]	Q3,Q8 [Nm]	Q4,Q7 [Nm]
Maximum performance	10,29	10,29	10,29	10,29	0,160	0,160	0,160	0,160
Roll (to the right)	9,82	10,28	10,28	9,82	0,153	0,160	0,160	0,153
Pitch (forward)	10,28	10,28	9,82	9,82	0,160	0,160	0,153	0,153
Yaw (clockwise)	10,28	9,82	10,28	9,82	0,160	0,153	0,160	0,153

Table 6 : Critical load cases

- Impact forces: This type of force is calculated with the impulse-momentum theorem considering the worst case where the drone falls from 20 meters and hits the ground. These forces would be mainly due to impacts in the corner of the arms and are considered to be applied at the center of the surface of the motor's supports and do not act simultaneously. Different impact load cases are set in different directions to ensure the structural integrity of the drone in all axes, as shown in figure 44.

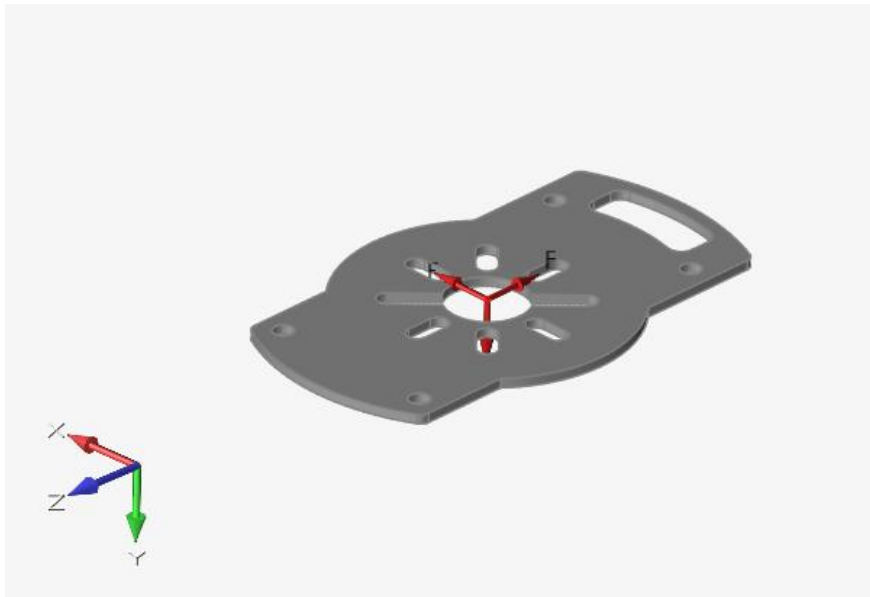


Fig 44 : Impact conditions over the motor support

✓ Main body

A rigid connection connects the two plates that compose the main body by the two facing surfaces, as shown in figure 45. This connection generates a point in the middle of the main body. This point is considered the system's mass center in which the concentrated mass due to the electronic components is put. This mass includes the total initial mass of the system, excluding the airframe.

Also, one structural support is applied in the middle of the main body. As the central body position is fixed and can not displace, this support is set to constrain the linear displacement in all directions (x,y,z). However, since the mass center coincides with the center of rotation, the drone can rotate around the mass center in all directions, so the support is set not to have constraints on the rotation. In addition, the impact forces generate the rotation of the structure around its mass center. Then this structural support is present in all the load cases.

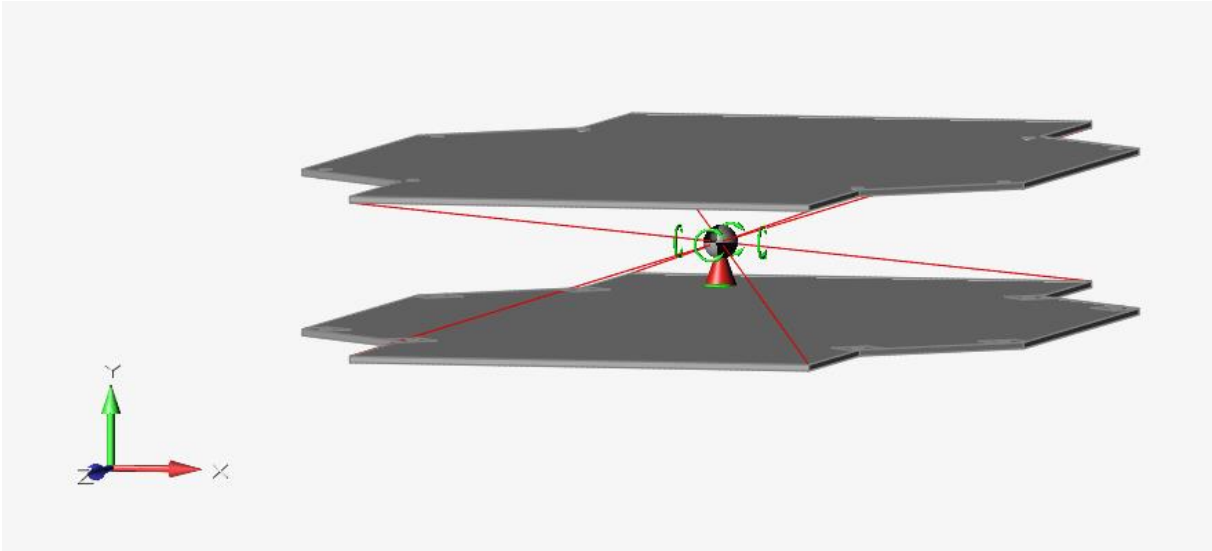


Fig 45 : Constraint and concentrated mass in the main body

4.4.5. Shape controls

The shape controls are features to constrain the design space to get geometries with specific patterns and symmetry or to ensure that the part can be physically manufactured. The symmetry shape controls are shown in figure 46. In this case, the topology optimization of the arm was performed with different symmetry conditions, alternating the symmetry planes.

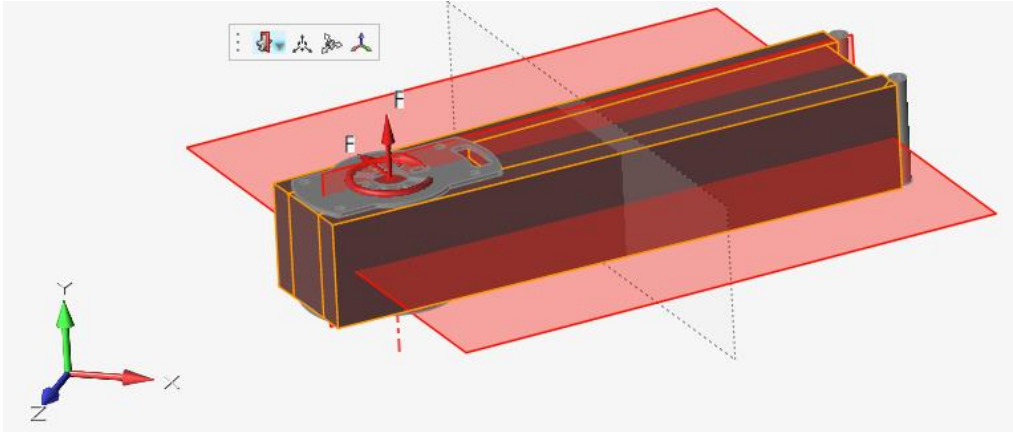


Fig 46 : Symmetric shape control

4.4.6. Optimization settings

The last phase is the configuration of parameters to run the topology optimization. The process is performed according to two main optimization objectives: maximize stiffness or minimize mass. In this case, the structure is first optimized to maximize stiffness, putting a mass target of around 30% of the total design space volume. Then a second optimization is performed to minimize mass, putting a minimum safety factor of 1,5 to improve the previous result and reduce the mass.

There are other parameters concerning the vibrations, the mesh, and the accuracy of the optimization. These parameters are set as follows:

- ✓ The frequency constraints are essential in the case in which it is necessary to change the system's natural frequency to avoid resonance. This is not the case, so there are no constraints about frequencies.
- ✓ Thickness constraints: The elements generated can have different thicknesses according to the flow of tensions that pass through them is crucial to control it. This feature can control the members' diameter and thickness by setting a minimum value. The recommended thickness is three times the average element size of the mesh. In this case, the minimum thickness is set at around 5mm. This element size defines the precision of discretizing the design space, so a minimal element size represents good precision but a high computational cost.
- ✓ Speed/accuracy: with this parameter is possible to prioritize the accuracy or the speed, but this feature is only needed when high accuracy is required for frequency constraints [64]. In this case, the speed is set as faster as the software recommends. A more accurate setting also increases the time significantly.
- ✓ Contacts: This feature has two options: sliding only or sliding with separation. In this case, "sliding only" is selected because, in reality, the bodies do not separate.
- ✓ Gravity: This feature should be activated when the structure's weight is significant concerning the loads it bears. In this case, it is not considered as the total system's weight is considered in the calculations of the loading conditions.

The algorithm of the optimization runs an iterative process. As the iterations run, it eliminates elements from the design space according to the tension to which they are subjected: unloaded elements provide a minor contribution to the structural stiffness compared to loaded elements. Then they are eliminated to lighten the structure. Elements with intermediate loads are

analyzed employing penalty algorithms, which are approximated to unloaded or loaded elements according to their associated value. This process proceeds until the local minimum point is found, minimizing the mass and complying with the constraints and parameters set.

4.5. Results

Once the optimization is performed, the structures are created using the Polynurbs tool according to the material distribution obtained from each configuration. Then each design is structurally analyzed through the finite element method. To select an optimum design, the main parameters to take into account are the weight, the minimum safety factor, and the facility to integrate the structure with the mounted components and the landing structure, complying with all the design constraints.

4.5.1. Quad X

The X type is one of the most common configurations due to its simplicity. This type of structure consists of four arms forming an X-geometry connected to the main body on one side and with the motor's supports on the other side. This structure was obtained from a parallelepiped with a 1-centimeter thickness and variable width as design space, shown in figure 39. The resulting structure is composed of a structural truss with variable thickness in its members. The thickness is more prominent in the zones where more significant stresses are generated, like in the joint with the main body, as shown in figure 47. The other thicknesses along the structure are designed in such a way as to obtain a minimum safety factor of 1,5, ensuring a lightweight, resistant design. Two planar surfaces are also integrated into the arm to put the electronic speed controllers on them and facilitate the connection with the motors.

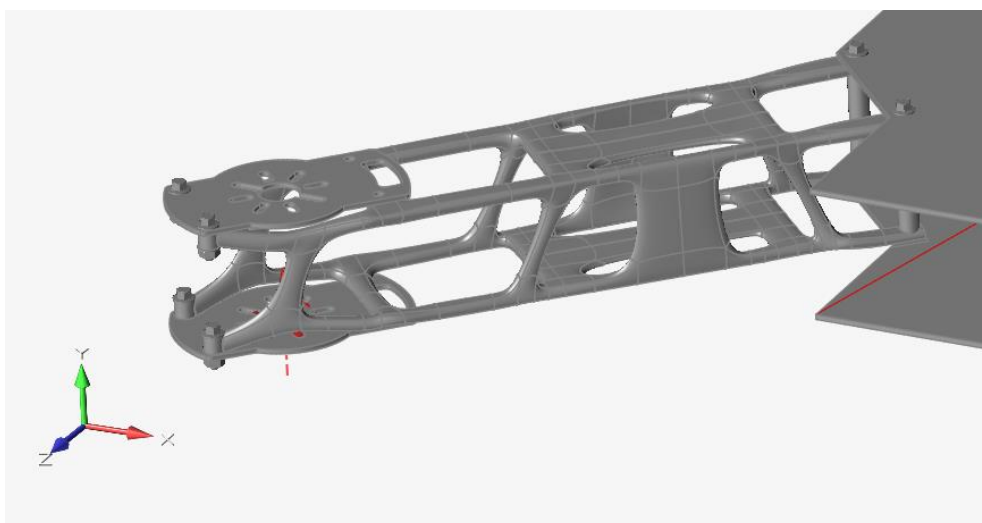


Fig 47 : Quad-X resulting structure

The advantages that offer this structure are described as follows:

- It is the easiest to produce. As the volume is not too large it is possible to print the entire arm in one piece and assemble each easily with the main body, ensuring excellent structural rigidity.
- It offers flexibility and modularity since it can be repaired and replaced quickly if one arm is crashed.
- The ease of assembly of the arm with the motor supports thanks to the compatibility of the planar section of the arm in this zone.
- This configuration offers optimum space for the integration and proper functioning of the electronic components.
- It has good space, which is suitable for linking the landing structure from the middle of the arm without modifying the structure's geometry.
- The planar structures, which support the electronic speed controllers, are integrated with the arms, avoiding additional supports that can increase the weight.

4.5.2. Quad X with cylindric section

This configuration is the most similar to the initial airframe, which is a quad X airframe with cylindric arms. The result is obtained from a solid cylindric arm as design space, shown in figure 39. In this case, the optimization process only reduces the thickness of the cylinder, decreasing the mass and ensuring the structural integrity and the safety factor imposed. The structure is shown in figure 48. From the point of view of structural performance, it is similar to the one before. However, this structure has the following disadvantages:

- From the point of view of the assembly with the main body and the motor supports, it is necessary to add the features shown in figure 48 in red because the plates of the main body and the motor supports have planar sections.
- Similarly, it is necessary to add a support structure, as shown in figure 48 in blue, compatible with the rectangular geometry of the electronic speed controller. This feature increases the weight of the entire structure.
- The integration of the landing structure is also more complicated than the previous design.

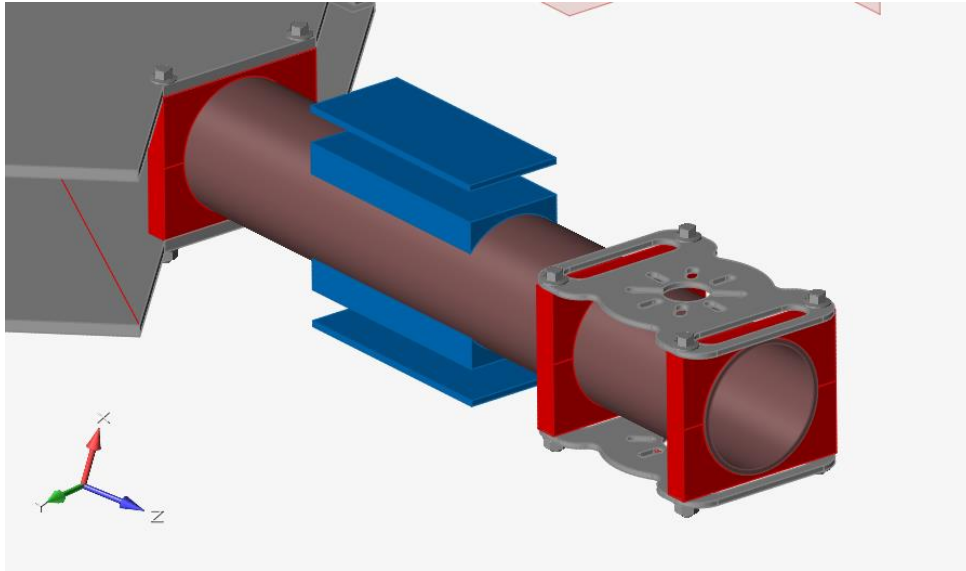


Fig 48 : Quad-X cylindric resulting structure

4.5.3. Quad H and Quad I

The results of these two types of configuration are similar between them. The optimization starts with a design space with the arms forming a geometry of H in one case and I in the other case as shown in figure 39. These types of structures consist of two main arms connected to the main body from which two secondary arms branch off and connect with the motor's supports. These designs are more complex than the X-design in which there are four main arms connected to the vertices in the middle of the main body. In this case, the primary arms are connected on the sides of the central body resulting in a structure where there are two sides completely occupied by the arms and two sides free to the integration with the electronic components. This configuration is suitable when the camera is located in the main body due to the wide range of vision, but in this case, the camera is located below it. The resulting structures are bigger than the X-design and therefore more complex to produce since the volume of each complete arm is too large to produce in one piece. Then the solution would be to divide the arm into two parts to assemble. A resulting structure composed of a structure with variable thickness according to the stress distribution is shown in figure 49.

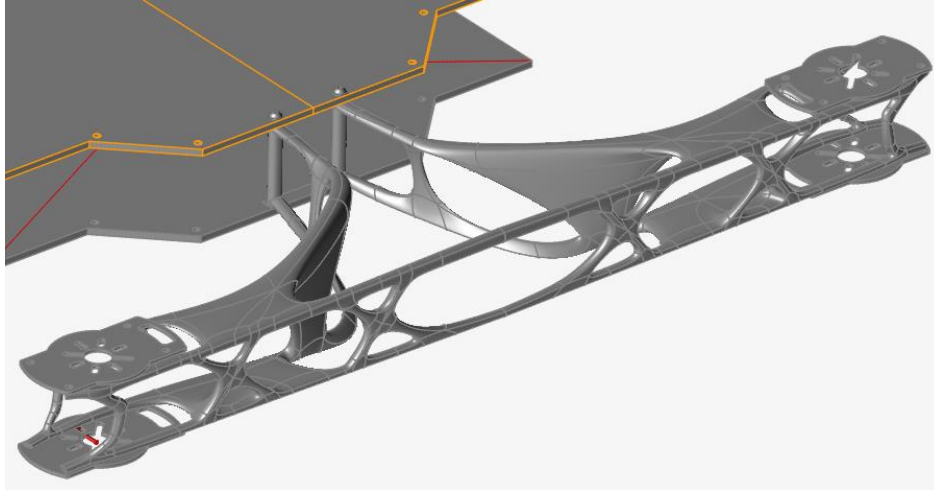


Fig 49 : Quad-H resulting structure

5. Optimum final design and printing

The next step is to define the final configuration of the airframe to perform the detailed design and integrate it with the other features of the system. In order to select the most optimum configuration among those described before, are considered mainly the following parameters: the weight, the minimum safety factor, the ease of assembly, and the integration with the electronic components and landing system.

The topology optimization process performed for all the configurations was similar, putting first the maximization of stiffness as the objective and then the minimization of mass. This is done to have a similar mass and perform a realistic comparison while all the design constraints are considered in each case. For each case is performed an iterative process in which the structure under all the load cases described, was analyzed by the finite element method, in *Inspire*, to verify the strength and the safety factor in each case. If the structure did not comply structurally, it was modified and analyzed again until the desired result was obtained. As the main requirement, the minimum safety factor was set to 1,5 in the worst condition. The final results of the FEM simulation are shown in figure 50 and the parameters are summarized in table 7.

Configuration	Mass (g)	Min SF	Max Von misses (MPa)	Cost (Euro)
Quad X	40,8	1,5	51,7	10,22
Quad X - cylindric	42,7	1,8	56,02	11,58
Quad H	39,5	1,5	61,13	12,76

Table 7 : FEM analysis results

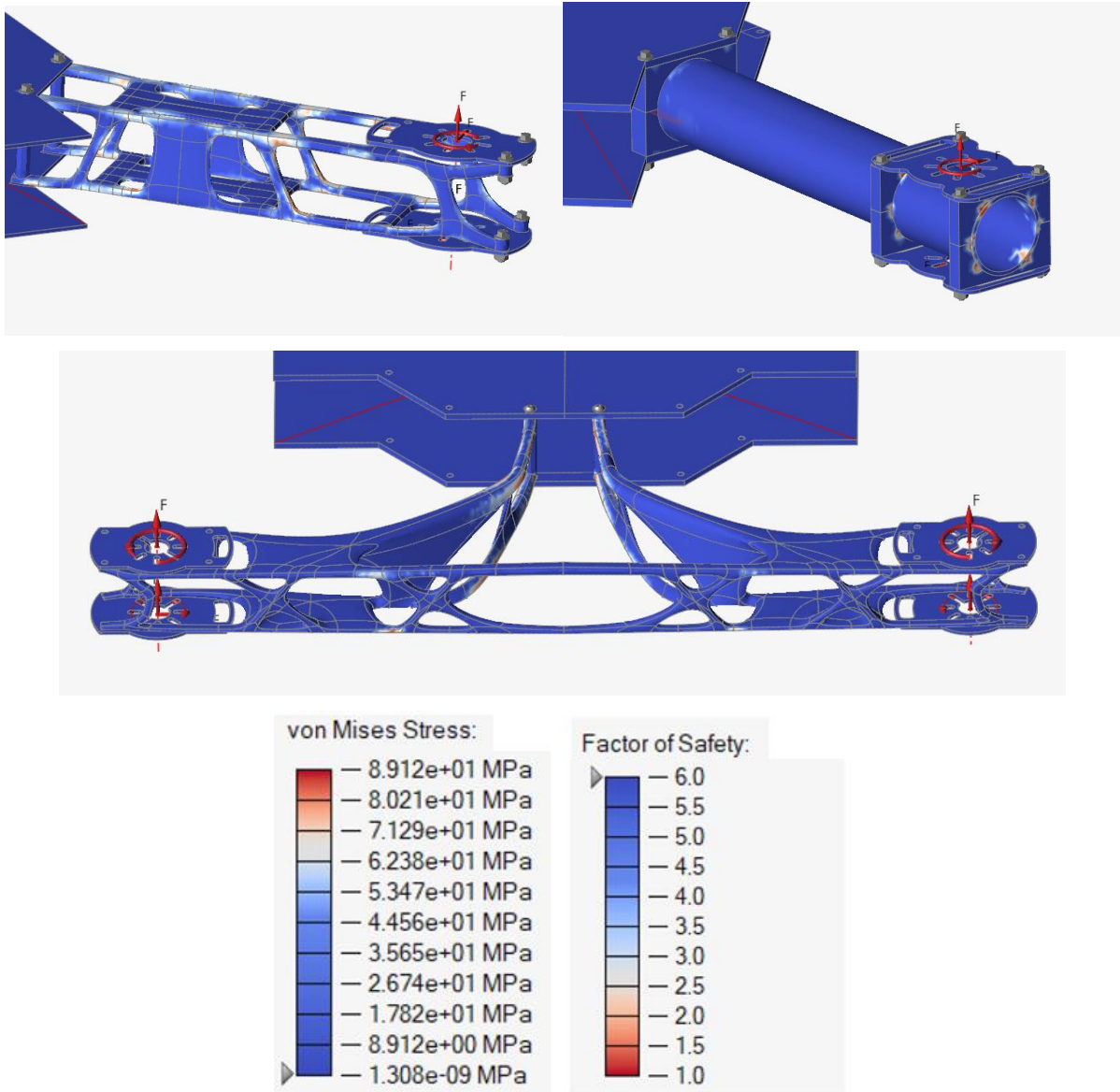


Fig 50 : Results of FEM simulation: Quad-X, Quad-X cylindric, Quad H – Divergent Scale

In the obtained results shown in figure 50 is possible to see the stress distribution along the structure and the structural behavior for each different configuration. All of these designs meet the minimum structural requirements but some differences between them are considered to select the most optimum. The mass of the arm is around 40g in all the cases which is a good point to compare the structural performance between them. The minimum safety factor is considered in the worst case of the loading conditions which is an impact case. The cost is obtained from the printing software Cura which considers the quantity of part material and support material required to produce the part.

The quad-X cylindric design presents the highest safety factor which is an indicator of good structural performance. However, the cylindric section is not suitable from the point of view of integration with the rest of the structure and components, which would complicate the complete design and this is the main drawback of this configuration. Also, the cost is on average but higher than the Quad-X. The quad-H design can be the lightest and this structure would be well integrated with the rest of the structure and components but this configuration is more complex to produce. This design must be divided into two parts to assemble due to its large volume and presents also the maximum stresses and the highest cost.

On the other side, the Quad-X design presents good structural integrity and the minimum von misses stress concerning the others. Also, it is the cheapest configuration and is simple to produce. This configuration is the most suitable from the point of view of functionality and integration with the whole system. It offers sufficient space for the assembly and proper functioning of electronic components. The landing structure is easily integrated due to the space and symmetry that the X-design presents. This configuration has a modular design in which each arm is well coupled to the main body with two bolts having a rigid assembly. Therefore this design is selected as the most optimum to produce.

5.1. Final design and other considerations

After defining the optimum configuration and structural design of the arms, other considerations are taken into account for the final design. The main body consisting of the top and bottom plate must be designed in detail to house the electronic components. The first modification is the reduction of the thickness of both plates from 3mm to 2mm. This is done after seeing that the safety factor in these plates was very big. The mass of the main body was reduced by one-third with this operation.

Then several extruded cut operations are done on both plates to create the holes to insert the bolts that join the components to the main body, and the holes to pass the cables through the plates and connect the components between them. These holes are located in a such way as to put each component in the proper position according to their geometry and the described requirements in the design constraints section, and to facilitate the connection between them. The design is flexible as permits locating the components which do not have a strict constraint, in different positions or orientations. The final design of the top and bottom plates is shown in figure 51.

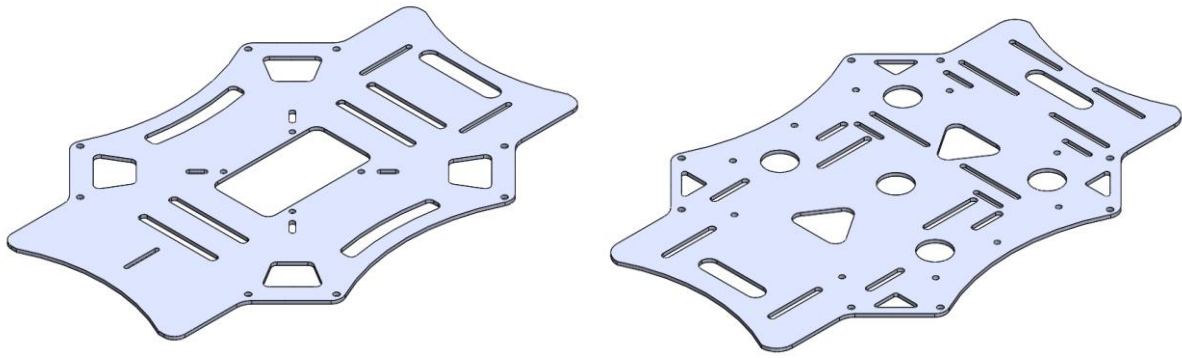


Fig 51 : Top and bottom plates' final design

The motor supports are also modified to fix the motor to the arm with rigidity. These elements are designed to be lightweight but with good mechanical properties. They are also integrated with the propeller guards to maintain a lightweight structure. These elements are useful to protect the structure in indoor flights and will be explained further. The modular structure which integrates these parts with the selected configuration is shown in figure 52. In the figure is possible to distinguish the elements, that are assembly by using threaded joints, by the following color distribution:

- Red = main body (top and bottom plates)
- Blue= X-design arms
- Yellow: motor supports integrated with the propeller guards

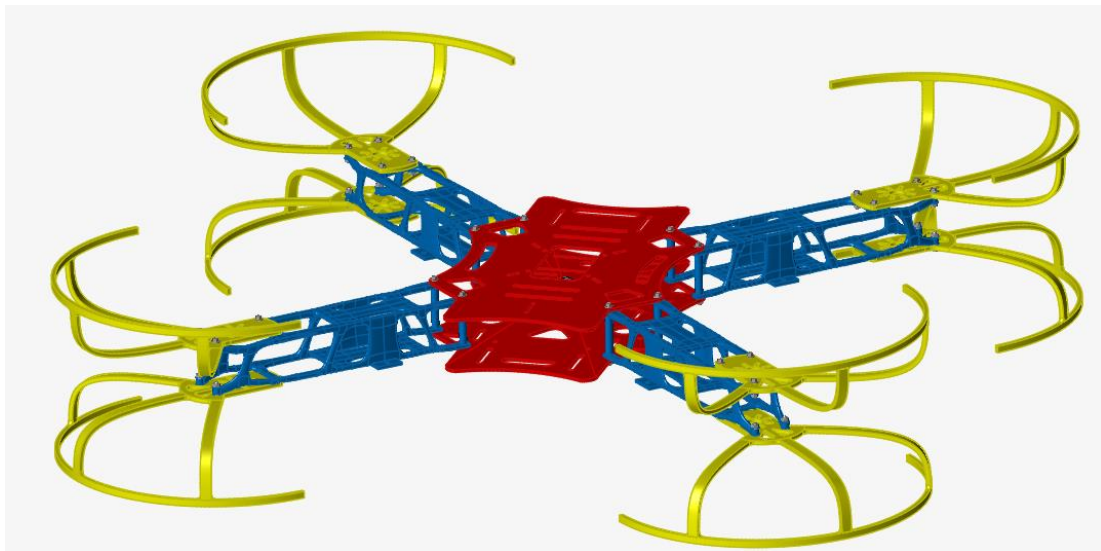


Fig 52 : Structure assembly – integrated with arms, main body, and motor supports

As a first result, the mass of the airframe is optimized with respect to the initial structure. The mass of the structure estimated with the two selected materials is 461,5g and 408g for the XT-CF20 and the PA6CF respectively. Then the mass reduction was around 32% using the XT-CF20 and 40% in the case of the PA6CF concerning the initial airframe with a mass of 675g. This assembly is also analyzed by the FEM to verify the structural strength. The minimum safety factor obtained in the worst load case is around 1,51 as shown in figure 53. Also, the stress distribution along the structure is evident with the divergent scale where the highest stresses are located in the corners of the arm structure and the joint of it with the main body. The maximum von mises stress is around 50Mpa.

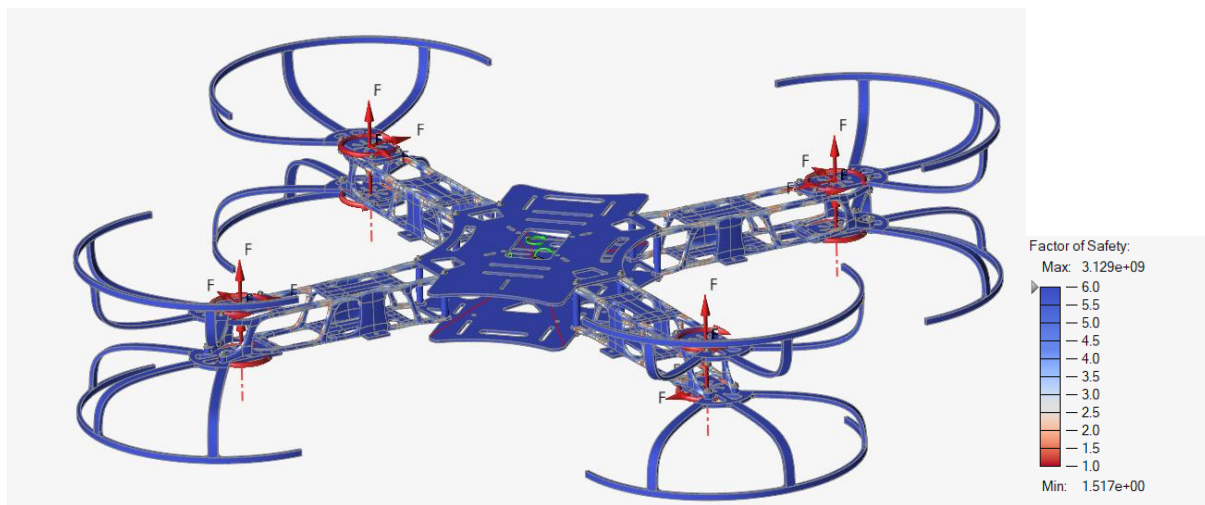


Fig 53 : Structural analysis of the optimized structure

5.2. Supports for electronic components

Other structures to support some electronic components in a specific position and orientation are also necessary for the optimum functioning of the whole system. The position of these supports and their geometry are defined by the geometrical features of the electronic components and their functioning constraints which were explained before. Also, how the supports are assembled in the main structure is considered for their design. These structures are lightweight and with small dimensions to don't increase so much the total weight but to fix the electronic components safely. The design is kept simple to have fast and cheap production. These elements do not support significant loads and they are filleted in the zones in which there are stress concentrations like the corners. The thickness is also minimum, between 2mm and 3,5mm being the smallest along the major portion of the piece and the largest around the holes where it is attached by the screws. In this sense, these structures can be printed in PLA to

maintain a minimum weight. They are assembled with bolts M3. The different support structures are described as follows:

- Battery support: It is attached to the bottom plate keeping fixed the battery, below this plate. The translation of the battery in the plane is blocked by the support at the corners and is vertically blocked by the bottom plate and the support as shown in figure 54.
- UWB support: The UWB module is attached to the support by pressing it and is kept fixed by interference by the two tabs as shown in figure 54.
- GPS support: The GPS is fixed by the support at the top in the highest position to avoid interference. This is attached in the corners as shown in figure 54.
- Depth camera support: This support is composed of two parts that cover the camera as shown in figure 54. It is assembled below the battery support since the camera must be in the lowest position facing down to capture the marker for landing.

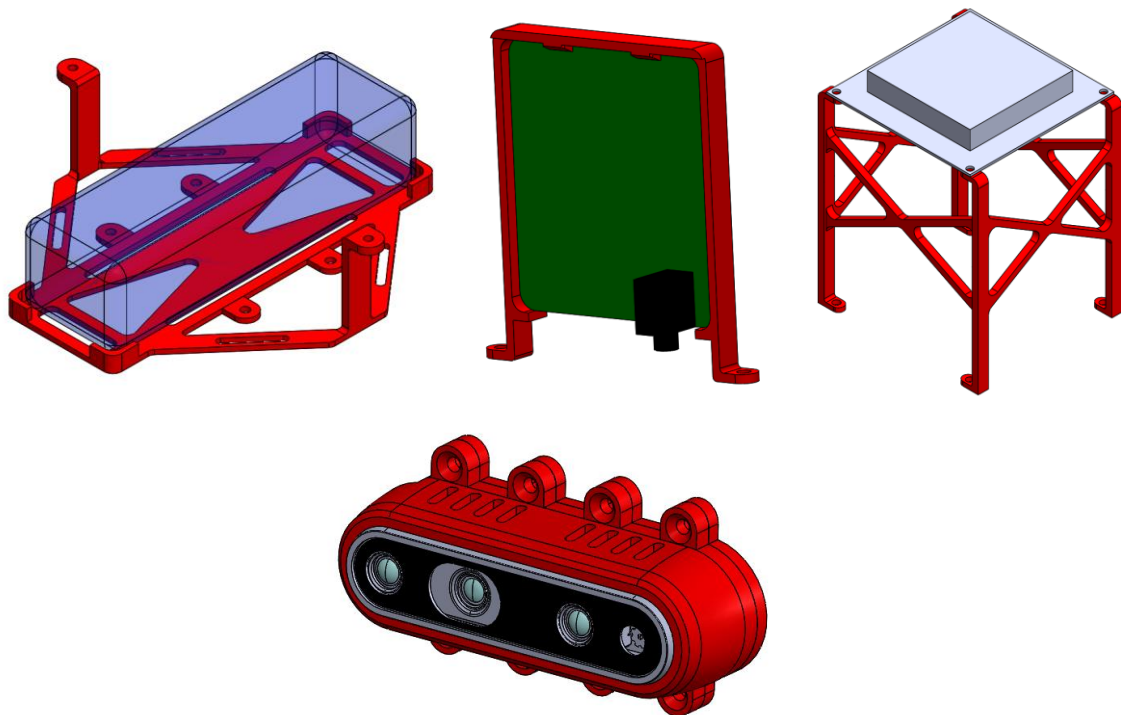


Fig 54 : Support structures for electronic components: Battery, UWB, GPS, and depth camera

5.3. Propellers protection for indoor flights

The propeller guards are protective elements of the propellers surrounding them, avoiding impact with objects. These guards must be light and protective to prevent the propellers from breaking in crashes. Furthermore, they must be sacrificial elements since, in the case of significant impacts, their breakage absorbs energy and further preserves the structure on which they are fixed. The propeller guards must also be designed so there is no interference with the propellers, especially considering the high deflection that this undergoes, being thin elements with a big length-to-thickness ratio. The result is a simple structure integrated with the motor support in one piece, with an arc of the circumference with a bigger radius than the propeller itself. Three lightweight elements connect these two components trying not to increase significantly the overall mass of the system to guarantee their stability, as shown in figure 55.

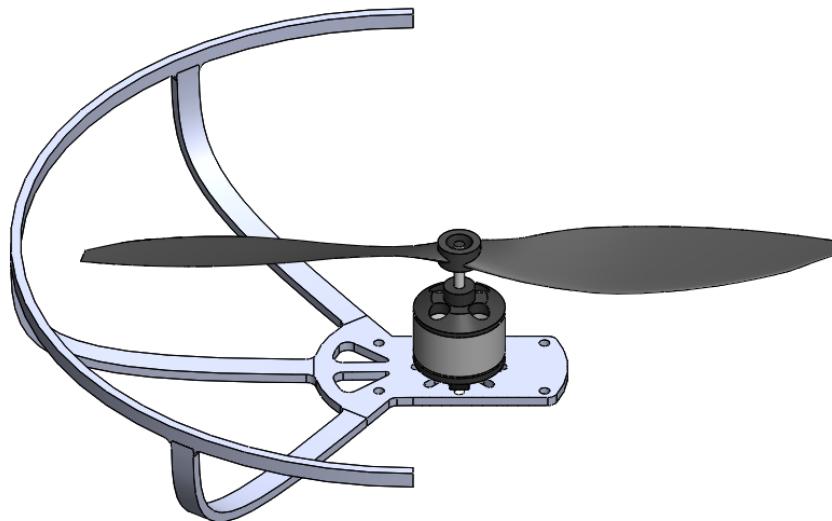


Fig 55 : Propeller guard integrated with the motor support

5.4. Landing structure

The scope of the Fixit project is to create a combined system in which the drone is integrated with the unmanned ground vehicle or also called, the rover. The idea is that the drone performs the flight activities and then can land on the UGV with precision. The drone is equipped with a depth camera under the main body that reads a marker in the ground to define the correct landing position. To perform this operation is necessary to design a landing system composed of a landing structure integrated into the drone and a landing base with the marker that will remain on the rover. The system is thought to have accurate and repeatable positioning, compatible with the precision of the landing system, avoiding falls, and a stable positioning,

which ensures the safe movement of the rover without the drone falling. This design results in a conical landing structure that comply with the main functioning requirements:

- Due to the circular geometry of the cone, the drone can land in any orientation on the landing base on the rover, which means a system more flexible and repeatable.
- The conical structure is suitable to do a precise landing as it serves as a guide to couple the drone with the landing base when the drone approaches it and comes into contact with it. In this sense, once the drone is aligned with the landing base, the motors can be turned off and the drone slides down the conical base. Also, the conical geometry offers good stability.

After performing diverse landing tests was verified that the following constraints must be satisfied to perform a correct landing:

- The depth camera is located at the center in the lowest part of the drone pointing down to the ground.
- The minimum distance from the camera to the marker to ensure recognition is 240mm. That means that when the drone reaches that safety distance between the camera and the marker the landing structure must be inside the landing base or at least at the same level because the final land command is given when the drone and the base approach complying this minimum distance, therefore to prevent the drone from landing early or outside the conical base is necessary that the drone has entered the base at this point.
- The radius of the landing structure in the lower part of the cone must be at least 100mm to guarantee the proper view range necessary for the camera.
- The space on the bottom of the landing base must be sufficient to locate the marker that has a square geometry with a 110mm side.

According to these requirements, an initial landing structure mounting into the drone is designed. The result is a conical structure joined to the drone at the bottom of the arms. The structure is coupled to each arm with two bolts as shown in figure 56. This integration is done by ensuring that the propellers at the bottom can rotate freely and do not interfere with the structure.

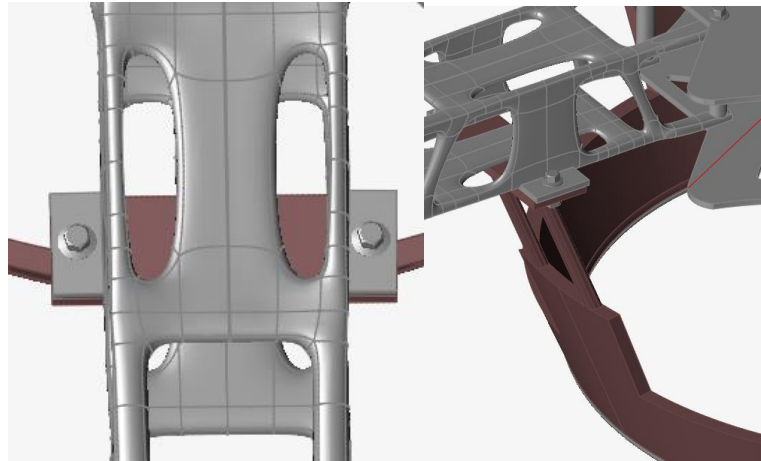


Fig 56 : Assembly of the structure with the arms

The structure assembled with the drone is shown in figure 57. As one of the main requirements of the system is to have a lightweight structure, topology optimization is performed on the landing structure to not increase so much the total weight of the airframe with it. In this case, the landing structure is set as the design space and the rest of the structure as non-design space, as shown in figure 57. To perform this optimization the following load cases are considered:

- Landing in normal condition: This is when the drone lands in an optimum way. The drone descends and lands in a controlled manner. In this case, the load is supposed like a little impact on the structure when it gets in contact with the landing base. This vertical force is higher than the weight of the system and is calculated with the impulse-moment theorem as before. The value is 100N and it is distributed in small forces around the circle at the bottom of the cone, as shown in figure 57a.
- Critical impact cases: These cases refer to impacts on the structures due to failures during flight. The landing structure is one of the most exposed components to impacts due to its position. The value of this impact force is 200N. It is the same calculated assuming a fall from 20m. Different impact cases are put in different directions along the circle at the bottom of the cone as shown in figure 57b in which each force represents one load case.

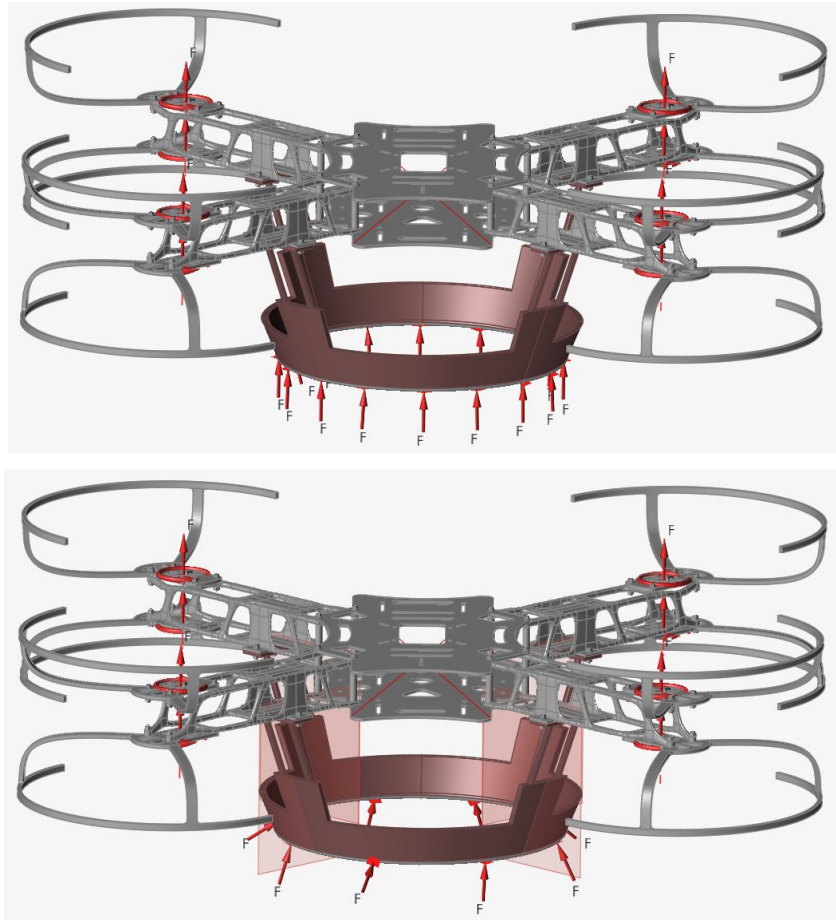


Fig 57 : Landing structure before optimization with load cases: case a)Top case b)Bottom

According to the results obtained with the topology optimization process, the structure shown in figure 58 is designed. The mass of the structure is 172g with the XT-CF20 and can not be produced in one part due to the large volume concerning the maximum volume of the Ultimaker S5. Then a modular design is created which is composed of four cone portions assembled with a male-female joint creating the cone. Each cone portion is assembled into an arm as shown in figure 58.

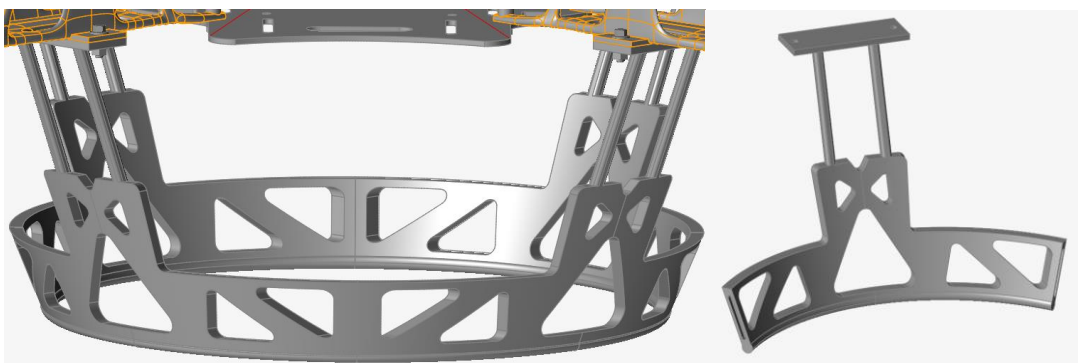


Fig 58 : Optimized landing structure

On the other side, the landing base located on the rover is designed also thinking in a lightweight structure that complies with the requirements described before about the dimensions of the system and the approach with the landing structure. The result is a conical structure that serves as a guide for the drone to land with precision on the rover. A description of the integration of the landing structure with the landing base is shown in figure 59, where are graphically described the design constraints for proper functioning.

The landing base is composed of four conic parts that are joined by bolts to a circular base at the bottom. The height of the landing base is 198mm and the height of the landing structure is 120mm. The radius for the view range of the camera is 118mm, the minimum distance between the camera and the marker when the drone approaches the landing base is 241mm, and the diameter at the bottom of the landing base where is located the marker is 170mm. All of these parameters comply with the mentioned constraints.

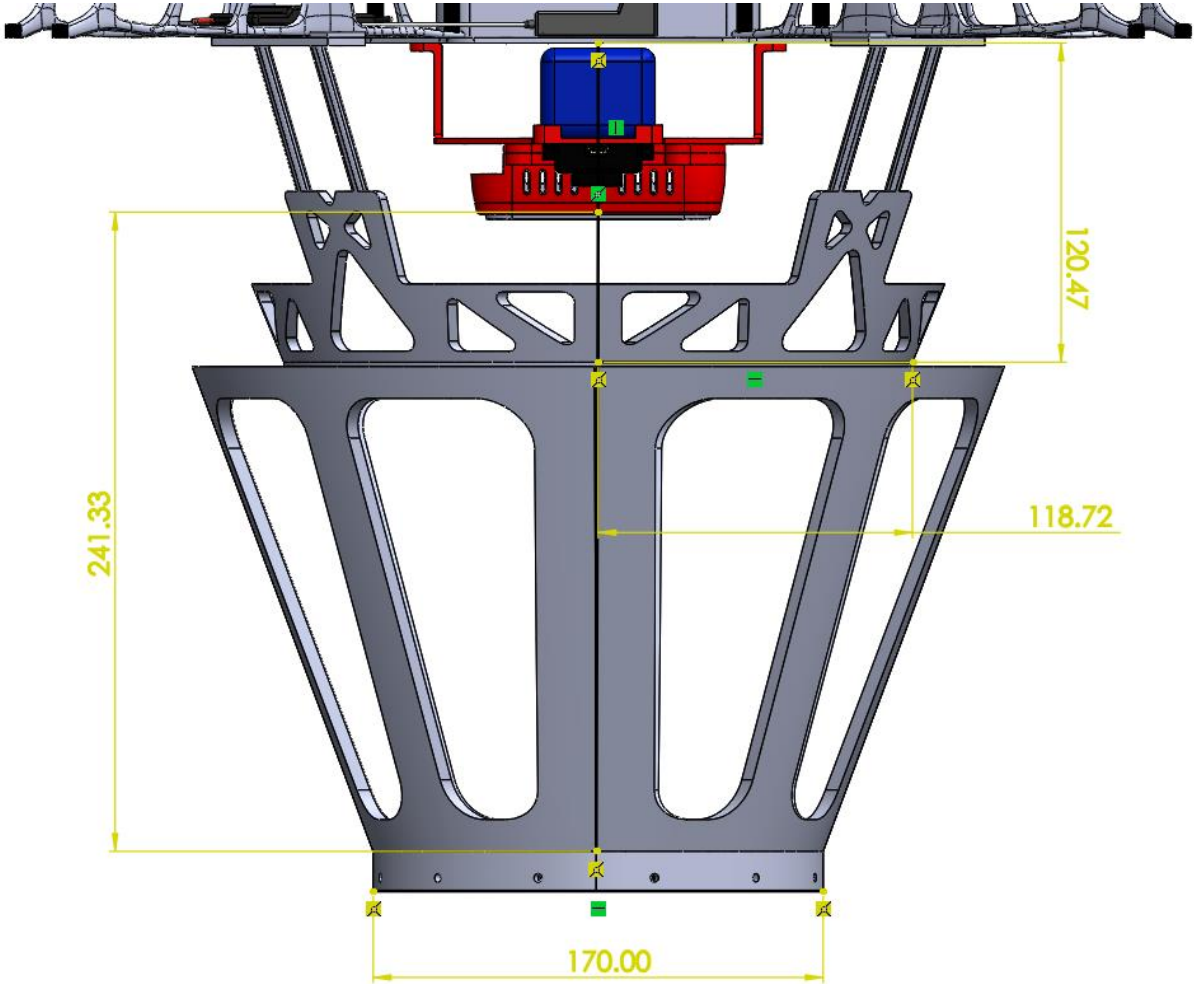


Fig 59 : Description of the landing system with the constraints

5.5. Final analysis

With the integration of the landing system, the complete structure design is finished. Then a final structural simulation is performed with all the load cases defined along the design. Also, other impact load cases are added to the propeller guards to see the maximum load that they can bear before breaking up. As a result, the safety factor in the landing structure, main body, and arms is over 1,5 but the propellers obtained a safety factor of 1 when the impact load on it is 60N, which means that over this force the propellers guards will break up. The result of this simulation is shown in figure 60.

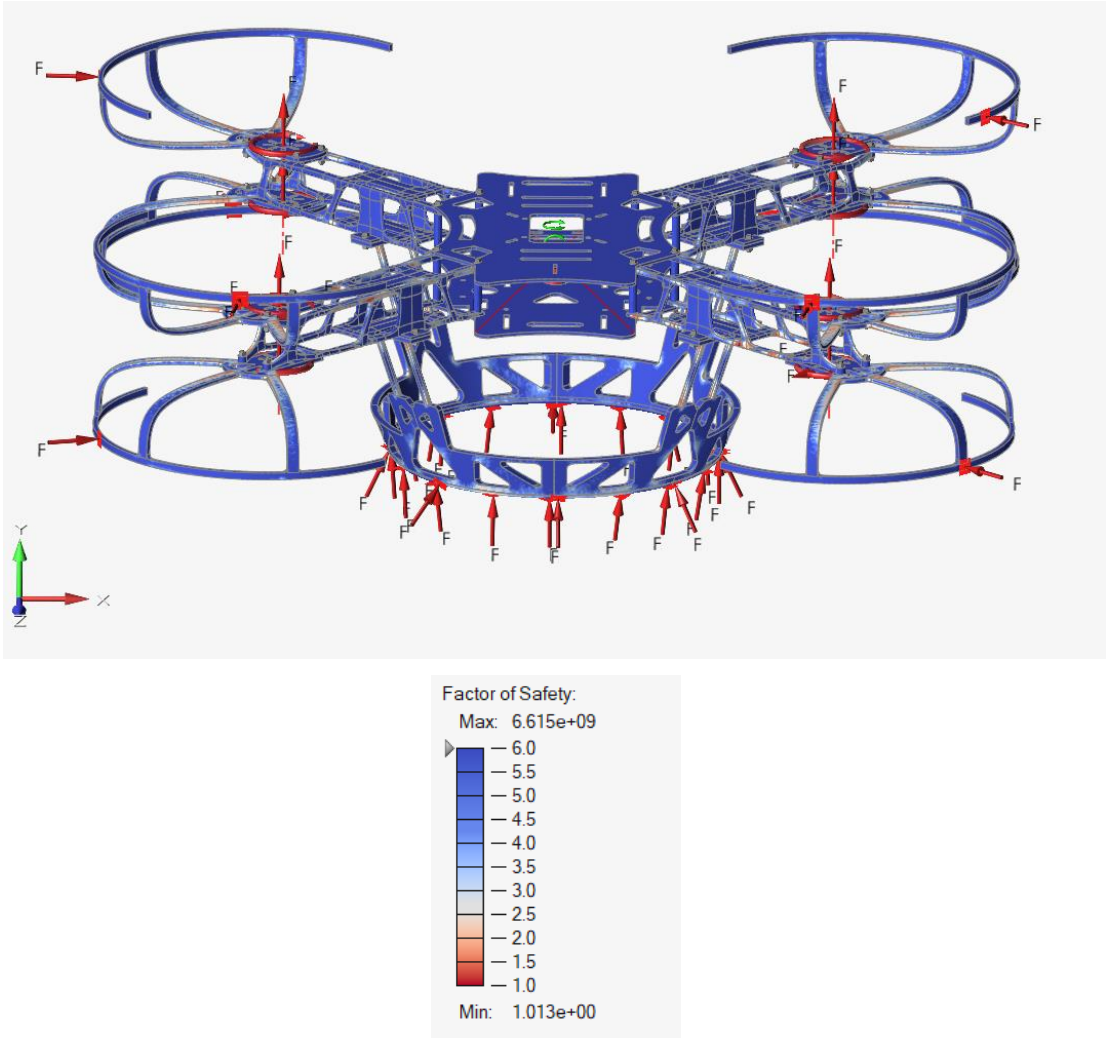


Fig 60 : Finite element analysis of the complete structure

At this point it is finished the design phase. The following point is about the production process through additive manufacturing and the description of the assembly. The complete assembly integrated with the electronic components is shown in figure 61.

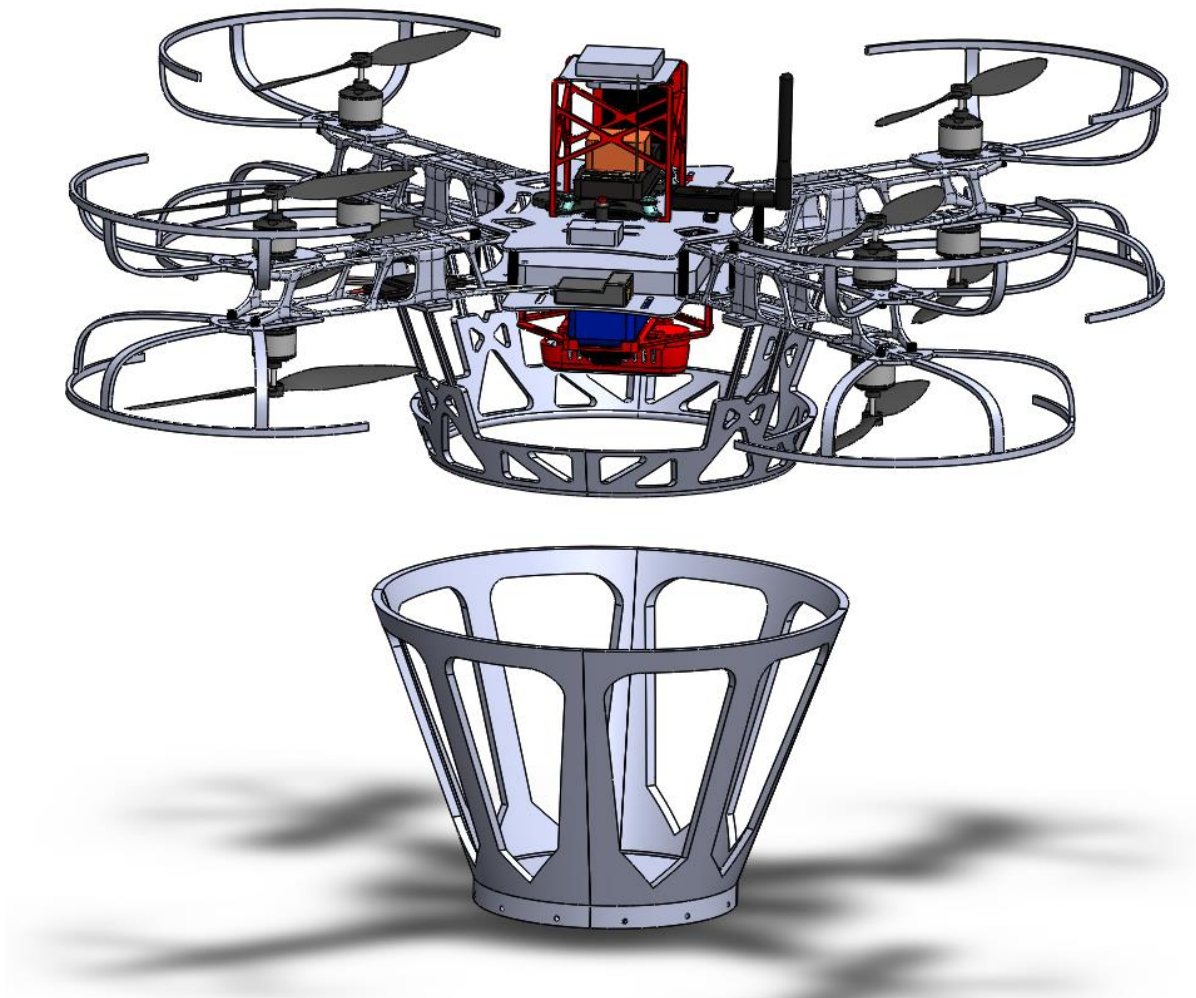


Fig 61 : The final model of the complete system

5.6. Printing process and assembly

The last phase is about the production process. The scope is to obtain a functional prototype in which the assembly of the structure and the performance of the complete system is verified. Therefore this phase is helpful to find eventual problems in the assembly due to the large variety of components mounted on the structure. These problems can be solved quickly by modifying the model and printing the new parts quickly. The additive manufacturing technology to produce this prototype is the FDM using the Ultimaker S5 machine as discussed before due to the low cost and the discussed advantages that it offers. The material used to produce the prototype is selected between the two material candidates (XT-CF20 and PA6 CF) according to the relation between the weight and cost of the structure that will be analyzed.

The Ultimaker S5 has a working volume of 330x240x300 mm. This is one of the reasons to produce a modular design which also offers more flexibility. As the idea is to have a functional prototype to test the performance of the structure, the printing settings are put with the scope to have optimum mechanical properties at the minimum cost. The assistant printing software used to configure the printing model, in STL format, is Ultimaker Cura. The main parameters considered to set the printing are:

- Infill density: The infill represents the fullness of the inside of a part. It is expressed in percentage. The infill affects directly the strength and weight of the parts. In this case, in which this is a structural application, the infill percentage is set at 100% to guarantee optimum mechanical properties. The infill pattern is set in triangles.
- Supports overhang angle: This parameter defines where is necessary a support to build the part. It is an inclination angle measured from the vertical axis. In this case, the overhang angle is 45°, which means that all the surfaces with a higher inclination angle would need supports to be built. Therefore each part is designed to have geometries with an inclination lower than 45° when it is possible to reduce the use of supports.
- Part orientation: This parameter is very important to reduce the time and therefore the cost of the parts. Each part is oriented in such a way as to have less amount of support material. The orientation is set also to avoid a big building direction along the axis perpendicular to the print bed because it causes an unstable building and increases the use of supports.
- Other parameters are predefined by the software Cura Ultimaker as it is the standard software of the machine and the building materials used are in its marketplace. These parameters include the layer height set at 0,2mm; the print speed set at 45mm/s; and the build plate temperature at 60 °C.

The printing process takes significant time due to the type of materials that are reinforced with carbon fibers and due to the infill density which is the maximum in this case. Each part of the structure is set in the Ultimaker Cura software with the two materials to compare the mass and the price. The XT-CF20 is a cheaper material than the Nylon PA6CF but it has a higher density, so more material is needed to build the same part and it also has lower strength. The material support used is the generic PVA which is soluble in water. It offers an easy way to remove the supports but the idea is to reduce the amount of support material when it is possible since it increases the total cost of the part due to its considerable price.

The STL files of the parts are introduced in the software and they are sliced to preview the printing process and estimate the mass and cost of the piece. The preview of the drone arm for the two materials is shown in figure 62, in which is possible to distinguish different layers. The red and yellow represent the part and the blue represents the material support. Also is possible to see other parameters such as the price, the mass, and the cost of the part. The information containing the price and mass of the structure produced with each material is summarized in table 8.

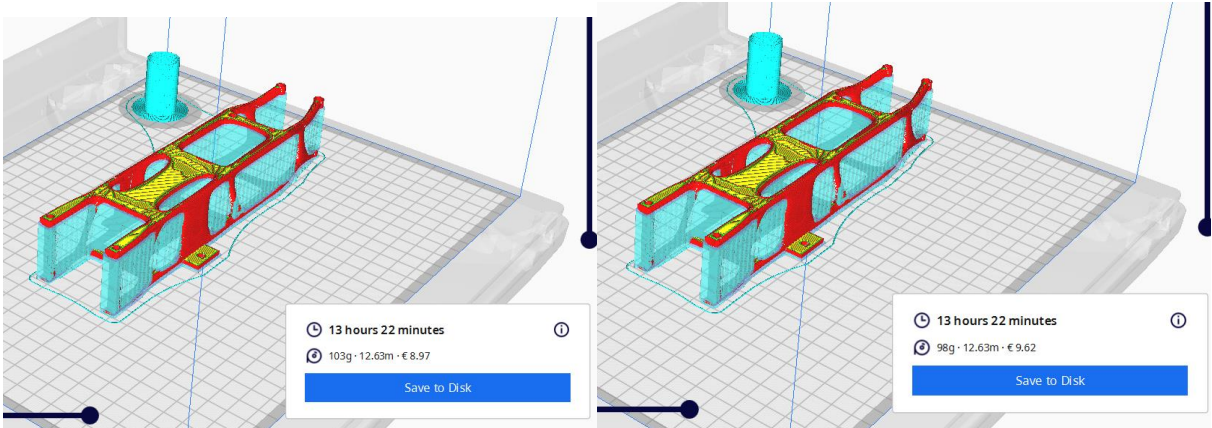


Fig 62 : Preview of the printing process: left: XT-CF20, right: PA6CF

Item	XT-CF20		Nylon PA6CF	
	Mass (g)	Cost (Euro)	Mass (g)	Cost (Euro)
Main structure	591	90,78	523,8	99,58
Landing structure on board	182	33,2	159,2	35,8
Electronic supports	72	8	72	8
Total drone structure	845	131,98	755	143,38
Landing base on the ground	539,2	33,76	474	40,76

Table 8 : Mass and cost of the system with each material

As a first result is possible to see that by producing the structure with PA6CF a lighter system is obtained and the difference in the cost is only around 20 Euro. The mass of the drone obtained with PA6CF is 755g while the one obtained with XT-CF20 is 845g. It represents a difference of 90g between the two designs. Also, the structure produced with PA6CF has higher strength and then a higher safety factor. Therefore the selected material to print the structure is the PA6CF.

The mass of the main structure of the final design is 523,8g. Considering the mass of the initial airframe which is 675, the mass reduction is 22,4%. The cost of the new design is around 100

euros while the cost of the initial frame is 194 euros, which represents about 48% of savings in producing the new structure considering only the costs related to the amount of material.

On the other side, the designed landing system, which is an additional feature concerning the initial frame, to perform the precision landing, increases the total mass and the price of the system. The landing structure on board increases the overall mass of the drone airframe by 159g. The price of the complete landing system, which includes the landing structure on board and the ground base is around 180 euros.

Regarding the support structures for the electronic components, they can be produced with cheap materials. These structures don't have to bear significant loads. The main function is to maintain the components in the desired position. Therefore these structures are planned to be printed with PLA. Due to the total volume of the parts, these can be printed in one session. In figure 63 is possible to see the preview of the printing process. The mass of all of these elements is 72g and the cost is 8 euros.

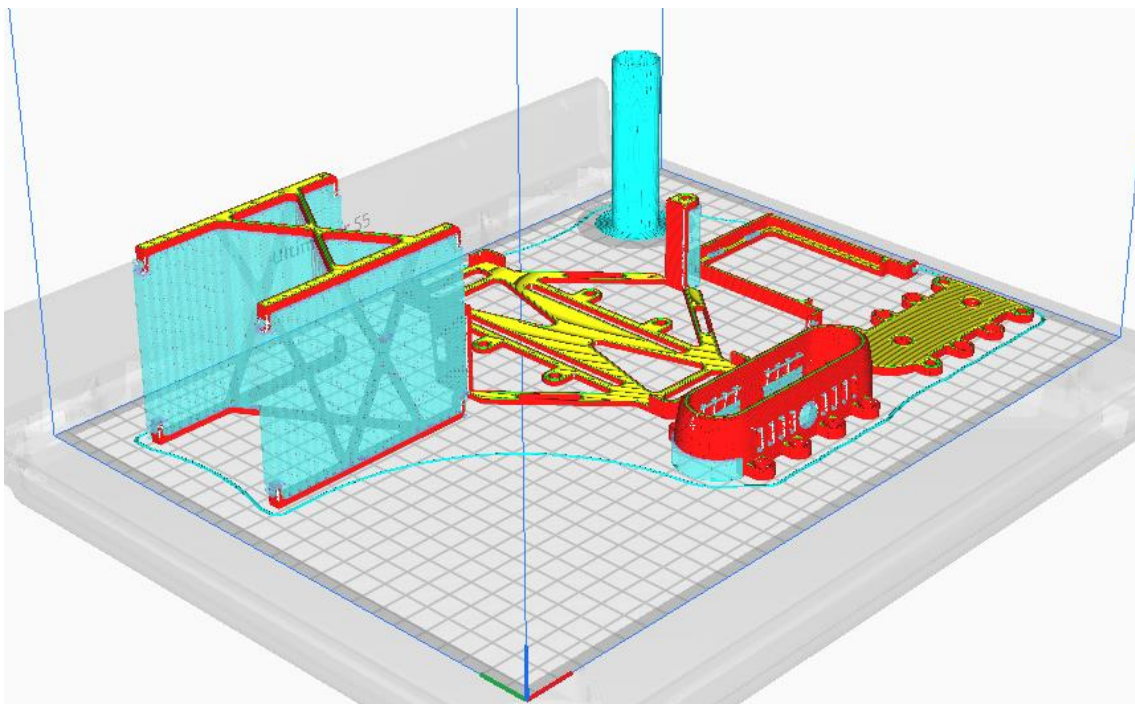


Fig 63 : Printing preview of the support structures for electronic components

After the printing process, the post-processing of the parts must be performed. This consists of the removal of the supports. This process can be done with mechanical methods, using some tools like pliers, wire cutters, and abrasive papers for small layers of material. With this method, there is the risk of damaging the part during the process, so must be done with

attention to avoid that. The other method is to use soluble support material. With this method, only it is necessary to introduce the part in the fluid and the support structures are chemically removed. In this case, is used as support material the PVA which is soluble in water and the supports are easily removed.

Regarding the structure assembly and the electronic components' mounting are used different join methods. To join the structural components, which include the main body, the arms, the propeller guards, the supports for the electronic components, and the landing structure on board, threaded fasteners are used. This type of join is suitable for structural parts. It is fast and is not permanent but adds weight to the structure. In this case, M3 bolts are used to join the parts. Some electronic components which have holes to be assembled are also joined with threaded connections. Other components, which do not allow the thread connection, are attached to the structure with cable ties and glue.

6. Conclusions

This thesis was focused on the optimization of a drone airframe using additive manufacturing technology. This is part of the FIXIT project developed at CIM 4.0, with the scope of creating an autonomous system for indoor and outdoor applications, integrated by a rover and a drone. The activity aims to design a customized, lightweight airframe with optimum mechanical properties at a low cost. The design includes the integration with the structure of the electronic components that are mounted and the design of a landing system that permits the precision landing of the drone on the rover without human intervention. This work is performed through different phases, considering an initial drone which was useful to test the functioning of the system with all the components.

The various phases in which the project was developed include the preliminary design in which the initial system is taken to define all the design constraints of the new structure, the selection of the material to print through the FDM technology, the topology optimization, the design of supports structures for electronic components, the design of the landing system and finally the printing process.

The design constraints considered are mainly related to the positional requirements of the electronic components for their functioning, the loading conditions evaluated in different cases such as the different flight manoeuvres, and critical impact cases. To perform the topology optimization different airframe configurations were considered and the best option was the quad X due to its good strength, the ease of printing it in a modular design, and the integration with the electronic components and the landing system. The landing system obtained is composed of a conical structure on board composed of four conical parts and a higher ground base with conical geometry that remains on the rover to receive the drone. This was obtained after performing several landing tests evaluating the landing precision with the depth camera.

Regarding the technology and the materials, the functional prototype is produced through FDM. Two materials reinforced with carbon fibers were first preselected to print the structure, the XT-CF20, and PA6CF. Then the printing process is previewed through the software Ultimaker Cura to estimate the mass of the airframe and the cost with the two options. The difference between the cost was only 20 euros and the mass difference was 90g. Finally, the PA6CF is selected for the printing process because a lighter structure with higher strength is obtained with it. A mass reduction is obtained. It was 22,4% concerning the initial frame and the cost is around 100 euros while the cost of the initial airframe is 194 euros.

Additive manufacturing is a very feasible technology to produce drone structures at all levels, from conceptual prototypes to small series. It offers the possibility of creating light airframes customized to specific applications with high-performance materials. With AM is possible to produce the most complex geometries and personalized shapes to fit the specific functional characteristics and the specific needed components. Also, it offers the possibility of creating and testing the drone parts quickly and modify in short times the design to reprint parts or add new modifications to the drone.

The topology optimization method is very useful to create this type of structure for drone applications in which mass is a critical parameter. With this method is possible to adjust the mass of the structure considering the constraints. Therefore the result is a structural truss with variable thickness where is possible to reduce the mass in the zones in which the safety factor is high and put more mass in the zones in which is necessary to bear the maximum stresses.

The implementation of a modular design offers flexibility and reduces production costs. The idea is to print a functional prototype to verify the assembly and perform functional flight and landing tests. The structure is produced in singular parts that are then assembled. It offers the possibility of swapping quickly the components if they are damaged due to crashes, only by printing the individual part again.

The feasibility of the production of drones with additive manufacturing will remain increasing as this technology is constantly growing, improving the process and developing new high-performance materials which make the production costs of high-quality drones with this technology decrease more and more.

Future works aligned with this project can be oriented to use the generative design method to optimize the structure. This is an analog method in which is possible to create different structural configurations without an initial design space as in the case of topology optimization. In this case, it would be only necessary to set the loading conditions, constraints about the space, and the preserved volume.

References

- [1] M. Javaid, I. Khan, R. Singh, S. Rab and R. Suman, "Exploring contributions of drones towards Industry 4.0," *Industrial Robot*, Vol. 49 No. 3, pp. 476-490. <https://doi.org/10.1108/IR-09-2021-0203>, 2022.
- [2] A. Haleem and M. Javaid, "Additive Manufacturing Applications in Industry 4.0: A Review," *Journal of Industrial Integration and Management*, DOI: 10.1142/S2424862219300011, 2019.
- [3] L. Amoroso, "Analisi delle traiettorie tecnologiche nel settore dei veicoli aerei senza equipaggio a uso commerciale," *Tesi di Laurea Magistrale*, 2018.
- [4] Y. K. & I. Nielsen, "A system of UAV application in indoor environment," *Production & Manufacturing Research*, 4:1, 2-22, DOI: 10.1080/21693277.2016.1195304, 2016.
- [5] Q.-V. Dang, I. Nielsen, K. Steger-Jensen and O. Madsen, "Scheduling a single mobile robot for part-feeding tasks of production lines," *Journal of Intelligent Manufacturing*, 25, 1271-1287., 2014.
- [6] K. C. T. Vivaldini, L. F. Rocha, M. Becker and A. P. Moreira, "Comprehensive review of the dispatching, scheduling and routing of AGVs.," *11th Portuguese Conference on Automatic Control (pp. 505-514).*, 2015.
- [7] A. Kumar and B. Muhammad, "On how internet of drones is going to revolutionise the technology application and business paradigms," *21st International Symposium on Wireless Personal Multimedia Communications (WPMC), IEEE*, pp. 405-410, 2018.
- [8] F. P. D. C. L. E. L. Dal Mas, G. Presch, M. Massaro, M. Skrap, A. Ferrario di Tor Vajana, S. D'Auria and C. Bagnoli, "The effects of artificial intelligence, robotics and industry 4.0 technologies. Insights from the healthcare sector," *Proceedings of the first European Conference on the Impact of Artificial Intelligence and Robotics*, pp. 88-95., 2019.
- [9] Grand view research, "Commercial Drone Market Size & Share Report, 2021-2028," 2020. [Online]. Available: <https://www.grandviewresearch.com/industry-analysis/global-commercial-drones-market>.
- [10] G. Bareth, H. Aasen and J. Bendig, "Low-weight and UAV-based hyperspectral full-frame cameras for monitoring crops: Spectral comparison with portable spectroradiometer measurements.," *Photogrammetrie - Fernerkundung - Geoinformation*, 69-79., 2015.
- [11] J. Kwon and S. Hailes, "Scheduling UAVs to bridge communications in delay-tolerant networks using real-time scheduling analysis techniques," *2014 IEEE/SICE international symposium on System Integration*. pp. 363-369, 2014.

- [12] D. Mellinger, N. Michael and V. Kumar, "Trajectory generation and control for precise aggressive maneuvers with quadrotors," *The International Journal of Robotics Research*, 31(5), 664–674., 2012.
- [13] S. H. Chung, B. Sah and J. Lee., "Optimization for drone and drone-truck combined operations: A review of the state of the art and future directions," *Computers and Operations Research* 123, doi: 10.1016/j.cor.2020.105004, 2020.
- [14] M. Ridolfi, N. Macoir, J. Vanhie-Van Gerwen, J. Rossey, J. Hoebeke and E. De Poorter, "Testbed for warehouse automation experiments using mobile AGVs and drones," *IEEE INFOCOM 2019-IEEE Conference on Computer Communications Workshops (INFOCOM WKSHPS)*, IEEE, pp. 919-920., 2019.
- [15] N. Zhang, Q. Jiang, L. Li, X. Ma and J. Ma, "An efficient three-factor remote user authentication protocol based on BPV-FourQ for internet of drones," *Peer-to-Peer Networking and Applications*, pp. 1-14., 2021.
- [16] G. Goh, S. Agarwala, G. Goh, V. Dikshit and W. Yeong, "Additive manufacturing in unmanned aerial vehicles (UAVs): Challenges and potential," *Aerospace Science and Technology*.
- [17] "Top 15 of the best 3D printed drone projects," 2018. [Online]. Available: <https://www.sculpteo.com/en/industries/drones/3d-printed-drone/>.
- [18] "The Marine Corps wants to 3D print cheaper drones," 2017. [Online]. Available: <https://www.popsci.com/marine-corps-3d-printed-drones/>.
- [19] "Disaster Inspires Japanese Designers: Generative Design & 3D Printing Create Relief Effort X VEIN Drone," 2017. [Online]. Available: <https://3dprint.com/181435/generative-design-x-vein-drone/>.
- [20] "CargoCopter, our latest generation of high-speed, long-range drones," [Online]. Available: https://www.youtube.com/watch?v=kqTu1IU_VoQ&ab_channel=BartTheys.
- [21] "Teal Group Predicts Worldwide Civil UAS Production Will Total \$65 Billion in Its 2016 UAS Market Profile and Forecast.," 2016. [Online]. Available: <https://tealgroup.com/index.php/about-teal-group-corporation/press-releases/129-teal-group-predicts-worldwide-civil-uas-production-will-total-65-billion-in-its-2016-uas-market-profile-and-forecast>.
- [22] A. Mishra, S. Pal and G. S. M. & P. Singh, "Structural analysis of UAV airframe by using FEM techniques: a review," *International Journal of Advanced Science and Technology*, 2020.
- [23] P. Kardasz and J. Doskocz, "Drones and Possibilities of Their Using," 2016.
- [24] Ardupilot, "Ardupilot - Motor order diagrams," [Online]. Available: <https://ardupilot.org/copter/docs/connect-escs-and-motors.html>.

- [25] P. Javir, K. Pawar, S. Dhudum³, N. Patale and S. Patil, "Design, analysis and fabrication of quadcopter," *Journal of Advance Research in Mechanical and Civil Engineering*, <https://doi.org/10.53555/nmce.v2i3.342>.
- [26] T-Motor, "AT2312 Long Shaft," [Online]. Available: <https://store.tmotor.com/goods.php?id=788>.
- [27] T. Robotics, *Drone Building and Optimization: How to Increase Your Flight Time, Payload and Overall Efficiency*, 2021.
- [28] HobbyKing, "Multistar Propeller 9x5," [Online]. Available: https://hobbyking.com/it_it/multistar-carbon-fiber-propeller-9x5-black-cw-ccw-2pcs.html.
- [29] Amazon, "Gens ace 4S Battery Lipo 14.8V," [Online]. Available: https://www.amazon.it/stores/gens+ace/page/3666955E-7DoF-4B56-8AA4-80ACF58B7018?ref_=ast_bln.
- [30] Amazon, "FEICHAO 4Pcs 40A Brushless ESC 2-4S Regolatore di velocità," [Online]. Available: https://www.amazon.it/FEICHAO-Brushless-Regolatore-Elicottero-Multi-ASSE/dp/B07Z684484/ref=sr_1_1_sspa?keywords=esc+40a&qid=1651130842&refinements=p_76:490211031&rnid=490209031&rps=1&s=toys&sprefix=esc+,toys,80&sr=1-1-spons&psc=1&spLa=ZW5jcmlwdGVkUXVhbGlm.
- [31] V. Alfonso, "Riprogettazione della struttura di un UAV a guida autonoma indirizzata alla produzione tramite tecnologie di additive manufacturing," 2021.
- [32] Amazon, "JMT PX4 PIX 2.4.8 32 Bit Flight Controller," [Online]. Available: https://www.amazon.it/JMT-Controller-Integrare-Interruttore-Multirotor/dp/B07RPTPSRP/ref=sr_1_23?keywords=pixhawk+2.4.8&qid=1649692255&sprefix=pixhawk+2.4,aps,70&sr=8-23.
- [33] Nvidia. [Online]. Available: <https://www.nvidia.com/it-it/autonomous-machines/embedded-systems/jetson-nano/product-development/>.
- [34] Pozyx, "Developer Tag," [Online]. Available: <https://www.pozyx.io/products/hardware/tags/developer-tag>.
- [35] LMIAOM, "Amazon," [Online]. Available: <https://www.amazon.it/>.
- [36] A. Salmi, *Additive Manufacturing Systems and Materials Course Notes*.
- [37] sculpteo, "Top tips for drone manufacturing with 3D printing".
- [38] Ultimaker. [Online]. Available: <https://ultimaker.com/es/3d-printers/ultimaker-s5>.
- [39] F. Calignano, F. Giuffrida and M. Galati, "Effect of the build orientation on the mechanical performance of polymeric parts produced by multi jet fusion and selective laser sintering," *Journal of Manufacturing Processes* doi:10.1016/j.jmapro.2021.03.018 , 2021.

- [40] Innovation News., "3-D Printers Could Recycle Old Plastic Bottles Into...Anything!," 2012. [Online]. Available: https://www.msnbc.msn.com/id/46058138/ns/technology_and_science-innovation/t/-d-printers-could-recycle-old-plastic-bottles-anything/#.UNtxQ-Q72eY.
- [41] H. V. Wang and D. Rosen, "Computer-aided design methods for the additive fabrication of truss structure," *School of Mechanical Engineering, Georgia Institute of Technology Atlanta*, 2001.
- [42] A.-J. Wang and D. McDowell, "Optimization of a metal honeycomb sandwich beam-bar subjected to torsion and bending," *International Journal of Solids and Structures*, 2003.
- [43] B. Vrancken, L. Thijs, J.-P. Kruth and a. J. V. Humbeeck, "Heat treatment of Ti6Al4V produced by selective laser melting: microstructure and mechanical properties," *Journal of Alloys and Compounds*, 2012.
- [44] S.-H. Ahn, M. Montero, D. Odell, S. Roundy and a. P. K. Wright, "Anisotropic material properties of fused deposition modeling ABS," *Rapid Prototyping Journal*, 2002.
- [45] S. Easter, J. Turman, D. Sheffler, M. Balazs, J. Rotner, T. Pham, M. A. Kolodny and K. L. Priddy, "Using advanced manufacturing to produce unmanned aerial vehicles: a feasibility study.," *Ground/Air Multisensor Interoperability, Integration, and Networking for Persistent ISR IV*, 2013.
- [46] I.-R. Popa, C. Ciofu and C. Carausu, "Process parameters influence on economic efficiency of 3D printing," *International Journal of Manufacturing Economics and Management*, 2021.
- [47] A. M. Leon, A. Rukavitsyn and S. Jatsun, "Topology optimization of a UAV airframe," *Proceedings of the 6th International Conference on Industrial Engineering (ICIE 2020) DOI: 10.1007/978-3-030-54814-8_41*, 2021.
- [48] H. M, N. M and S. H, "Multidisciplinary design optimization of UAV under uncertainty.," *Journal of Aerospace Technology and Management*, 2017.
- [49] I. P. Rosinha, K. V. Gernaeya, J. M. Woodley and U. Krühnea, "Topology optimization for biocatalytic microreactor configurations," *Computer Aided Process Engineering Volume 37*, 2015.
- [50] M. Bendsoe and O. Sigmund, *Topology Optimization: Theory, Methods, and Applications.*, Springer Berlin Heidelberg, 2013.
- [51] "Engineering Product Design," [Online]. Available: <https://engineeringproductdesign.com/knowledge-base/topology-optimization/>.
- [52] G. Belingardi, *Il metodo degli elementi finiti nella progettazione meccanica*, Torino: ISBN: 9788882180898, 1995.
- [53] BASF, "Technical Datasheet," [Online]. Available: <https://www.crea3d.com/it/ricerca?controller=search&s=basf>.

- [54] Fabbrix, "Technical Datasheet," [Online]. Available: <https://www.fabbrix.com/it/materiali-fabbrix>.
- [55] Colorfabb, "Technical Datasheet," [Online]. Available: https://colorfabb.com/filaments/materials/2_85_mm.
- [56] Polymaker, "Technical Datasheet," [Online]. Available: <https://eu.polymaker.com/product/polymide-pa6-cf/>.
- [57] Sinterit, "Technical Datasheet," [Online]. Available: <https://sinterit.com/materials/pa11-cf-carbon-fiber/>.
- [58] M. Habib, W. Abdelaal and M. Saad, "Dynamic modeling and control of a quadrotor using linear and nonlinear approaches.," 2014.
- [59] B. d. a. B. B. Blue, "Understanding The Physics Of Drones," 2022. [Online]. Available: <https://beaglebluevoyager.com/understanding-the-physics-of-drones/>.
- [60] T. Luukkonen, "Modelling and control of quadcopter," *Independent research project in applied mathematics, Espoo*, 2011.
- [61] C. A. Amadi, "Design and Implementation of Model Predictive Control on Pixhawk Flight Controller," *Thesis*, 2018.
- [62] C. Luis and J. Ny, "Design of a trajectory tracking controller for a nanoquadcopter.," *arXiv preprint arXiv:1608.05786*, 2016.
- [63] APC Propellers, "APC Propeller Performance Data," 2014. [Online]. Available: https://www.apcprop.com/files/PER3_9x5.dat.
- [64] A. Inspire, "Speed/Accuracy (optimization)," [Online]. Available: https://2021.help.altair.com/2021/inspire/en_us/topics/inspire/structure/optimization_speed_accuracy.htm.